




Original Article

Systematics of minute strabomantid frogs allocated to the genus *Noblella* (Amphibia: Anura) with description of a new genus, seven new species, and insights into historical biogeography

Jhael A. Ortega¹,, Diego F. Cisneros-Heredia^{2,3}, Jeffrey D. Camper⁴,
Andrés Romero-Carvajal¹,, Leonardo Negrete¹ and Santiago R. Ron^{1,*},

¹Museo de Zoología, Escuela de Biología, Pontificia Universidad Católica del Ecuador, Avenida 12 de Octubre 1076 y Roca, Apartado 17-01-2184, Quito, Ecuador

²Universidad San Francisco de Quito USFQ, Colegio de Ciencias Biológicas y Ambientales, Instituto de Biodiversidad Tropical IBIOTROP, Museo de Zoología/Laboratorio de Zoología Terrestre, Quito, Ecuador

³Instituto Nacional de Biodiversidad INABIO, División de Herpetología, Quito, Ecuador

⁴Department of Biology, Francis Marion University, Florence, SC 29506, USA

*Corresponding author. Museo de Zoología, Escuela de Biología, Pontificia Universidad Católica del Ecuador, Avenida 12 de Octubre 1076 y Roca, Apartado 17-01-2184, Quito, Ecuador. E-mail: santiago.ron@gmail.com

ABSTRACT

Noblella is a genus of 17 recognized nominal species of ground-dwelling, direct-developing frogs. It consists of two clades that do not form a monophyletic group: a northern clade from northern Peru, Ecuador, Colombia, and Brazil and a southern clade from southern Peru and Bolivia. Herein, we present a systematic review of *Noblella* with emphasis on the northern clade, including a new phylogeny based on DNA sequences of mitochondrial and nuclear genes. We also describe the osteology of five species from the northern clade using X-ray computed tomography. Based on our results, we resurrect the genus *Phyllonastes* for species of the northern clade (i.e. eight described species plus six new species described herein) and restrict the genus *Noblella* to the southern clade. We describe a new genus of Holoadeninae, sister to *Phyllonastes*: *Urkuphryne* gen. nov., from northern Ecuador. The new genus is distinguished by unique morphological characteristics that are diagnostic of different genera in Strabomantidae. We describe seven new species diagnosable based on morphology. *Phyllonastes* has five morphological synapomorphies, including the absence of vomerine teeth. *Phyllonastes* originated in the Pacific basin, Chocó region, ~21 Mya.

Keywords: Andes; biogeography; Chocó; Holoadeninae; phylogeny; systematics; taxonomy

INTRODUCTION

Noblella Barbour, 1930 is a genus of small strabomantid frogs known from Andean montane forests and lowland rainforests in Colombia, Ecuador, Peru, Bolivia, and Brazil. As currently defined, it is composed of 17 nominal species (Frost 2023) and includes species that are among the smallest Neotropical vertebrates, with *Noblella pygmaea* Lehr & Catenazzi, 2009 being the smallest Andean frog species (Lehr and Catenazzi 2009a). The genus *Noblella* was erected by Barbour (1930) to allocate a single species, *Sminthillus peruvianus* Noble, 1921 (= *Noblella peruviana* Noble, 1921) from the Department of Puno in southern Peru (De la Riva *et al.* 2008b). Lynch (1971) synonymized *Noblella*

with *Eleutherodactylus* Duméril & Bibron, 1841. A few years later, Lynch (1975) synonymized *Noblella* with *Phrynopus* Peters, 1873 based on finger morphology. Lynch (1975) noted that the type species of *Noblella* has several osteological differences relative to *Phrynopus*, including the absence of vomerine teeth. However, he considered that trait to be irrelevant for genus definition. Lynch (1975) acknowledged that *Phrynopus peruvianus* was 'osteologically isolated from the other species of the genus [*Phrynopus*]'. Nevertheless, he did not regard those traits as enough evidence to consider *Noblella* a valid genus (Lynch 1975).

Noblella was resurrected by De la Riva *et al.* (2008b), who, after examining the type series of *Sminthillus peruvianus*, concluded

Received 25 March 2024; revised 12 November 2024; accepted 19 November 2024

[Version of Record, first published online 13 January 2025, with fixed content and layout in compliance with Art. 8.1.3.2 ICZN. <http://zoobank.org/urn:lsid:zoobank.org:pub:10ED7D3B-C7E9-4FAS-BD47-45D87308D3AA>]

© The Author(s) 2025. Published by Oxford University Press on behalf of The Linnean Society of London. All rights reserved. For commercial re-use, please contact reprints@oup.com for reprints and translation rights for reprints. All other permissions can be obtained through our RightsLink service via the Permissions link on the article page on our site—for further information please contact journals.permissions@oup.com.

that it did not belong to *Phrynopus*. Furthermore, they considered *Phyllonastes* Heyer, 1977 a junior synonym of *Noblella*. Heyer (1977) described the genus *Phyllonastes* to resolve the taxonomic and geographical inconsistencies of the genus *Euparkerella* Griffiths, 1959. He placed *Euparkerella lochites* (Lynch, 1976) and *Euparkerella myrmecoides* (Lynch, 1976) within *Phyllonastes*, restricting *Euparkerella* to species from the Brazilian Atlantic Forest. Unfortunately, most diagnostic characters of *Phyllonastes* proposed by Heyer (1977) became invalid as new species were added to the genus [e.g. tympanum distinct, but absent in *Noblella carrascoicola* (De la Riva & Köhler, 1998)]; toes circumferentially grooved, but toes without circumferential grooves in *N. carrascoicola* (De la Riva & Köhler, 1998); tips of fingers pointed, bearing papilla, but slightly expanded without papilla in *N. carrascoicola* (De la Riva & Köhler, 1998); two phalanges in finger IV, but three phalanges in finger IV in *Noblella lynchi* (Duellman, 1991) and *Noblella heyeri* (Lynch, 1986)]. Eventually, the only remaining morphological diagnostic character was the pointed toe tips (especially toes III and IV).

As currently defined, *Noblella* is characterized by the following combination of characters (*sensu* De la Riva et al. 2008b): (1) head narrower than body; (2) cranial crests absent; (3) dentigerous processes of vomers absent; (4) 'S' condition of adductor muscle; (5) terminal phalanges narrowly T-shaped; (6) finger I < finger II; (7) toe III shorter than toe V; (8) tips of at least toes III–IV acuminate; and (9) small size [snout-vent length (SVL) < 22 mm]. Miniaturization of *Noblella* is accompanied by the reduced number of phalanges in finger IV in some species (i.e. *Noblella lochites*, *N. myrmecoides*, and *Noblella naturetrekii* Reyes-Puig et al. 2019).

Despite having a relatively small number of species, *Noblella* presents some taxonomic problems awaiting resolution. *Noblella* was found to be polyphyletic by Reyes-Puig et al. (2019), with two geographically disjunct clades: one northern clade, closely related to *Barycholos* Heyer, 1969 and *Bahius* Dubois et al. 2021, and a southern clade closely related to *Psychrophrynella* Hedges et al. 2008 and *Microkayla* De la Riva et al. 2017 (see also Santa-Cruz et al. 2019, Reyes-Puig et al. 2021). The lack of genetic information on the type species, *Noblella peruviana*, which presumably belongs to the southern clade given the location of its type locality, along with its morphological similarity to some species of *Psychrophrynella* and the paraphyly of the latter (e.g. Catenazzi and Tito 2019, Motta et al. 2021, Reyes-Puig et al. 2021) have made it challenging to resolve the polyphyly of *Noblella*.

In this study, we integrate several lines of evidence (i.e. molecular, ecological, morphological, and biogeographical) to solve the polyphyly of *Noblella* by resurrecting the genus *Phyllonastes*. In addition, we analyse genetic and morphological variation of populations distributed in Ecuador and northern Peru to describe six new species and a new genus from the Andes of northern Ecuador.

MATERIALS AND METHODS

Ethics statement

Voucher specimens and tissue samples were obtained following ethical and technical protocols (Esselstyn et al. 2008). We conducted this research under the following collection and mobilization permits: MAE-DNB-ARRGG-CM-2014-0002,

MAE-DPMS-2015-06, 002-16 IC-FAU-DNB/MA, 005-14 IC-FAU-DNB/MA, MAE-DPMS-2015-09, 008-2015, 001-11 IC-FAU-DNB/MA, MAE-DNB-CM-2015-0025, MAE-DPMS-2018-04, 002-16 IC-FAU-DNB/MA, and 008-09 IC-FAU-DNB/MA issued by the Ministerio de Ambiente, Agua y Transición Ecológica del Ecuador (MAE) to the Pontificia Universidad Católica del Ecuador (PUCE); MAE-DNB-CM-2019-0120 issued to the Instituto Nacional de Biodiversidad INABIO; and 006-2015-FAU-DPAP-MA issued to the Universidad San Francisco de Quito.

Sampling of species and populations

Our analysis focused mainly on *Noblella* specimens and tissue samples deposited at the Museum of Zoology of Pontificia Universidad Católica del Ecuador (QCAZ). Most specimens were collected during field trips by QCAZ staff and students as part of the Arca de Noé initiative. The sample size was expanded to include relevant type material and specimens from División de Herpetología, Instituto Nacional de Biodiversidad, Quito (DHMECN), and Museo de Zoología, Universidad San Francisco de Quito, Quito (ZSFQ). The QCAZ tissue collection has samples from 196 individuals of *Noblella*. Of them, we selected 44 individuals for sequencing based on preliminary morphological examination and distribution. The specimens chosen for sequencing included one representative from each population and morphological variants suggestive of cryptic diversity within populations. We also included all available GenBank sequences of *Bahius*, *Bryophryne*, *Microkayla*, *Noblella*, *Psychrophrynella*, and *Qosqophryne*. In addition, we added sequences of representative species of other Terrarana (= Brachycephaloidea) genera from GenBank.

DNA extraction, amplification, and sequencing

DNA was extracted from muscle or liver tissue preserved in 95% ethanol. We performed a standard PCR to amplify DNA fragments for mitochondrial genes 12S rRNA (12S), 16S rRNA (16S), and the nuclear genes recombination-activating 1 (*RAG1*) and tyrosinase (*TYR*). PCR amplification was carried out following standardized protocols using the following primers: 12Sh and 12SKH (Goebel et al. 1999), tPhe2-frog (Smith et al. 2005), and tVal3-frog (Moen and Wiens 2009) for 12S rRNA; 12L34, 16H48E, 16H36E, 16L19, 16H47, and 16L34 (Heinicke et al. 2007) for 16S rRNA; Tyr1C and Tyr1G (Bossuyt and Milinkovitch 2000) for *TYR*; and R182 and R270 (Hedges et al. 2008) for *RAG1*. Sequencing in both directions was carried out by the MacroGen Sequencing Team (MacroGen Inc., Seoul, Korea).

Phylogenetic analyses

The new sequences (17 of 12S, 40 of 16S, 33 of *RAG1*, and 24 of *TYR*) from 44 individuals were assembled and edited with GENEIOUS v.7.1.7 (GeneMatters Corp.). The sequences generated in this study were deposited in GenBank (accession numbers shown in Table 1). We blasted our 12S, 16S, *TYR*, and *RAG1* sequences with the GenBank database (*blastn* procedure) to find similar sequences of *Noblella* and related lineages and added them to the matrix. We included sequences of *Ceuthomantis smaragdinus* (ROM40161) available in GenBank for the outgroup. GenBank sequences

Table 1. GenBank accession numbers for newly generated DNA sequences used in the phylogenetic analyses.

Species	Voucher QCAZ	Voucher GenBank	16S	12S	RAG1	TYR
<i>Lynchius simmonsii</i>	QCAZ41639	QCAZ41639	PP536451	PP536493	PP536416	PP536390
<i>Lynchius simmonsii</i>	QCAZ41640	QCAZ41640	PP536452		PP536417	
<i>Niceforonia nigrovittata</i>	QCAZ33258	QCAZ33258	PP536448			
<i>Niceforonia nigrovittata</i>	QCAZ41145	QCAZ41145	PP536450			
<i>Oreobates quixensis</i>	QCAZ25520	QCAZ25520			PP536411	
<i>Phyllonastes cerrogolondrinus</i>	QCAZ66086	QCAZ66086	PP536470		PP536431	PP536401
<i>Phyllonastes cerrogolondrinus</i>	QCAZ66089	QCAZ66089	PP536471		PP536432	PP536402
<i>Phyllonastes cerrogolondrinus</i>	QCAZ66090	QCAZ66090	PP536472			
<i>Phyllonastes dicaprio</i>	QCAZ72212	DHMECN13723	PP536476	PP536488	PP536437	PP536407
<i>Phyllonastes dicaprio</i>	QCAZ72213	DHMECN13724	PP536477	PP536489	PP536438	PP536408
<i>Phyllonastes dicaprio</i>	QCAZ72216	DHMECN13727	PP536478		PP536439	
<i>Phyllonastes ecuadoriensis</i>	QCAZ48916	QCAZ48916	PP536454		PP536419	PP536392
<i>Phyllonastes ecuadoriensis</i>	QCAZ57064	QCAZ57064	PP536459	PP536494	PP536422	
<i>Phyllonastes heyeri</i>	QCAZ24875	QCAZ24875	PP536445			
<i>Phyllonastes heyeri</i>	QCAZ31471	QCAZ31471			PP536414	PP536388
<i>Phyllonastes lochites</i>	QCAZ72220	DHMECN11227	PP536481	PP536486	PP536442	PP536410
<i>Phyllonastes lochites</i>	QCAZ51766/EPN14255	QCAZ51766	PP536455		PP536420	PP536393
<i>Phyllonastes lochites</i>	QCAZ51767/EPN14253	QCAZ51767	PP536456			
<i>Phyllonastes macuma</i>	QCAZ40180	QCAZ40180			PP536415	PP536389
<i>Phyllonastes myrmecoides</i>	QCAZ53583	QCAZ53583	PP536458		PP536421	PP536394
<i>Phyllonastes naturetrekii</i>	QCAZ71337	QCAZ71337			PP536434	PP536404
<i>Phyllonastes naturetrekii</i>	QCAZ72217	QCAZ72217	PP536479	PP536503	PP536440	
<i>Phyllonastes personinus</i>	QCAZ31115	QCAZ31115	PP536446	PP536491	PP536412	PP536387
<i>Phyllonastes personinus</i>	QCAZ71452	QCAZ71452	PP536474	PP536501	PP536435	PP536405
<i>Phyllonastes personinus</i>	QCAZ71453	QCAZ71453	PP536475	PP536502	PP536436	PP536406
<i>Phyllonastes personinus</i>	QCAZ40332	QCAZ40332	PP536449			
<i>Phyllonastes personinus</i>	QCAZ52716	QCAZ52716	PP536457			
<i>Phyllonastes personinus</i>	QCAZ58816	QCAZ58816	PP536460	PP536495	PP536423	PP536395
<i>Phyllonastes personinus</i>	QCAZ58819	QCAZ58819	PP536461	PP536496	PP536424	
<i>Phyllonastes personinus</i>	QCAZ58820	QCAZ58820	PP536462	PP536497	PP536425	
<i>Phyllonastes personinus</i>	QCAZ59121	QCAZ59121	PP536464	PP536499		
<i>Phyllonastes personinus</i>	QCAZ59433	QCAZ59433	PP536465			
<i>Phyllonastes personinus</i>	QCAZ59437	QCAZ59437	PP536466		PP536427	PP536397
<i>Phyllonastes personinus</i>	QCAZ72222	DHMECN9721	PP536483	PP536490	PP536444	
<i>Phyllonastes plateadensis</i>	QCAZ65015	QCAZ65015	PP536467		PP536428	PP536398
<i>Phyllonastes sardinayacu</i>	QCAZ58822	QCAZ58822	PP536463	PP536498	PP536426	PP536396
<i>Phyllonastes</i> sp.	QCAZ31165	QCAZ31165	PP536447	PP536492	PP536413	
<i>Phyllonastes</i> sp.	QCAZ72221	DHMECN12012	PP536482	PP536487	PP536443	
<i>Phyllonastes</i> sp.	QCAZ72218	DHMECN10226	PP536480	PP536485	PP536441	PP536409
<i>Urkuphryne merinoi</i>	QCAZ41813	QCAZ41813	PP536453		PP536418	PP536391
<i>Urkuphryne merinoi</i>	QCAZ66078	QCAZ66078	PP536468		PP536429	PP536399
<i>Urkuphryne merinoi</i>	QCAZ66082	QCAZ66082	PP536469		PP536430	PP536400
<i>Urkuphryne merinoi</i>	QCAZ66091	QCAZ66091	PP536473	PP536500	PP536433	PP536403

were originally published by Faivovich *et al.* (2005), Lehr *et al.* (2005), Heinicke *et al.* (2007, 2009, 2011), Hedges *et al.* (2008), Padial *et al.* (2008, 2009, 2012, Canedo and Haddad (2012), Catenazzi *et al.* (2015, 2017, 2020), Chaparro *et al.* (2015), Catenazzi and Tito (2016, 2018, 2019), Motta *et al.* (2016), von May *et al.* (2017), De la Riva *et al.* (2018), Reyes-Puig *et al.* (2019, 2020, 2021), and Santa-Cruz *et al.* (2019).

Accessions numbers for previously published specimens are listed by Catenazzi *et al.* (2020), Motta *et al.* (2021), and Reyes-Puig *et al.* (2021).

We imported the sequences into MESQUITE v.3.70 (Maddison and Maddison 2019). Sequences were aligned using the MUSCLE extension under default parameters (Edgar 2004) in MESQUITE. The matrix was inspected visually for alignment errors that were

adjusted manually. The aligned and concatenated matrix is available at: <https://doi.org/10.5281/zenodo.14498155>.

We partitioned the matrix by gene and codon position to find the best evolution model for each and the best partition scheme. We used the command MFP + MERGE (Chernomor *et al.* 2016, Kalyaanamoorthy *et al.* 2017) in the software IQ-TREE v.1.6.8 (Nguyen *et al.* 2015). Phylogenetic relationships were inferred for all genes (nuclear and mitochondrial) concatenated using maximum likelihood as an optimality criterion. To find the best tree, we used IQ-TREE under default settings (i.e. heuristic search algorithm to find the maximum likelihood tree, gamma distribution with four discrete categories to account for rate heterogeneity among sites, initial tree using neighbour-joining method, automatic optimizing of the parameters of the chosen evolutionary model, and estimating base frequencies). We also made 200 non-parametric bootstrap searches and 1000 searches for the approximate likelihood ratio test also in IQ-TREE (-b 200 and -alrt 1000 commands, respectively) to evaluate branch support.

Owing to its matrilineal inheritance, mitochondrial gene trees can differ from species trees as a result of introgression or incomplete lineage sorting. Therefore, species descriptions need to rely on additional independent sets of characters: genomic, phenotypic, or both. To identify potential problems in the concatenated phylogeny (which is influenced mainly by our mitochondrial genes), we carried out two additional phylogenetic analyses (nuclear and mitochondrial separately) using maximum likelihood as the optimality criterion. These analyses were inferred using an IQ-TREE webserver (Trifinopoulos *et al.* 2016) and the command TEST (Chernomor *et al.* 2016) to find the best evolution model and partition scheme. To evaluate branch support, we made 100 non-parametric bootstrap searches and 1000 searches for the approximate likelihood ratio test in IQ-TREE (-b 100 and -alrt 1000 commands, respectively). In addition, we compared the concatenated phylogeny with a phylogenetic network for *RAG1* built with SPLITSTREE v.4.19.2 (Huson and Bryant 2006) using the NeighborNet method under HKY85 distances.

Morphology

Our morphological descriptions follow the format proposed by Lynch and Duellman (1997). Terminology and definition of diagnostic characters follow Duellman and Lehr (2009). Sex was determined by gonad inspection and by the presence secondary sexual characters. Adult males were determined by the presence of vocal slits and testes morphology (i.e. active males have larger and more swollen testes; Duellman and Lehr 2009). Adult females were determined by the high convolution of the oviducts and the presence of ovarian eggs (Duellman and Lehr 2009). Descriptions of coloration in life were based on digital photographs. Measurements were taken using digital callipers (accuracy of ± 0.01 mm and rounded to the nearest 0.1 mm) and following Duellman and Lehr (2009). Holotypes were measured for the following: snout-vent length (SVL), tibia length (TL), foot length (FL; distance from proximal margin of inner metatarsal tubercle to tip of toe IV), head length (HL), head width (HW), eye diameter (ED), tympanum diameter (TD), interorbital distance (IOD), upper eyelid width (EW), internarial distance (IND), and eye-nostril distance (EN). For the paratypes, we measured SVL only. We did not measure paratypes for other

morphometric variables because in Strabomantidae, morphometric measurements, other than SVL, are of limited diagnostic utility (e.g. Páez and Ron 2019, Carrión-Olmedo and Ron 2021). Fingers and toes are numbered from inner to outer from I to IV and I to V, respectively. Lengths of toes III and V were determined by addressing both against toe IV; lengths of fingers I and II were compared when addressed midways against each other. Examined specimens (Supporting Information, Tables S1a and S1b) are stored in the herpetological collection of the Museo de Zoología, Pontificia Universidad Católica del Ecuador, Quito (QCAZ), División de Herpetología, Instituto Nacional de Biodiversidad, Quito (DHMECN), and Museo de Zoología, Universidad San Francisco de Quito, Quito (ZSFQ).

Species delimitation

In this taxonomic review, we adhere to the evolutionary species concept, which defines a species as ‘a single lineage of ancestor-descendant populations of organisms which maintains its identity from other such lineages, and which has its own evolutionary tendencies and historical fate’ (Wiley 1978). Species were delimited using integrative taxonomy criteria (Dayrat 2005, Padial and de la Riva 2010, Padial *et al.* 2010) by combining genetic and morphological evidence. To identify candidate species, we followed the protocol by Vieites *et al.* (2009) and considered confirmed candidate species those where genetic variation aligns with morphological characters of diagnostic relevance.

For genetic species delimitation within the *Noblella* northern clade, we partitioned genetic lineages using a Poisson tree processes (PTP) model (Zhang *et al.* 2013) through the bPTP web server (<http://species.h-its.org/ptp/>). The input tree was obtained from the 16S gene matrix using maximum likelihood as optimality criterion. We performed the analysis with 200 000 Markov chain Monte Carlo generations, burn-in of 0.1, a thinning of 100, and a seed of 123. To designate confirmed candidate species, we adopted a conservative approach: in cases of discordance between genetic and morphological criteria, we prioritized the delimitation method that suggested the fewest number of species.

Ancestral morphological trait reconstruction analyses

To identify morphological synapomorphies for the northern clade, we carried out ancestral character reconstructions on the best tree obtained from the DNA-based maximum likelihood search (see above). Taxon sampling focused on the northern clade and its closely related genera, *Barycholos* and *Bahius*, and on the southern clade and its closest related genera, *Psychrophrynella*, *Qosqophryne*, and *Microkayla*. For these genera, our sampling was thorough but necessarily incomplete, because character data for several species were unavailable in the literature. We excluded from the analysis distant genera outside our focal groups, such as *Phrynopus*, *Lynchius*, *Oreobates*, *Pristimantis*, *Craugastor*, *Haddadus*, *Niceforonia*, *Eleutherodactylus*, and *Bryophryne*. We analysed 17 binary discrete characters (Supporting Information, Table S2) and two continuous characters (Supporting Information, Table S3). For the binary discrete characters, we used maximum likelihood as the optimality criterion for the reconstruction. Analyses were performed using MESQUITE (Maddison and Maddison 2019) under the asymmetrical two-parameter Markov-k model.

Information on the character states for species described prior to this study was obtained from Boulenger (1898), Miranda-Ribeiro (1920), Parker (1926, 1932), Miranda-Ribeiro (1937), Cochran (1955), Lutz (1958), Griffiths (1959), Bokermann (1966), Heyer (1969, 1977), Bokermann (1975), Lynch (1975, 1976, 1986), De la Riva (1992, 2007), Köhler (2000), Aguayo-Vedia and Harvey (2001), Caramaschi and Pombal (2006), Lehr (2006), Heinicke *et al.* (2007), De la Riva *et al.* (2008a, b, 2018), Hedges *et al.* (2008), Guayasamin and Terán-Valdez (2009), Lehr and Catenazzi (2009a, b, 2010), Harvey *et al.* (2013), De la Riva and Burrows (2014), Catenazzi *et al.* (2015, 2020), Catenazzi and Tito (2016, 2018, 2019), Mamani *et al.* (2017), Reyes-Puig *et al.* (2019, 2020); Santa Cruz *et al.* (2019), Dubois *et al.* (2021), Motta *et al.* (2021), and Reyes-Puig *et al.* (2021).

Given that the expansion of finger discs (and the underlying width of the terminal expansion of the distal phalanx) is a diagnostic character differentiating frog genera (Duellman and Lehr 2009, Dubois *et al.* 2021), we also analysed the width of the terminal expansion of the distal phalanx as a continuous character using specimens from the QCAZ Museum of Zoology collection. We obtained the ratio between the expansion and the length of the distal phalanx of finger III and toe IV from X-ray images obtained using the Thermo Kevex X-ray Imaging System at the QCAZ museum, following the protocol proposed by Ron *et al.* (2020). Measurements were performed on the images using IMAGEJ2 v.1.53 software (Rueden *et al.* 2017). We measured the distal phalanx of finger III and toe IV of the right hand and foot, respectively, except when specimens had crooked digits owing to fixation problems. The ratio was obtained by dividing the expansion of the distal phalanx by the length of the distal phalanx. For the reconstruction analyses, we used parsimony as the optimality criterion using MESQUITE (Maddison and Maddison 2019) under the linear model.

Osteology and geometric morphometry

We described osteological characters for the new genus using high-resolution X-ray computed tomography (CT-scanning) images. Cranial and postcranial osteology follows the terminology proposed by Trueb (1993). Scans were made at the Department of Ecology & Evolutionary Biology of Toronto University using a Bruker SkyScan 1173 X-ray Micro-CT scanner. We followed the protocol by Ortega *et al.* (2022) for specimen manipulation during scanning, equipment setting, and the reconstruction and rendering of three-dimensional models. Scans were used to perform exploratory analyses of geometric morphometry of the skulls.

A total of 44 landmarks were placed on all the scanned skulls, mainly located at sutures, joints, protuberances, and bony angles. Landmarks followed those proposed by Ponssa and Candiotti (2012), Acevedo *et al.* (2016), and Ortega *et al.* (2022) and are as follows (Fig. 1): (1) premaxillary suture; (2) rostral end of right nasal; (3) rostral end of left nasal; (4) right lateral end of nasal; (5) left lateral end of nasal; (6) crest between frontoparietal and right prootic; (7) crest between frontoparietal and left prootic; (8) otic ramus of right squamosal; (9) otic ramus of left squamosal; (10) angle at the anterior end of quadratojugal–squamosal articulation (right side); (11) angle at the anterior end of quadratojugal–squamosal articulation (left side); (12) point between vertical and transverse branch of left

squamosal; (13) point between vertical and transverse branch of right squamosal; (14) lower rostral angle of the left orbit; (15) lower rostral angle of right orbit; (16) vertex between right ala and cultriform process of parasphenoid; (17) vertex between left ala and cultriform process of parasphenoid; (18) caudal end of left angulosplenic; (19) caudal end of right angulosplenic; (20) end of the right pterygoid medial branch; (21) end of the left pterygoid medial branch; (22) left atlanto-occipital articulation; (23) right atlanto-occipital articulation; (24) upper caudal angle of right orbit; (25) upper caudal angle of left orbit; (26) rostral angle of right maxilla; (27) rostral angle of left maxilla; (28) upper rostral angle of left orbit; (29) upper rostral angle of right orbit; (30) end of the right squamosal zygomatic ramus; (31) end of the left squamosal zygomatic ramus; (32) lateral end of the left prootic foramen; (33) medial end of the left prootic foramen; (34) lateral end of the right prootic foramen; (35) medial end of the left prootic foramen; (36) end of the right pterygoid posterior branch; (37) end of left pterygoid posterior branch; (38) midpoint of the left quadratojugal arch; (39) midpoint of the right quadratojugal arch; (40) posterior suture of the frontoparietals; (41) anterior end of the ridge formed by the right frontoparietal + right otoccipital; (42) anterior end of the ridge formed by the left frontoparietal + left otoccipital; (43) posterior end of the ridge formed by right prootic + right exoccipital; and (44) posterior end of the ridge formed by left prootic + left exoccipital. Data obtained from the landmarks were analysed using the GEOMORPH v.3.2.1 package (Adams *et al.* 2020) available in R and following the protocol proposed by Adams and Otárola-Castillo (2013) and Ortega *et al.* (2022) considering that each landmark varies in a three-dimensional space (x , y , and z).

Analyses of divergence times and biogeographical origin

To estimate divergence times among species, we used the same matrix and partitions as those for assessing phylogenetic relationships (see above), using Bayesian inference in BEAST 2 software. Estimates of divergence times were based on the node ages of the dated phylogeny from Hime *et al.* (2021). We set one calibration point at the divergence between *Ceuthomantis smaragdinus* Heinicke *et al.* 2009 and *Pristimantis* Jiménez de la Espada, 1870, corresponding to 54.4 Mya. We implemented a Yule model for speciation, with a uniform prior on the birth rate. Molecular dates were estimated using a relaxed Bayesian clock, specifically using an uncorrelated lognormal clock model with a uniform prior for the mean substitution rate. This approach was implemented under the HKY evolutionary model for all partitions. We performed a single Markov chain Monte Carlo run with a total chain length of 250 million iterations, recording every 5000th iteration and with the first 10% of the iterations as burn-in. The search included topological monophyletic constraints to mirror the maximum likelihood phylogeny, which should be more reliable because its search is less parameterized and allowed to use the best evolution model for each partition (see above). We extracted a maximum clade credibility tree using TREEANNOTATOR v.2.6.6.

All species in the ingroup live either on the western flank of the Andes (Pacific Basin) or on the eastern flank (Amazon Basin), but not both. To determine the role of the Andes as a barrier between species living in opposite flanks of the Andes,

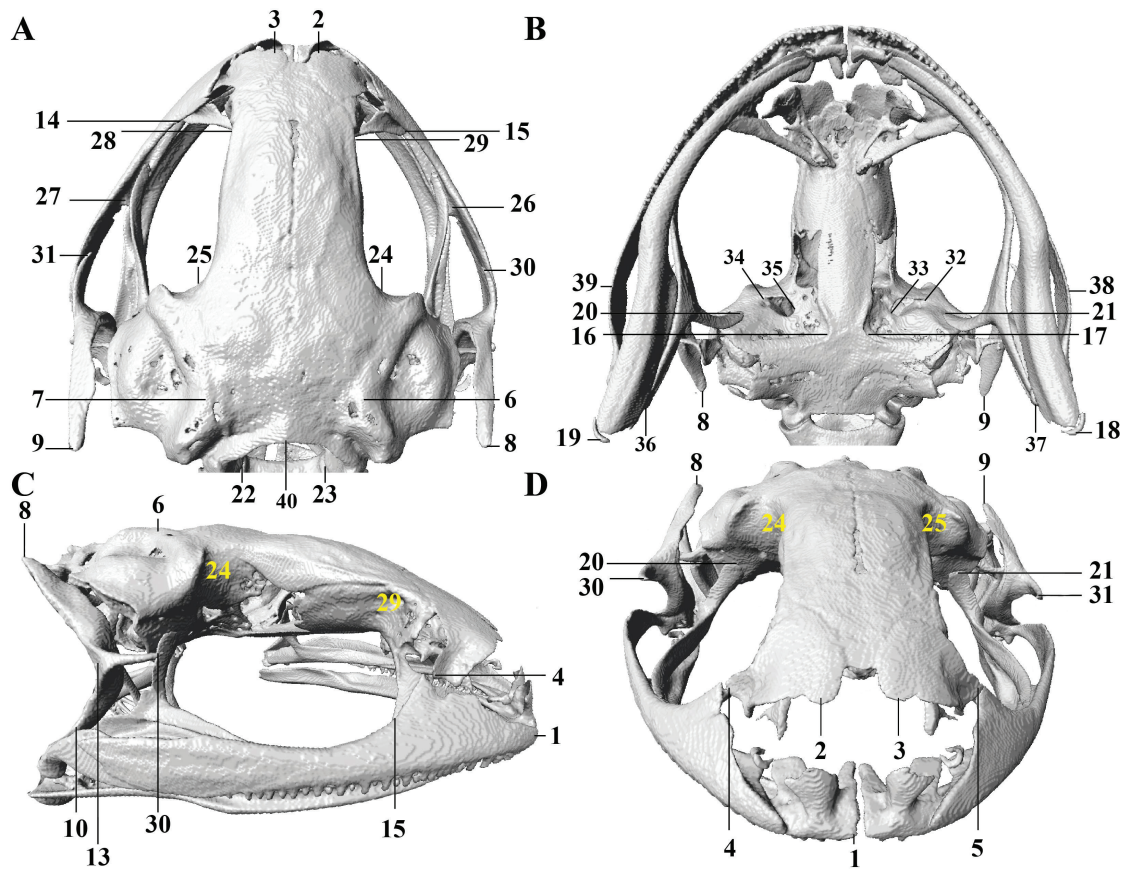


Figure 1. Landmarks for geometric morphometric analyses of skulls of *Phyllonastes* and *Urkuphryne*. The numbers show the landmarks for geometric morphometry analysis. A, dorsal view. B, ventral view. C, right lateral view (corresponding landmarks on the left side are not shown). D, frontal view. The images correspond to the holotype of *Urkuphryne merinoi* (QCAZ 66078).

we performed ancestral character reconstruction for a discrete binary character with two states: (1) cis-Andean (eastern flank, Amazon Basin); and (2) trans-Andean (western flank, Pacific Basin). Ancestral states were traced on the consensus dated phylogeny from the Bayesian inference search (see above). The reconstruction used maximum likelihood as the optimality criterion. The reconstruction was performed using MESQUITE v.3.70 (Maddison and Maddison 2019) under the asymmetrical two-parameter Markov-k model. Anfibios del Ecuador (Ron et al. 2024) and AmphibiaWeb (AmphibiaWeb 2021) databases were used to determine species distributions.

Environmental envelope and conservation status

Climatic envelope analysis is a powerful tool providing key evidence for taxonomic delimitation within integrative frameworks (Raxworthy et al. 2007, Padiál and De la Riva 2010). We made a principal component analysis of 19 bioclimatic variables (see Supporting Information, Table S4) to compare the environmental envelope of the southern and northern clades of *Noblella*. Initially, we obtained occurrence localities for all species of the northern and southern clades (see Supporting Information, Table S4). We excluded unverified records of *N. myrmecoides* from Bolivia, Brazil, and central and southern Peru, because they are distant from the type locality, and our results indicate that *N. myrmecoides* is a species complex, even among populations separated by short distances in Ecuador and northern Peru. To avoid

pseudo-replication from spatial autocorrelation, we randomly deleted localities falling at distances <10 km. The final set had 33 localities for the northern clade and 15 for the southern clade. The point sampling tool plugin in QGIS v.3.34 (QGIS.org 2023) was used to extract values for 19 bioclimatic raster maps downloaded from CHELSA (<https://chelsa-climate.org>) (Karger et al. 2021). Bioclimatic variables represent climate measurements based on temperature and precipitation, including annual averages, monthly and daily variation, and seasonality. These values were used to run a principal component analysis as implemented by the *prcomp* function in R (R Core Team 2021).

We classified the extinction risk of the newly described species based on the Red List categories under criteria by the International Union for Conservation of Nature (IUCN) (IUCN Standards and Petitions Committee 2023). Ecosystem classification follows the proposal by Ron et al. (2024).

Early development

We describe, for the first time, the early development of one species of the new genus and one species of *Phyllonastes*. One clutch of eggs of the new genus was found next to an adult female (QCAZ 66078) at Cerro Golondrinas, Carchi, Ecuador. The other clutch was obtained in captivity from a couple of *Phyllonastes personinus* (QCAZ 71452–71453) collected at Kutuku mountain range. The couple was found in amplexus *in situ*, and the clutch was laid during transport to the laboratory

facilities of the Amphibian Division of the Museum of Zoology QCAZ of the Pontificia Universidad Católica del Ecuador, in a plastic container with moistened paper towels. Both nests were incubated at room temperature (18–20°C) in humid boxes, following del Pino *et al.* (2004). To describe embryonic development, we used the staging system (TS#) for *Eleutherodactylus coqui* Thomas, 1966 by Townsend and Stewart (1985).

RESULTS

Phylogenetic analyses and species delimitation

Our concatenated phylogeny shows that *Noblella*, as defined by De la Riva *et al.* (2008b), is polyphyletic, comprising a northern clade that is more closely related to *Barycholos* than to the southern clade (Fig. 2). Both clades are strongly supported and show high support values for the relationships among species within the northern and southern clades. The northern clade is distributed in the northern Andes and western Amazonia (Ecuador and northern Peru) and is sister clade to the genus *Barycholos* Heyer, 1969. The southern clade is distributed in the Andes of southern Peru and Bolivia. It includes a mixture of species that have been identified as *Noblella* or *Psychrophrynella* Hedges *et al.*, 2008 with neither genus being monophyletic within this southern clade. The southern clade is sister to *Qosqophryne* Catenazzi *et al.*, 2020 and *Microkayla* De la Riva *et al.*, 2018. The distribution limits of both clades remain unclear; apparently, there is a geographical gap of ~1200 km separating them (Fig. 3).

The complete DNA sequence data matrix included ≤3846 bp for 170 samples. For the analyses based on the concatenated genes, the best partition scheme indicated eight partitions as the best strategy (Supporting Information, Table S5). The topology of the phylogeny and the relationships recovered (Supporting Information, Fig. S1) are generally consistent with those obtained in previous studies (Hedges *et al.* 2008, Pyron and Wiens 2011, Padial *et al.* 2014, Reyes-Puig *et al.* 2019, 2020, 2021, Portik *et al.* 2023); topological differences correspond principally to deep nodes and nodes with low support values. However, we observed inconsistencies at nodes with high support values in the phylogenies of both Motta *et al.* (2021) and Catenazzi *et al.* (2020). In the phylogeny proposed by Motta *et al.* (2021), the genus *Bryophryne* appears as sister to *Noblella* southern clade + *Psychrophrynella* + *Microkayla* and together they form the sister group to *Euparkerella* + *Holoaden* + *Bahius* + *Barycholos* + *Noblella* northern clade. That topology differs from our phylogeny, in which *Bryophryne* is basal and sister to *Noblella* northern clade + *Psychrophrynella* + *Microkayla* + *Qosqophryne* + *Euparkerella* + *Holoaden* + *Bahius* + *Barycholos* + *Noblella* southern clade, with slightly higher support than that obtained by Motta *et al.* (2021). In the phylogeny of Catenazzi *et al.* (2020), the genus *Bahius* is sister to *Noblella* northern clade, and together they are sister to *Barycholos*, unlike in our phylogeny, where *Bahius* is sister to *Noblella* northern clade + *Barycholos*.

Within the northern clade, which is the primary focus of our study, the concatenated phylogeny revealed four clades (for which we are resurrecting the genus *Phyllonastes*, see below) sister to a highly divergent lineage, which we are assigning to a new genus, *Urkuphryne*. The reasons to describe it as a new genus, instead of assigning it to extant genera, are provided in

the ‘Systematic accounts’ section. The first clade (clade A; Fig. 4) consists of a single species, *Phyllonastes cerrogolondrinus*, sister to all other species. The second clade (clade B) includes two groups: the first group comprises *Phyllonastes heyeri*, *Phyllonastes dicaprioi*, and *Phyllonastes plateadensis*, which together are sister to the second group: *Phyllonastes lochites*, *Phyllonastes myrmecoides*, *Phyllonastes macuma*, *Phyllonastes sardinayacu*, and two undescribed species. The third clade (clade C) contains *P. naturetrekii* and is sister to the fourth clade (clade D), which includes two groups: the first group is formed by *Phyllonastes personinus*, *Phyllonastes ecuadoriensis*, and *Phyllonastes coloma*, which are sister to *Phyllonastes worleyae*, *Phyllonastes mindo*, and an undescribed species (*P. sp.* QCAZ 31165). Clades C and D together are sister to clade B.

For the analyses based on the nuclear genes (i.e. *RAG1* and *TYR*) only, the best partition scheme indicated six partitions as the best strategy (Supporting Information, Table S6). The nuclear phylogeny (Supporting Information, Fig. S2) presents one incongruence with the concatenated matrix phylogeny concerning the placement of *P. heyeri* (QCAZ 31471). However, the support value for this inconsistency is low. In the nuclear phylogeny, *P. heyeri* (QCAZ 31471) is sister to a clade of species composed by *P. plateadensis* + *P. dicaprioi* + *P. sardinayacu* + *P. macuma* + *P. myrmecoides* + *P. lochites* + *P. sp.* (DHMECN 10226 and DHMECN 12012), whereas in the concatenated matrix phylogeny, this species is sister only to *P. dicaprioi* (Fig. 4), and together they form the sister clade of *P. plateadensis*. The phylogenetic network for *RAG1* (Supporting Information, Fig. S3) is consistent with the concatenated phylogeny in showing a close relationship between *P. heyeri* and *P. dicaprioi*.

For the analyses based on the mitochondrial genes only, the best partition scheme indicated two partitions (Supporting Information, Table S6). The phylogeny (Supporting Information, Fig. S4) bears one inconsistency relative to the concatenated phylogeny, regarding our study group. In the mitochondrial analysis, *P. dicaprioi* appears as paraphyletic, relative to *P. heyeri*. However, in the concatenated matrix phylogeny, *P. dicaprioi* is recovered as monophyletic and sister to *P. heyeri*. This discrepancy is likely to arise because *P. dicaprioi* specimen DHMECN 13727 lacks overlapping mitochondrial sequences with its conspecifics, DHMECN 13723 and DHMECN 13724. That issue is solved with the *RAG1* sequences, for which the three individuals overlap and form a monophyletic group (Supporting Information, Fig. S3). Inconsistencies between nuclear and mitochondrial phylogenies, for other genera, have low support values.

The species delimitation bPTP analysis recovered 18 candidate species within the northern clade (= *Urkuphryne* + *Phyllonastes*) (Fig. 4). By contrasting the results of bPTP with the morphological information (see below) and using conservative criteria, we recovered a total of 17 confirmed candidate species within the northern clade, of which eight species have already been described formally. The bPTP analysis suggests that *P. worleyae* and *P. mindo* constitute a single species. According to the species description (Reyes-Puig *et al.* 2021), they are separated by an uncorrected p-genetic distance of 1.2% for 16S, which is low for interspecies divergences in *Phyllonastes* (Supporting Information, Table S7). Morphological differences between both species are listed in Table 2.

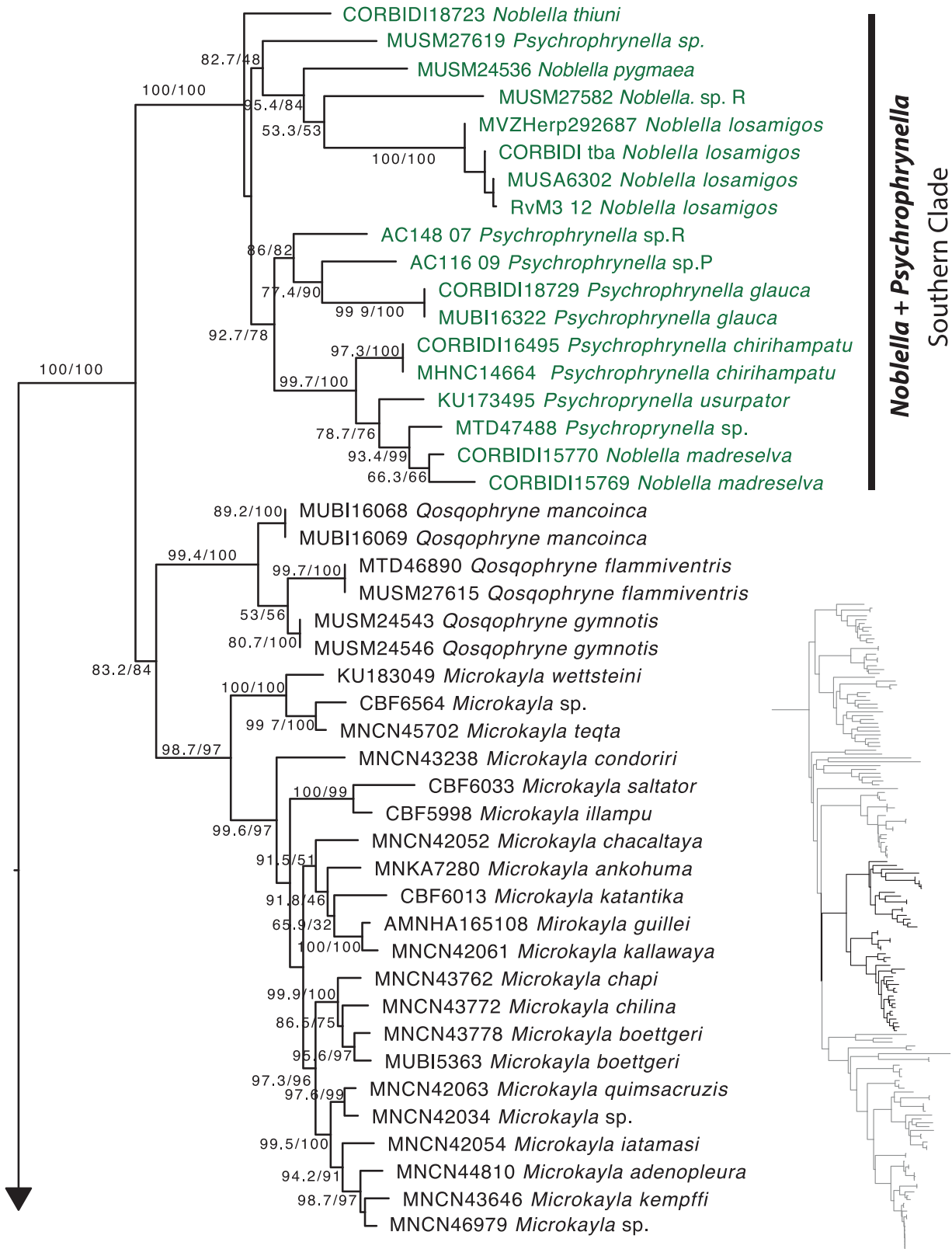


Figure 2. Phylogenetic relationships of *Noblella*. Maximum likelihood tree obtained for genes 16S, 12S, *TYR*, and *RAG1* from a matrix of 3846 bp for 170 taxa. Support values are on the corresponding branches: aLRT values before the slash and non-parametric bootstrap after the slash. For each specimen, the voucher number is shown or, in its absence, the GenBank accession number. The outgroup is not shown.

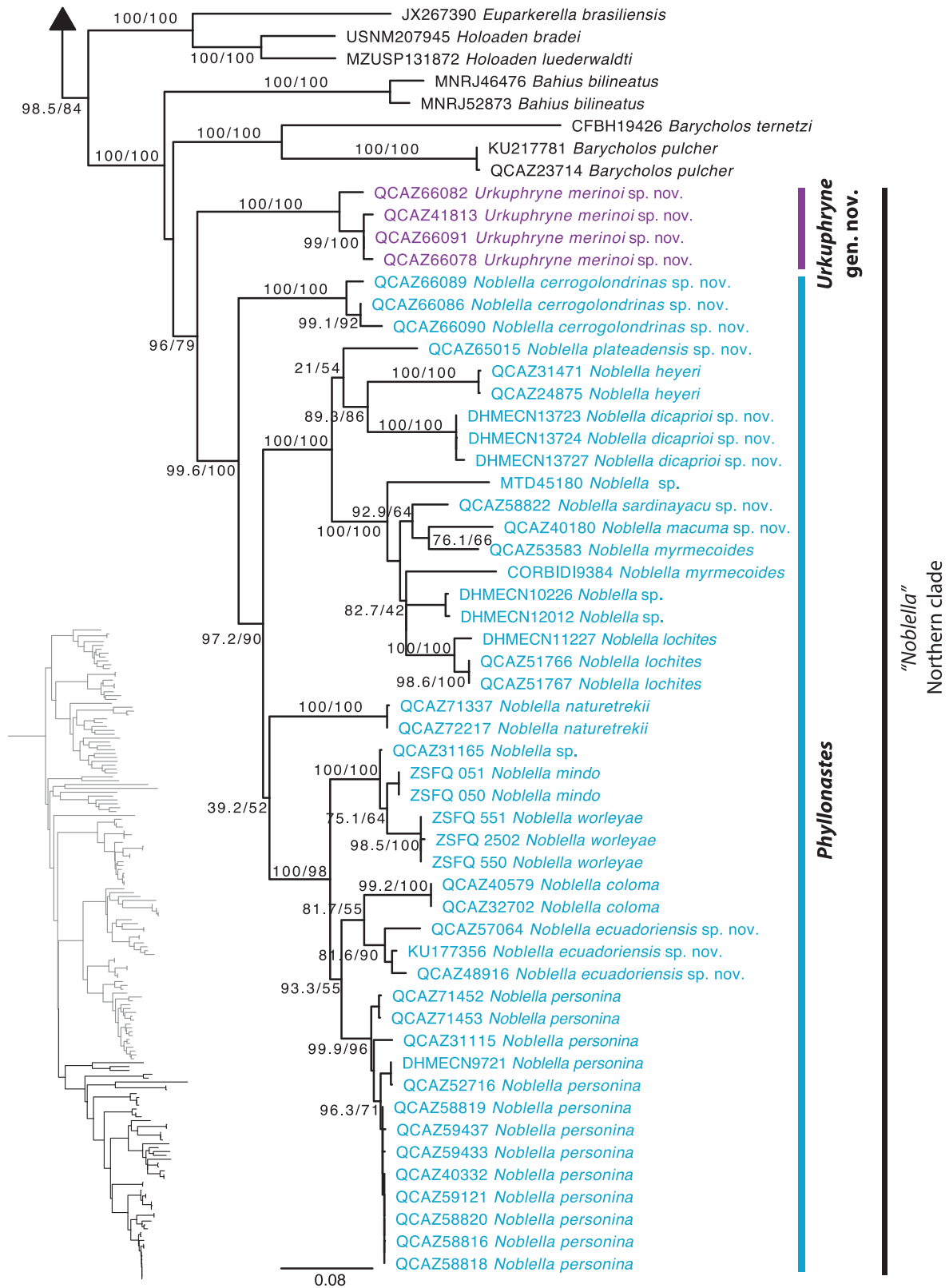


Figure 2. Continued

Geometric morphometry

Skull geometric morphometry shows a separation of specimens of *Urkuphyrne* (QCAZ 41813, QCAZ 66078 and QCAZ 66091) from those of the remaining species of the northern clade

(Fig. 5). The new genus is characterized by having lower values along principal components PC1 and PC2, which correspond to a shorter skull and a slightly broader maxilla with a broader space between angulosplenials. Within the latter, it is not possible to

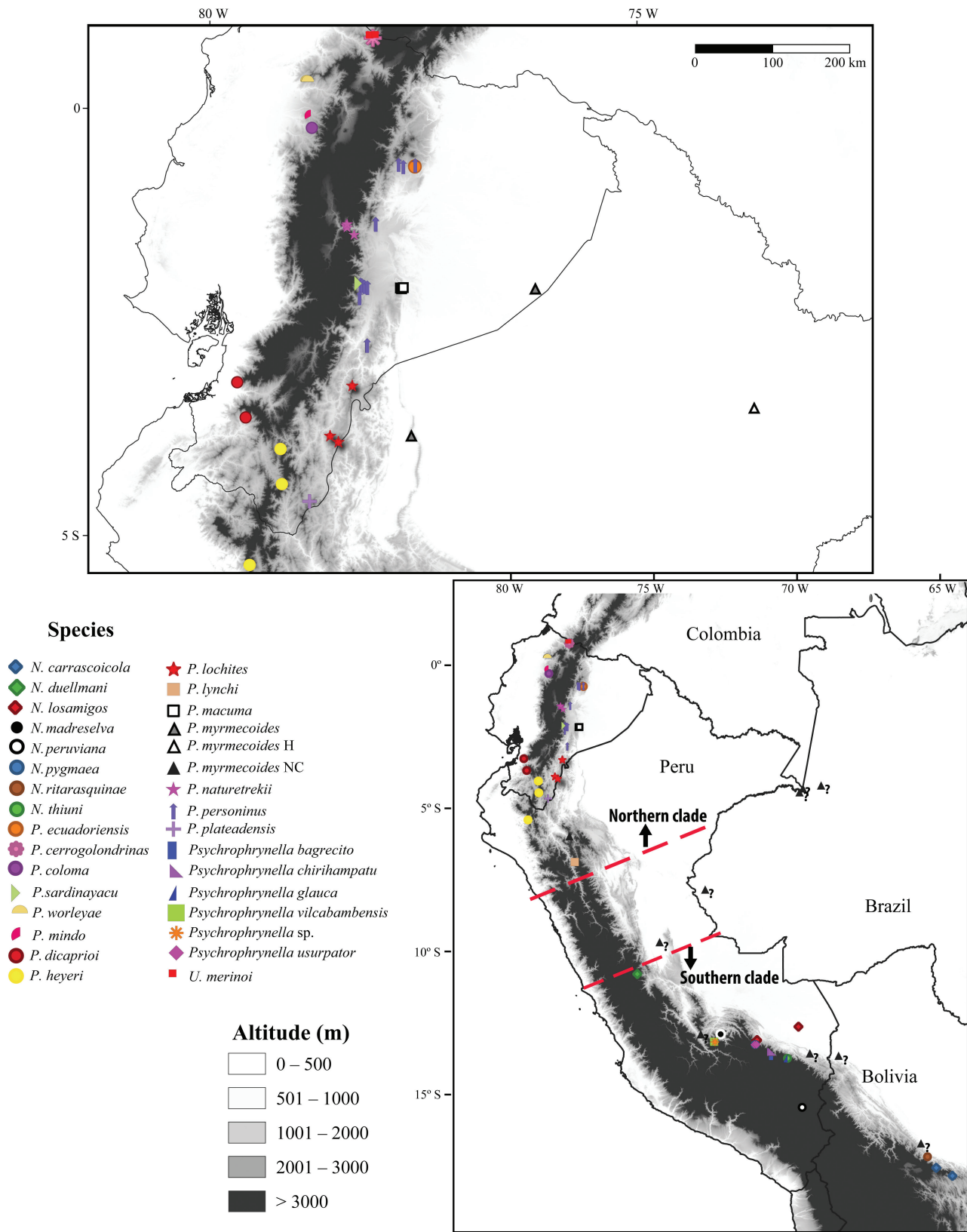


Figure 3. Collection localities of *Noblella* northern clade and southern clade species. The map shows the geographical gap between the two clades. The dashed lines indicate the southernmost boundary of the northern clade and the northernmost boundary of the southern clade. The question marks denote individuals identified as *Phyllonastes myrmecoides* whose identification has not been confirmed; their localities are not assigned to either clade owing to uncertainty regarding their true species assignment. Localities are based on specimens deposited at Museo de Zoología of Pontificia Universidad Católica del Ecuador (QCAZ), Instituto Nacional de Biodiversidad (DHMECN), Museo de Zoología of Universidad San Francisco de Quito (ZSFQ), and from Lynch (1976, 1986), Hoogmoed and Lescure (1984), Reichle et al. (2004), De la Riva et al. (2008a), Guayasamin and Terán-Valdez (2009), Lehr and Catenazzi (2009a), Harvey et al. (2013), Catenazzi et al. (2015), Catenazzi and Tito (2016, 2018, 2019), Reyes-Puig et al. (2019, 2020), Santa Cruz et al. (2019), Reyes-Puig et al. (2021), Frost (2023), and GBIF.org (2023). Abbreviations: H, holotype; NC, not confirmed.

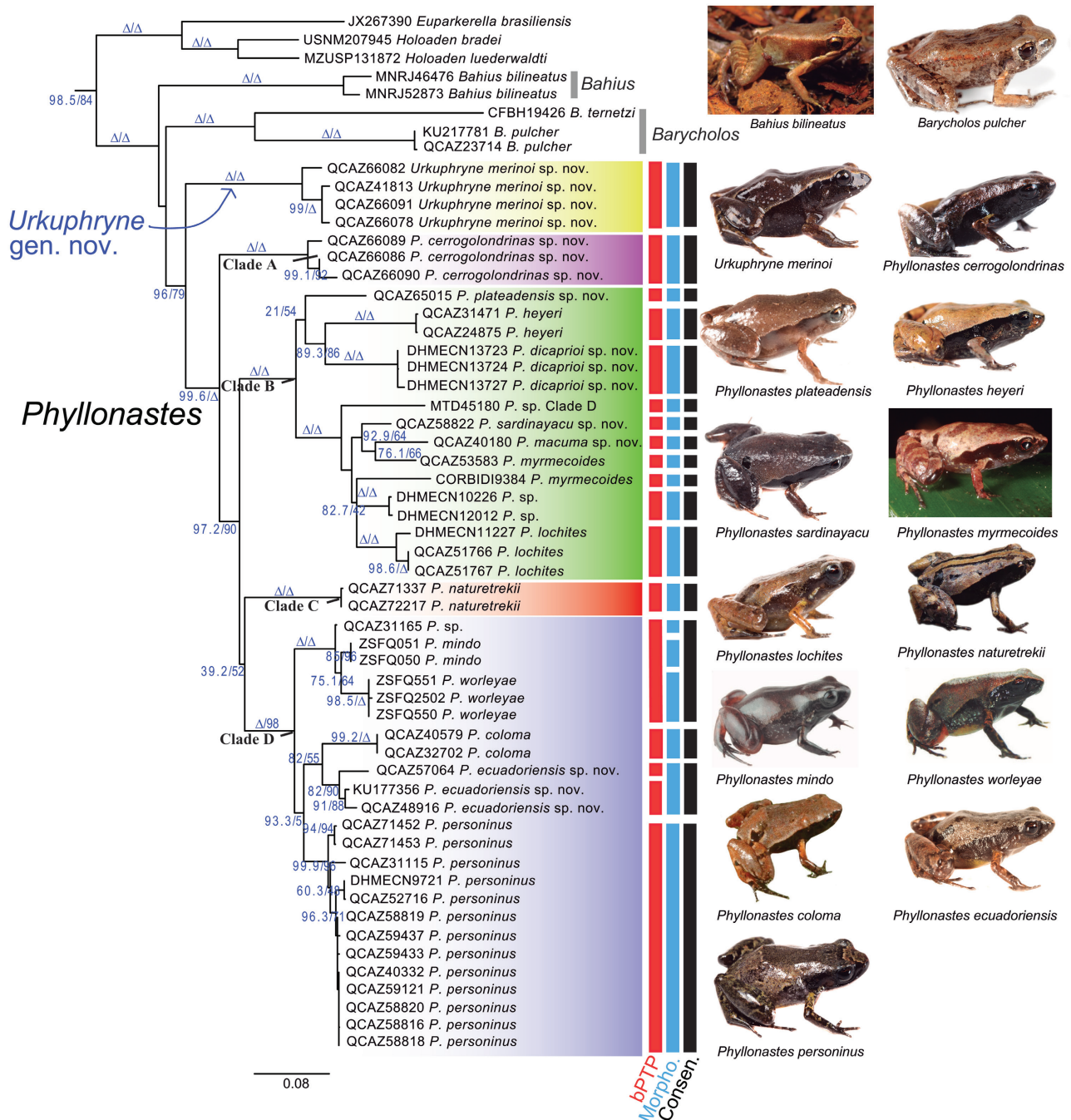


Figure 4. Phylogenetic relationships of *Phyllonastes* + *Urkuphryne* gen. nov. (= *Noblella* northern clade). Maximum likelihood tree obtained for genes 16S, 12S, *TYR* and *RAG1* from a matrix of 3846 bp for 170 terminals. Support values are on the corresponding branches: aLRT values before the slash and non-parametric bootstrap after the slash; triangles on the branches represent aLRT or bootstrap support values of 100%. For each specimen the voucher number is shown, or in its absence, the GenBank accession number. The outgroup is not shown. Black bars represent species recovered by contrasting morphological and genetic information. Red boxes represent species recovered by bPTP analysis. Abbreviations: Morpho. = Morphology; Consens. = Consensus. Photography of *Bahiush bilineatus* by Mauro Teixeira Jr. Photography of *Phyllonastes coloma* by Luis A. Coloma. Photography of *Phyllonastes mindo* by Matthijs Hollanders. Photography of *Phyllonastes myrmecoides* by Mauricio Ortega. Photography of *Phyllonastes naturetrekii* by Juan Pablo Reyes. Photography of *Phyllonastes worleyae* by David Brito.

assess differences among species owing to the small sample size of each; however, they are grouped into two clusters. The first cluster groups species part of clade B (i.e. *P. plateadensis*, *P. macuma*, *P. myrmecoides*, and *P. sardinayacu*). The second cluster groups species of clade D (i.e. *Phyllonastes ecuadoriensis*, *P. personinus*, and *P. sp.* QCAZ 31165) and *P. heyeri* (Figs 4, 5). PC1

explains 32.99% of the variance and PC2 19.79%. The landmarks that explain the most variation in PC1 are the upper caudal angle of left orbit (x -axis; inverse relationship) and the otic ramus of the right and left squamosals; in PC2 they pertain to the position of the nasal bones and the posterior end of angulosplenials (y -axis) (Fig. 5; Supporting Information, Table S8).

Table 2. General morphological characters of *Phyllonastes* and *Urkuphryne* species. Abbreviations: A, absent; Exp, expanded; I, indistinct; NExp, not expanded; P, present; SExp, slightly expanded; Und, undifferentiated; Ukn, unknown; Wdef, weakly defined. Character states are based on specimens deposited at Museo de Zoología of Pontificia Universidad Católica del Ecuador (QCAZ) and from the literature: Boulenger (1898), Miranda-Ribeiro (1920), Parker (1926, 1932), Miranda-Ribeiro (1937), Cochran (1955), Lutz (1958), Griffiths (1959), Bokermann (1966), Heyer (1969), Bokermann (1975), Lynch (1975, 1976, 1986), Heyer (1977), De la Riva (1992, 2007), Köhler (2000), Aguayo-Vedia and Harvey (2001), Caramaschi and Pombal (2006), Lehr (2006), Heinicke et al. (2007), De la Riva et al. (2008a, b, 2018), Hedges et al. (2008), Guayasamin and Terán-Valdez (2009), Lehr and Catenazzi (2009a, b, 2010), Harvey et al. (2013), De la Riva and Burrows (2014), Catenazzi et al. (2015, 2020), Catenazzi and Tito (2016, 2018, 2019), Mamani et al. (2017), Reyes-Puig et al. (2019, 2020); Santa Cruz et al. (2019), Dubois et al. (2021), Motta et al. (2021), Reyes-Puig et al. (2021).

Species	Teeth	Tympanic annulus	Tympanic membrane	Supratympanic fold	Snout dorsal	Snout lateral	Mask	Mask extension	Vocal slits	Ulnar tubercle	Inner tarsal tubercle	Inner tarsal tubercle shape
<i>P. ecuadoriensis</i>	A	P	P	P	Truncate	Round	P	Groin		A	P	Subconic
<i>P. cerrogolondrinas</i>	A	P	P	A	Truncate	Round	P	Flank half	P	A	P	Round
<i>P. coloma</i>	A	P	P	P	Round	Round	P	Groin	P	A	P	Subconic
<i>P. dicaprio</i>	A	P	Und	P	Round	Round	P	Groin	A	P or A	P	Conic
<i>P. heyeri</i>	A	P	P	P	Subacuminate	Round	P	Groin	P	A	P	Conic
<i>P. plateadensis</i>	A	P	Und	A	Broadly rounded	Round	P	Groin	Ukn	A	P	Round
<i>P. lochites</i>	A	P	P	A	Truncate	Truncate	P or A	Groin	A	A	P	Conic
<i>P. macuma</i>	A	P	P	A	Broadly rounded	Round	P	Flank half	P	A	P	Round
<i>P. mundo</i>	A	P	P	P	Round	Round	P	Groin	P	P	P	Subconic
<i>P. nyrmecoides</i>	A	P	P	A	Truncate	Round	P	Flank half	A	A	P	Conic
<i>P. naturetrekii</i>	A	Wdef	Und	A	Elongated	Round	P	Groin	P	A	P	Subconic
<i>P. personinus</i>	A	P	P	P	Round	Subtruncate	P	Flank (first third)	P	A	P	Round
<i>P. sardinayacu</i>	A	P	P	A	Round to truncate	Round	P	Groin	Ukn	A	P	Subconic
<i>P. worleyae</i>	A	P	P	P	Round	Round	P	Flank half	P	P	P	Subconic
<i>U. merinoi</i>	P	P	P	P	Round	Round	P	Groin	P	A	P	Round

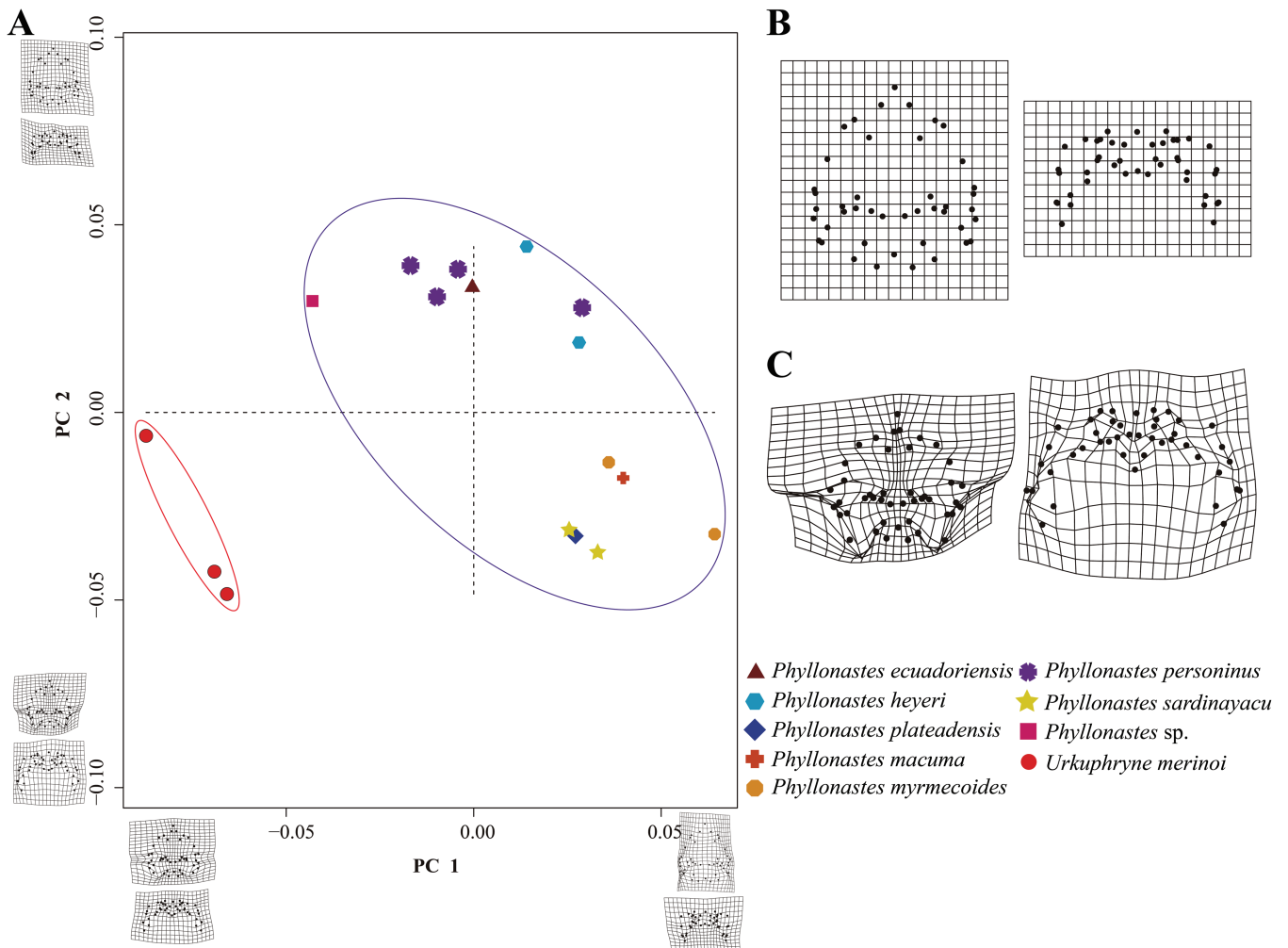


Figure 5. Geometric morphometry of skulls of *Phyllonastes* + *Urkuphryne*. **A**, principal component analysis showing the variation of skulls in the morphometric space. Principal component 1 (PC1) explains 32.99% of the variance and principal component 2 (PC2) 19.8%. **B**, morphometric plane showing the average shape of the total shapes of all skulls analysed. The diagrams show the landmarks set on the skull in dorsal and posterior views. **C**, morphometric plane showing the deformation suffered by the average plane (**B**) when plotting only the skull of *Urkuphryne*.

Divergence times and biogeographical origin

Our ancestral area reconstruction reveals that the northern clade has a trans-Andean origin, in the western Andean slopes and lowlands, Pacific Basin, of northern South America, >25 Mya (Fig. 6; Supporting Information, Fig. S5). Within the northern clade, our reconstruction supports a scenario with five colonizations from the Pacific to the Amazon Basin and none in the opposite direction. Most events took place during the Miocene, but the youngest event (colonization of the Amazon Basin by *P. ecuadoriensis*) took place during the Pliocene (>4 Mya). Although the northern clade originated in the Pacific Basin, there are more species in the Amazon Basin, suggesting a higher diversification rate. Across all the tree (northern clade, southern clade, and closely related genera), the colonization rate from Pacific to Amazon was 0.044 and only 0.003 from Amazon to Pacific. Two species from the Amazonian Basin (i.e. *P. plateadensis* and *P. ecuadoriensis*) have each sister species from the Pacific Basin (i.e. *P. dicaprio* + *P. heyeri*, and *P. coloma*, respectively) (Fig. 6). Intriguingly, *Barycholos* consists of a species from the Pacific Basin of northern

South America sister to a species from the geographically distant Atlantic Forest of Brazil.

All studied species belonging to the southern clade of *Noblella* have a *cis*-Andean distribution and a biogeographical origin in the Amazon Basin. The same is true for its sister clade (i.e. *Qosqophryne* and *Microkayla*). The southern clade of *Noblella* has a similar age to the northern clade (~25 Mya; Fig. 6).

Ancestral morphological trait reconstruction

We found five morphological synapomorphies for the northern clade, excluding *Urkuphryne* (= *Phyllonastes*) (Fig. 7): (1) absence of vomerine teeth (Supporting Information, Fig. S6); (2) subacuminate to acuminate fingertips (with two reversals) (Supporting Information, Fig. S7); (3) subacuminate to acuminate toe tips (with one reversal) (Supporting Information, Fig. S8); (4) toe distal expansion (with two reversals) (Supporting Information, Fig. S9); and (5) circumferential grooves on toes (Supporting Information, Fig. S10). Absence of vomerine teeth and the presence of acuminate toe tips are shared convergently

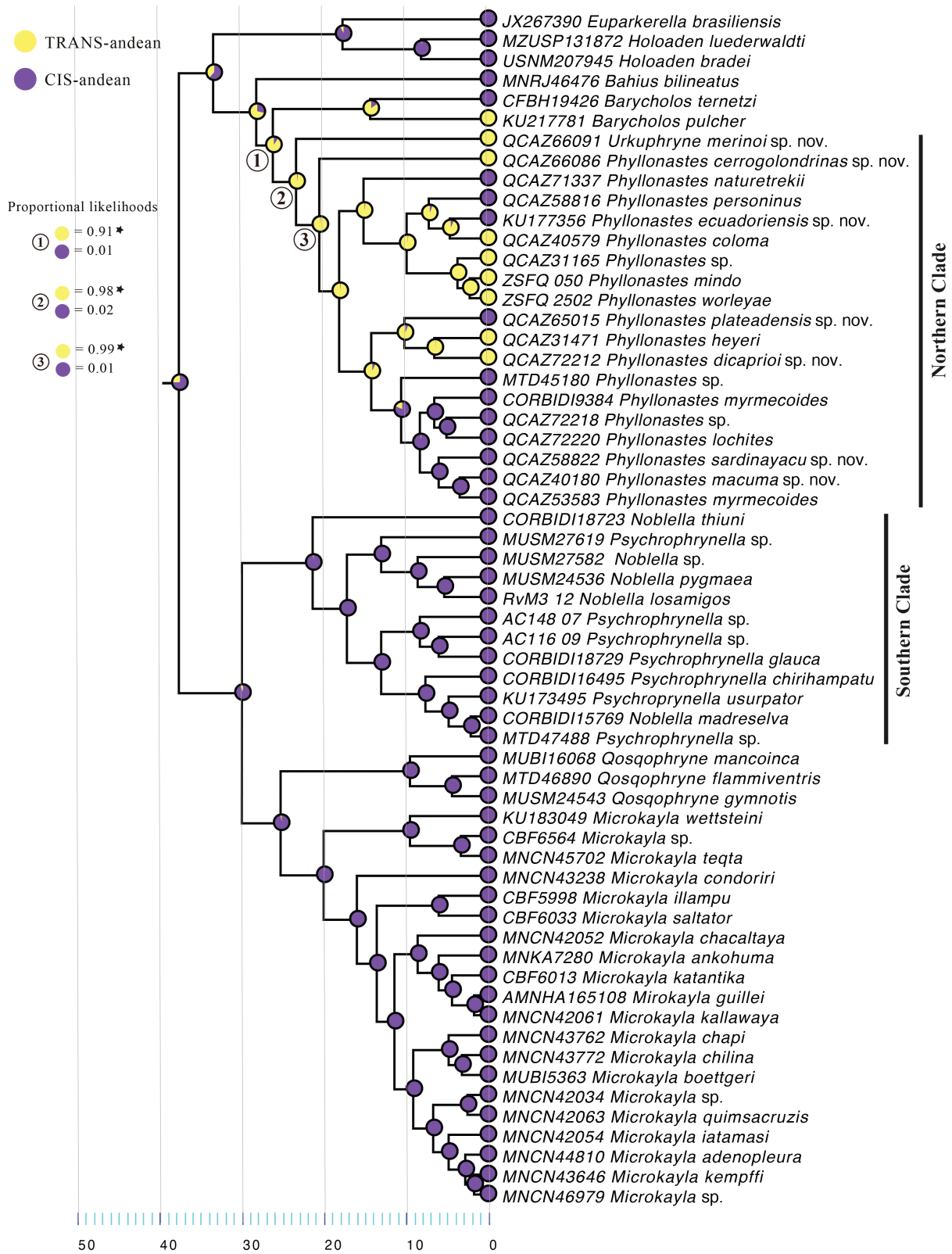


Figure 6. Chronogram and ancestral area reconstruction of *Phyllonastes*, *Noblella*, and their closest genera. Proportional likelihood values are shown for the divergence nodes of *Barycholos*, *Urkuphryne*, and *Phyllonastes*. Stars indicate statistically significant support for the most likely character state.

with the southern clade of *Noblella* (Supporting Information, Figs S6, S8). However, note that vomerine teeth are present in most closely related genera of *Phyllonastes* (*Urkuphryne*, *Barycholos*, and *Bahius*). Therefore, loss of teeth is an

evolutionary change that occurred in the most recent common ancestor of *Phyllonastes* (node 3 in Fig. 7A). Hence, absence of teeth is a synapomorphy for *Phyllonastes*. The remaining characters were symplesiomorphic or homoplastic relative to other

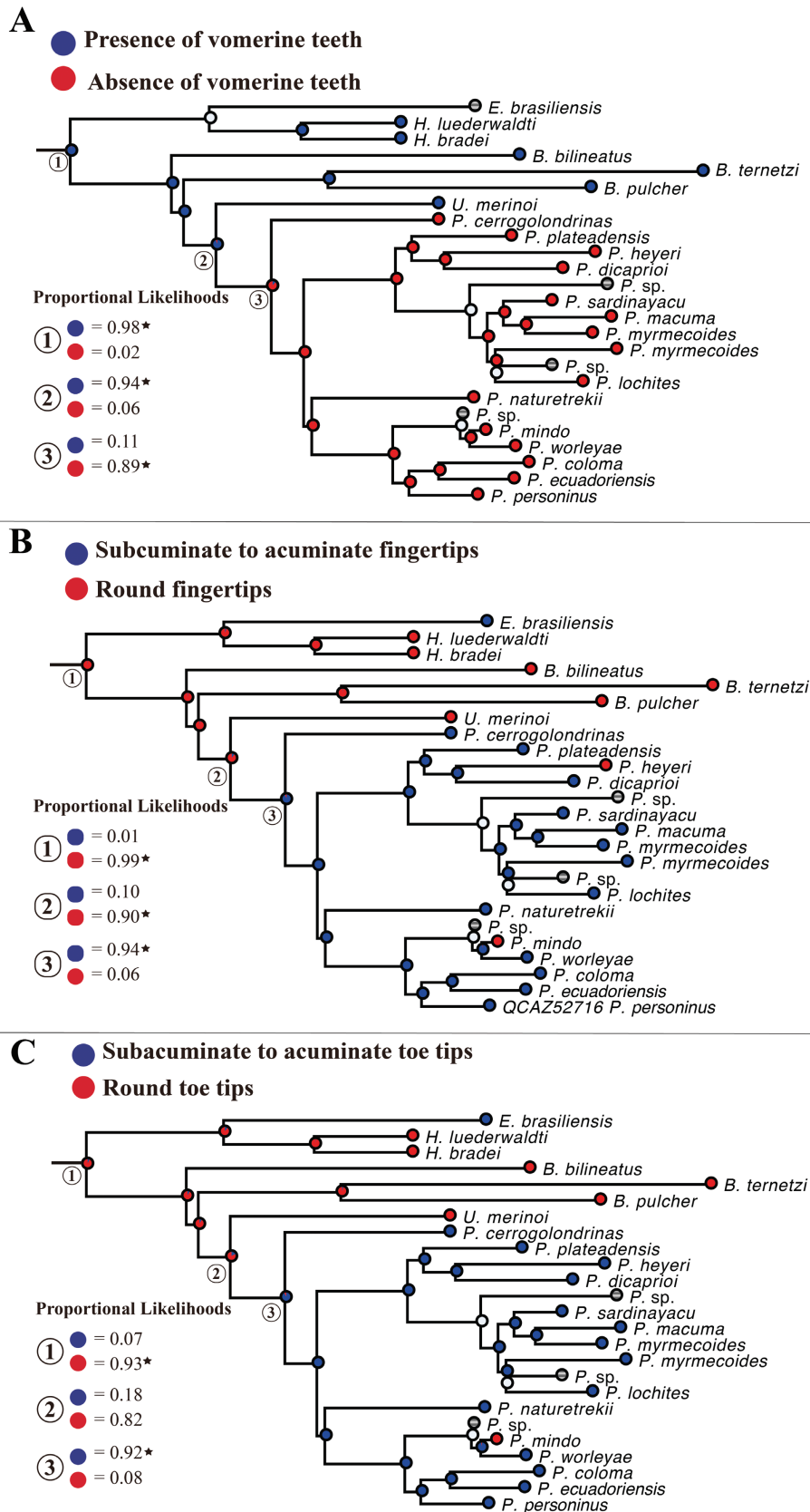


Figure 7. Ancestral trait reconstruction for discrete morphological characters for *Phyllonastes* and related genera. The five synapomorphic characters of *Phyllonastes* are shown. Stars indicate statistically significant support for the most likely character state.

Holoadeninae genera (Supporting Information, Figs S11–S20). We found two synapomorphies for the clade *Phyllonastes* + *Urku phryne* + *Barycholos* + *Bahius* Dubois *et al.*, 2021: (1) presence

of a tympanic membrane (Supporting Information, Fig. S21); and (2) presence of an inner tarsal tubercle (Supporting Information, Fig. S22).

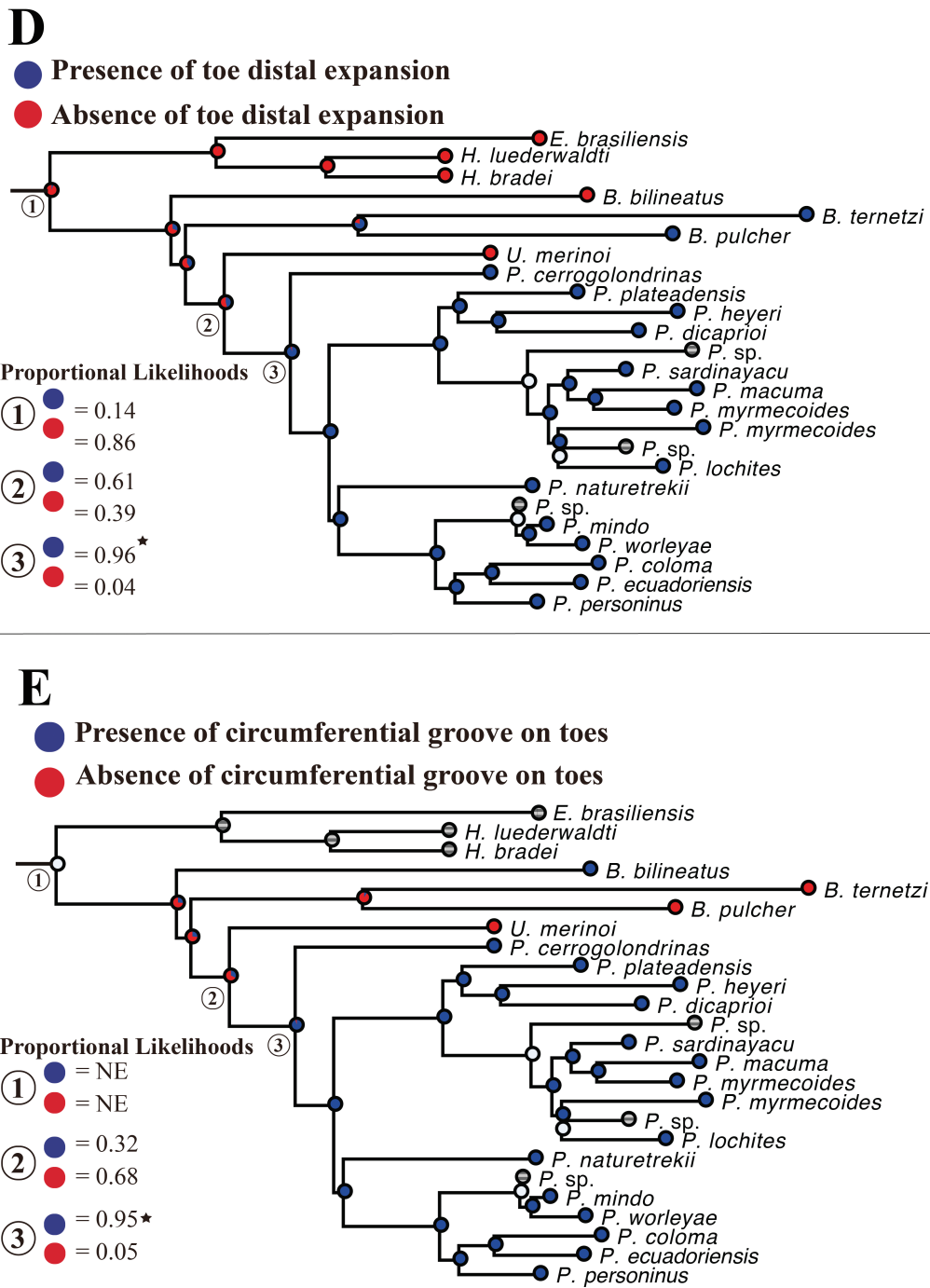


Figure 7. Continued

With respect to the terminal (T-shaped) expansion of distal phalanges, we found that the northern clade, excluding *Urkuphryne*, has expansion ratios (expansion width/phalange length) >0.63 with respect to the length of the distal phalanx in fingers and >0.52 in toes. In contrast, *Urkuphryne* (0.18–0.25 in fingers and 0.10–0.12 in toes) and *Barycholos* (0.40–0.74 in fingers and 0.34–0.47 in toes) have narrower expansions in both fingers and toes (Fig. 8).

Environmental envelope analyses

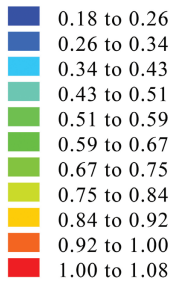
The principal component analysis on bioclimatic variables shows a partial overlap in environmental space (PC I vs. PC

II) between the northern and southern clades. Overall, species from the northern clade (genera *Urkuphryne* + *Phyllonastes*) tend to occur in warmer and drier habitats than species from the southern clade (Fig. 9; significant differences: PC I Welch's t -test = 3.067, $P = .005$; PC II Welch's t -test = 4.360, $P < .001$). *Noblella peruviana*, the type species for the genus, lies at the lower end of variation for PC I and outside the 95% confidence ellipsoid for the northern clade. *Noblella peruviana* occurs in much colder climates than the northern clade. At the type locality of *N. peruviana*, mean annual temperature is 7.8°C; at localities of the northern clade, average mean annual temperature is 17.3°C

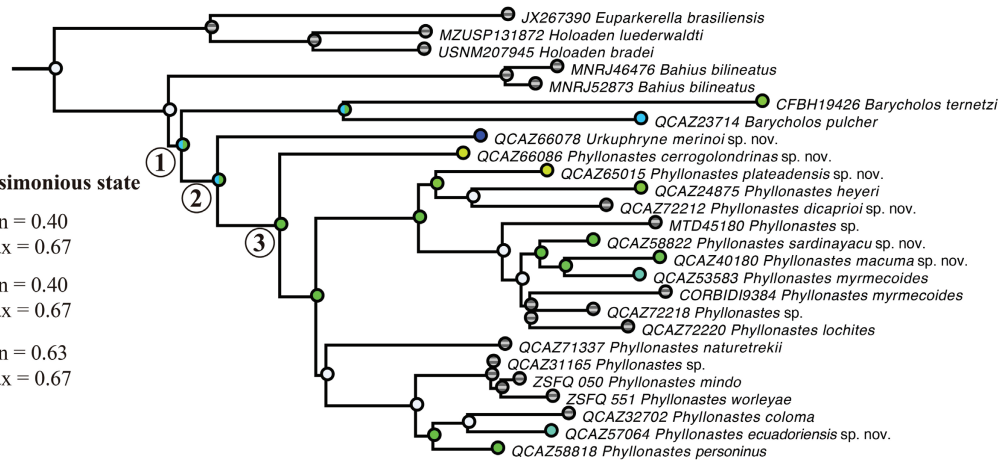
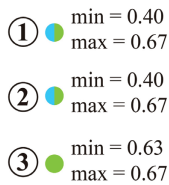
Relationship between distal phalanx expansion and distal phalanx length

Finger III

Parsimony reconstruction

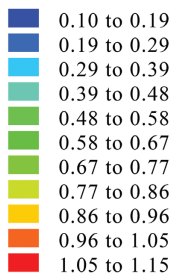


Most parsimonious state



Toe IV

Parsimony reconstruction



Most parsimonious state

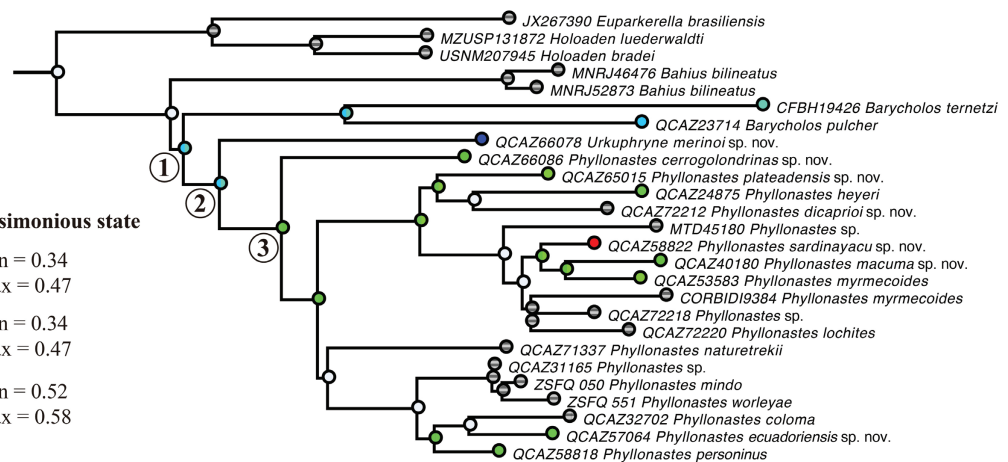
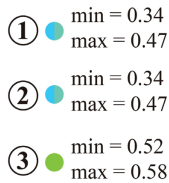


Figure 8. Ancestral trait reconstruction for the terminal expansion of distal phalanges for *Phyllonastes* and related genera. The characters analysed are the ratio between the terminal expansion and the length of the distal phalanx of the third finger and the fourth toe.

(SD = 38.4°C, range 9.8°C–25.3°C). An outlier within the southern clade is *Noblella losamigos* Santa Cruz *et al.*, 2019, the only species with one locality that occurs in lowland Amazonian rainforests.

SYSTEMATIC ACCOUNTS

The genetic, morphological, and environmental evidence presented above clearly shows that the northern clade represents a distinct evolutionary lineage, not closely related to the southern clade. To solve, in part, the polyphyly of the genus *Noblella*, we propose restricting the genus *Noblella* to the southern clade (as shown in Fig. 2). An available genus name for the northern clade is *Phyllonastes* Heyer, 1977. The type species of *Phyllonastes* is *Euparkerella myrmecoides* Lynch, 1976 (= *N. myrmecoides*), which in the phylogeny falls within the northern clade (Fig. 4). Moreover, its type locality lies within the distribution range of the northern clade (Mishana, Departamento Loreto, Peru; Fig. 3). Morphological evidence also indicates that *N. myrmecoides* belongs to the northern clade because it shares four of five diagnostic synapomorphies. Finally, *N. myrmecoides* lies within the environmental envelope of the northern clade (Fig. 9). The only

species of the southern clade occurring in hot and humid conditions is *N. losamigos*, which differs by having a supratympanic fold, a round snout in dorsal view, round fingertips, elongate inner tarsal tubercle, supernumerary plantar tubercles, mask extending to the groins, males with vocal slits, and fingers with circumferential grooves (*P. myrmecoides* lacks a supratympanic fold, supernumerary plantar tubercles, vocal slits, and circumferential grooves in fingers, and has a truncate snout in dorsal view, acuminate fingertips, conical inner tarsal tubercle, and mask extending only halfway down the flank).

The assignment of *Noblella* to the southern clade is based on: (1) location of the type locality of *Noblella*, Departamento de Puno, Peru (De la Riva *et al.* 2008b), which lies within the distribution range of the southern clade and is at ~1303 km in a straight line from the closest locality of the northern clade; (2) morphology of the type species of *Noblella*, *N. peruviana*, because it differs from species of the northern clade by lacking a tympanic membrane (according to Catenazzi and Tito 2019), circumferential grooves on toes, and toe distal expansion (Parker 1926, Lynch 1975, Hedges *et al.* 2008); and (3) environmental envelope, because *N. peruviana* is adapted to much colder habitats than any species of the northern clade and lies within climate

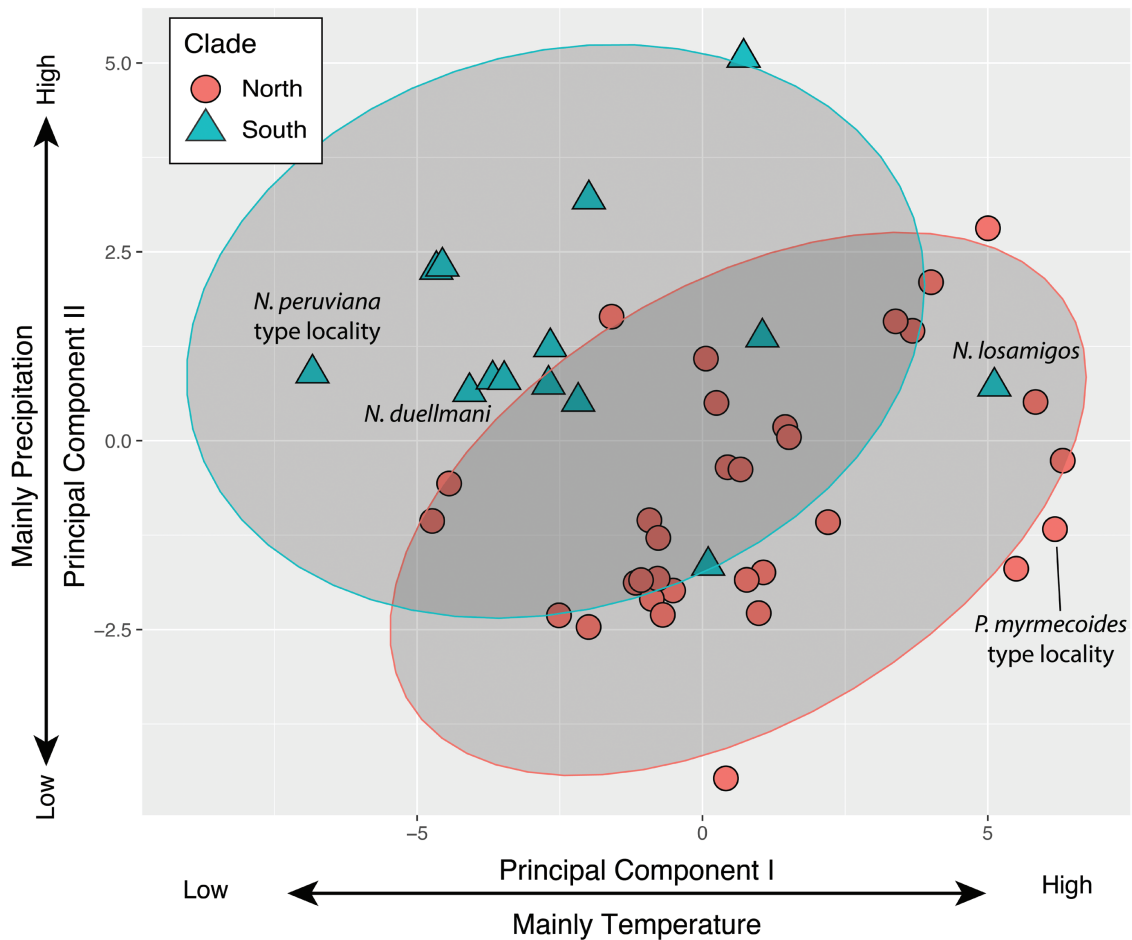


Figure 9. Principal component analysis of 19 bioclimatic variables for localities of the Northern and Southern clades of *Noblella s.l.* The ellipses are drawn at the 95% confidence level.

conditions typical for the southern clade (Fig. 9). After resurrecting *Phyllonastes*, the genus *Noblella* contains eight species [i.e. *Noblella carrascoicola*, *Noblella duellmani* (Lehr et al., 2004), *Noblella losamigos*, *Noblella madrevela* Catenazzi et al. 2015, *Noblella peruviana*, *Noblella pygmaea*, *Noblella ritarasquinae* (Köhler, 2000), and *Noblella thiuni* Catenazzi and Tito, 2019] restricted to southern Peru and Bolivia (Fig. 2). In addition to the new generic arrangement, our genetic and morphological data revealed the existence of six new species that we describe below.

We are also describing as a new genus the lineage sister to *Phyllonastes*. The reasons to describe *Urkuphryne* as a new genus (instead of assigning it to *Phyllonastes*) are in adherence to three primary taxon naming conventions described by Vences et al. (2013): (1) monophyly, which is strongly supported for *Urkuphryne* (Fig. 4), not only by molecular evidence but also by the presence of three morphological autapomorphies (see ‘Diagnosis’ sections); (2) clade stability, because a newly named genus, by definition, cannot change previous binomina; in addition, the monophyly of the closely related genera *Phyllonastes*, *Barycholos*, and *Bahius* has strong support (Fig. 4), making taxonomic instability from future topological changes unlikely; and (3) phenotypic diagnosability, because the new genus can easily be diagnosed from closely related genera by morphological diagnostic characters (see ‘Diagnosis’ sections of each genus below).

In addition, the description of the new genus is also supported by a secondary taxon naming criterion, time banding (Vences et al. 2013), because there is an old divergence time between *Urkuphryne* and its sister genus (23 Mya; Fig. 6), similar to the divergence times separating closely related genera within Terrarana (i.e. 25 Mya between *Qosqophryne* and *Microkayla*, ~18 Mya between *Euparkerella* and *Holoaden*). For all these reasons, we have opted to describe *Urkuphryne* as a new genus.

Phyllonastes Heyer, 1977

(Fig. 4)

Type species: *Euparkerella myrmecoides* Lynch, 1976, by original designation.

Definition (Tables 2 and 3): (1) Adult female average SVL < 17.5 mm, adult male < 15.6 mm, Table 4; (2) head narrower than body, wide body; (3) tympanic annulus present; (4) cranial crest absent; (5) finger I < finger II; (6) distal phalanges of fingers and toes narrowly T-shaped; (7) knees and heels without tubercles; (8) presence of inner tarsal tubercle; (9) toes bearing circumferential grooves; (10) toe V < toe III; (11) foot phalangeal formula 2-2-3-4-3; (12) dark facial mask extending at least to the middle of the flanks, triangular cloacal blotch present; (13) frontoparietals longer than wide, narrower at the anterior

Table 3. General morphological characters of *Phyllonastes* and *Urkuiphryne* species. Finger and toe characters of *Phyllonastes* and *Urkuiphryne* species. Abbreviations: A, absent; Exp, expanded; I, indistinct; NExp, not expanded; P, present; SExp, slightly expanded; Und, undifferentiated; Ukn, unknown; WDef, weakly defined. Character states are based on specimens deposited at Museo de Zoología of Pontificia Universidad Católica del Ecuador (QCAZ) and from the literature: Boulenger (1898), Miranda-Ribeiro (1920), Parker (1926, 1932), Miranda-Ribeiro (1937), Cochran (1955), Lutz (1958), Griffiths (1959), Bokermann (1966), Heyer (1969), Lynch (1975, 1976, 1986), Heyer (1977), De la Riva (1992, 2007), Köhler (2000), Aguayo-Vedia and Harvey (2001), Caramaschi and Pombal (2006), Lehr (2006), Heinicke *et al.* (2007), De la Riva *et al.* (2008a, b, 2018), Hedges *et al.* (2008), Guayasamin and Terán-Valdez (2009), Lehr and Catenazzi (2009a, b, 2010), Harvey *et al.* (2013), De la Riva and Burrows (2014), Catenazzi *et al.* (2015, 2020), Catenazzi and Tito (2016, 2018, 2019), Mamani *et al.* (2017), Reyes-Puig *et al.* (2019, 2020); Santa Cruz *et al.* (2021), Dubois *et al.* (2021), Motta *et al.* (2021), Reyes-Puig *et al.* (2021).

Species	Finger tip	Finger expansion	Finger groove	Finger papilla	Finger I < II	Supernumerary palmar tubercles	Hand phalangeal formula	Toe tip	Toe expansion	Toes groove	Papilla toe tip	Toe V < III	Supernumerary plantar tubercles
<i>P. ecuadoriensis</i>	Acuminate	SExp	A	P	P	A	2-2-3-2	Acuminate	Exp	P	P	P	P
<i>P. cerrogolondrinus</i>	Acuminate	NExp	P	A	P	P	2-2-3-2	Acuminate	SExp	P	A	P	P
<i>P. coloma</i>	Acuminate	NExp	A	A	P	P	2-2-3-3	Acuminate	NExp	P	A	P	A
<i>P. dicaprio</i>	Acuminate	NExp	A	A	P	P	2-2-3-3	Acuminate	Exp	P	A	P	A
<i>P. heyeri</i>	Round	SExp	A	A	P	P	2-2-3-3	Subacuminate	SExp	P	A	P	A
<i>P. plateadensis</i>	Subacuminate	NExp	P	A	P	P	2-2-3-3	Acuminate	SExp	P	A	P	P
<i>P. lochites</i>	Acuminate	NExp	A	A	P	P	2-2-3-2	Acuminate	SExp	P	A	P	P
<i>P. macuma</i>	Acuminate	NExp	A	A	P	P	2-2-3-3	Acuminate	Exp	P	P	P	P
<i>P. mindo</i>	Round	NExp	A	A	P	P	2-2-3-3	Round	SExp	P	A	P	A
<i>P. myrmecoides</i>	Acuminate	Exp	A	P	P	P	2-2-3-2	Acuminate	Exp	P	P	P	A
<i>P. naturetrekii</i>	Acuminate	NExp	A	A	P	A	2-2-3-2	Acuminate	SExp	P	A	P	A
<i>P. personinus</i>	Acuminate	NExp	I	A	P	P	2-2-3-3	Acuminate	SExp	P	A	P	A
<i>P. sardimayacu</i>	Subacuminate	NExp	A	A	P	P	2-2-3-3	Acuminate	SExp	P	A	P	P
<i>P. worleyae</i>	Subacuminate/ acuminate	NExp	A	A	P	P	2-2-3-3	Acuminate	SExp	P	A	P	P
<i>U. merinoi</i>	Round to broadly rounded	NExp	A	A	P	P	2-2-3-3	Round	NExp	A	A	P	A

end; (14) premaxillary and maxillary teeth present; (15) nasal bones small, separate from maxilla; (16) zygomatic branch of squamosal much shorter than otic branch; (17) vomers reduced, broadly separated from each other, vomerine teeth absent; (18) occipital condyles widely separated from each other; (19) medial ridges present at least on presacral vertebrae III–IV; (20) urostyle crest very prominent; (21) expanded to broadly expanded sacral diapophyses; and (22) small prepollex and prehallux present.

Content (15 species): *Phyllonastes cerrogolondrinus*, *Phyllonastes coloma* (Guayasamin & Terán-Valdez, 2009) comb. nov., *Phyllonastes ecuadoriensis*, *Phyllonastes dicaprioi*, *Phyllonastes heyeri* Lynch, 1986, *Phyllonastes lynchi* Duellman, 1991, *Phyllonastes lochites* (Lynch, 1976), *Phyllonastes mindo* (Reyes-Puig et al., 2021) comb. nov., *Phyllonastes macuma*, *Phyllonastes myrmecoides* (Lynch, 1976); *Phyllonastes naturetrekii* (Reyes-Puig et al., 2019) comb. nov., *Phyllonastes personinus* (Harvey et al., 2013) comb. nov., *Phyllonastes plateadensis*, *Phyllonastes sardinayacu*, and *Phyllonastes worleyae* (Reyes-Puig et al., 2020) comb. nov.

Distribution: Pacific foothills and western slopes of the Andes of Ecuador, in Western Foothill Forest and Western Montane Forest between 1100 and 2554 m a.s.l.; on the western Amazon Basin, eastern Andean slopes of Ecuador, in Eastern Montane Forest, Eastern Foothill Forest ≤ 2400 m a.s.l. in Ecuador and Amazonian Tropical Rainforest from southeastern Colombia to northern and central Peru, and northwestern Brazil, ≥ 90 m a.s.l. (Fig. 3).

Remarks: The specific epithet *personina* is replaced by the specific epithet *personinus* to match the masculine gender of the genus *Phyllonastes*. Thus, *Noblella personina* becomes *Phyllonastes personinus*. In the new specific epithet, the root *person-* is maintained, and the diminutive suffix *-ina* is replaced by the Latin suffix *-us*. We include *P. lynchi* in the genus *Phyllonastes* because it has the synapomorphies of the group: (1) absence of vomerine teeth; (2) subacuminate toe tips; (3) toes distally expanded; and (4) presence of circumferential grooves in toes (Duellman 1991). Additionally, it presents characteristics more frequently found within the northern clade: (1) presence of tympanic membrane; and (2) presence of inner tarsal tubercle. In addition, its distribution range is closer to the northern clade (Fig. 3). It is ~218 km in a straight line from the confirmed record of *P. lynchi* to the nearest confirmed record of the northern clade (*P. heyeri*) and ~490 km to the nearest record of the southern clade (*N. duellmani*).

***Phyllonastes cerrogolondrinus* sp. nov.**

LSID: urn:lsid:zoobank.org:act:2E34387F-A763-4337-87AF-BE7843D1DCEA

Holotype (Figs 10, 11): QCAZ 66090 (field no. SC-PUCE 48711) adult male from Ecuador, Carchi Province, Canton Espejo, El Goaltal Parish, Bosque Protector Cerro Golondrin, trail to Santa Blanca (0.8224°N, 78.0923°W), 2554 m. Collected by Diego Almeida, Kunam Nusirquia, Darwin Núñez, Fernando Ayala, David Mantilla, Santiago Recalde, Carlos Castro, Polibio Malte, and Josué Quintanchala on 14 December 2016.

Paratypes (N = 4; Fig. 10): Same locality and collectors as holotype, QCAZ 66086–87 adult females; QCAZ 66088 juvenile; QCAZ 66089 adult male. Collected on 12 and 14 December 2016.

Proposed standard English name: Golondrin leaf litter frog.

Proposed standard Spanish name: Cutín de Hojarasca de Golondrin.

Definition (Figs 10, 11; Tables 2 and 3): We assign the new species to the genus *Phyllonastes* based on its phylogenetic relationships. The new species is characterized by: (1) dorsal skin smooth to finely shagreen, dorsolateral folds absent, ventral surfaces weakly areolate, flanks finely shagreen, discoidal fold present; (2) tympanic membrane and tympanic annulus defined, supratympanic fold and postrectal tubercle absent; (3) snout truncate in dorsal view, round in profile; (4) upper eyelid without tubercles, cranial crests absent; (5) vomerine teeth absent; (6) vocal slits present, nuptial pads absent; (7) fingers not expanded distally, with fingertips acuminate lacking papillae, finger I shorter than finger II, supernumerary tubercles present; (8) fingers bearing broad lateral fringes and ill-defined circumferential grooves; (9) distal phalanges blunt or T-shaped, phalangeal formula of hand 2-2-3-2; (10) ulnar tubercles absent; (11) knees and heels without tubercles, outer edge of tarsus without tubercles, inner edge of tarsus bearing one rounded tubercle; (12) inner metatarsal tubercle elongate in ventral view and flat in lateral view, bigger than rounded outer metatarsal tubercle; (13) toes slightly expanded distally, with acuminate toe tips and lacking papillae, supernumerary tubercles well defined, toes with narrow lateral fringes, toe basal webbing present, all toes bearing ill-defined circumferential grooves, toe V shorter than toe III; (14) in life, dorsum light brown, with darker tubercles and a darker hourglass-shaped blotch, circular dark brown sacral lateral patches, facial mask dark brown extending from the tip of snout to the midflank, ventral surfaces bearing irregular white flecks, distal half of shanks and heels bearing yellowish brown spots; and (15) SVL in adult males 11.53 mm (N = 2) and SVL in adult females 13.65 mm (N = 2) (Table 4).

Diagnosis: *Phyllonastes cerrogolondrinus* resembles the other *Phyllonastes* species from the western foothills of Ecuadorian Andes: *P. coloma*, *P. dicaprioi*, *P. mindo*, and *P. worleyae* by having tympanic annulus, supernumerary palmar tubercles, fingers not expanded distally, and circumferential grooves on toes. It differs from all of them by having a dark brown belly with irregular white flecks, in life (belly bright orange in *P. coloma*, brown with brown marks in *P. dicaprioi*, yellowish cream in *P. mindo* and yellowish cream with minute speckling in *P. worleyae*), truncate snout in dorsal view (snout rounded in *P. coloma*, *P. dicaprioi*, *P. mindo*, and *P. worleyae*), and rounded tarsal tubercle (subconic tarsal tubercle in *P. coloma*, *P. mindo*, and *P. worleyae*, and conical tarsal tubercle in *P. dicaprioi*). *Phyllonastes cerrogolondrinus* also differs from *P. coloma* by the presence of supernumerary plantar tubercles (supernumerary plantar tubercles absent in *P. coloma*) and circumferential grooves in fingers (fingers without circumferential grooves in *P. coloma*). *Phyllonastes cerrogolondrinus* can also be distinguished



Figure 10. Live and preserved specimens of *Phyllonastes cerrogolondrinus*. Lateral, dorsal, and ventral views of: A, B, holotype QCAZ 66090, adult male, SVL = 10.89 mm; C, paratype QCAZ 66087, adult female, SVL = 13.75 mm; and D, paratype QCAZ 66089, adult male, SVL = 12.17 mm. A, in life. B–D, in preservative. Scale bars are given only for preserved adults. The depigmentation visible in the specimens is attributable to preservation defects.

from *P. dicaprioi* by the presence of vocal slits in males (males without vocal slits in *P. dicaprioi*) and by the presence of supernumerary plantar tubercles (supernumerary plantar tubercles absent in *P. dicaprioi*). It also differs from *P. mindo* and *P. worleyae* by having weakly areolate ventral surfaces (ventral surfaces smooth in *P. mindo* and *P. worleyae*), acuminate toe tips (toe tips rounded in *P. mindo* and *P. worleyae*), circumferential grooves in fingers (fingers lacking circumferential grooves in *P. mindo* and *P. worleyae*), and by the absence of a supratympanic fold and ulnar tubercles (both present in *P. mindo* and *P. worleyae*). For a comparison with other *Phyllonastes* species that are more phylogenetically distant, see [Tables 2](#) and [3](#).

Description of the holotype (Figs 10, 11): Adult male (QCAZ 66090). Measurements (in millimetres): SVL, 10.89; tibia length, 6.07; foot length, 5.91; head length, 3.36; head width, 3.64; eye diameter, 1.32; tympanum diameter, 0.48; interorbital

distance, 1.93; upper eyelid width, 1.31; internarial distance, 1.38; eye–nostril distance, 0.76.

Body robust, head slightly wider than long, narrower than body; snout truncate in dorsal view, short and rounded in lateral profile, without rostral papilla; canthus rostralis straight in dorsal view; loreal region slightly concave; eyelids without tubercles; interorbital space flat, with no cranial crests; tympanic membrane and annulus distinct (more conspicuous in its anterior half), without supratympanic fold; postrictal tubercles absent; vomerine teeth absent, vocal slits present; and nuptial pads absent.

Skin on dorsum and flanks finely shagreen; dorsolateral folds absent; ventral surfaces weakly areolate; skin in cloacal region areolate; discoidal fold present. Ulnar tubercles absent, palmar tubercles low, outer palmar tubercle circular, larger than elongate thenar tubercle; subarticular tubercles well defined, round in ventral and lateral view; well-defined rounded supernumerary

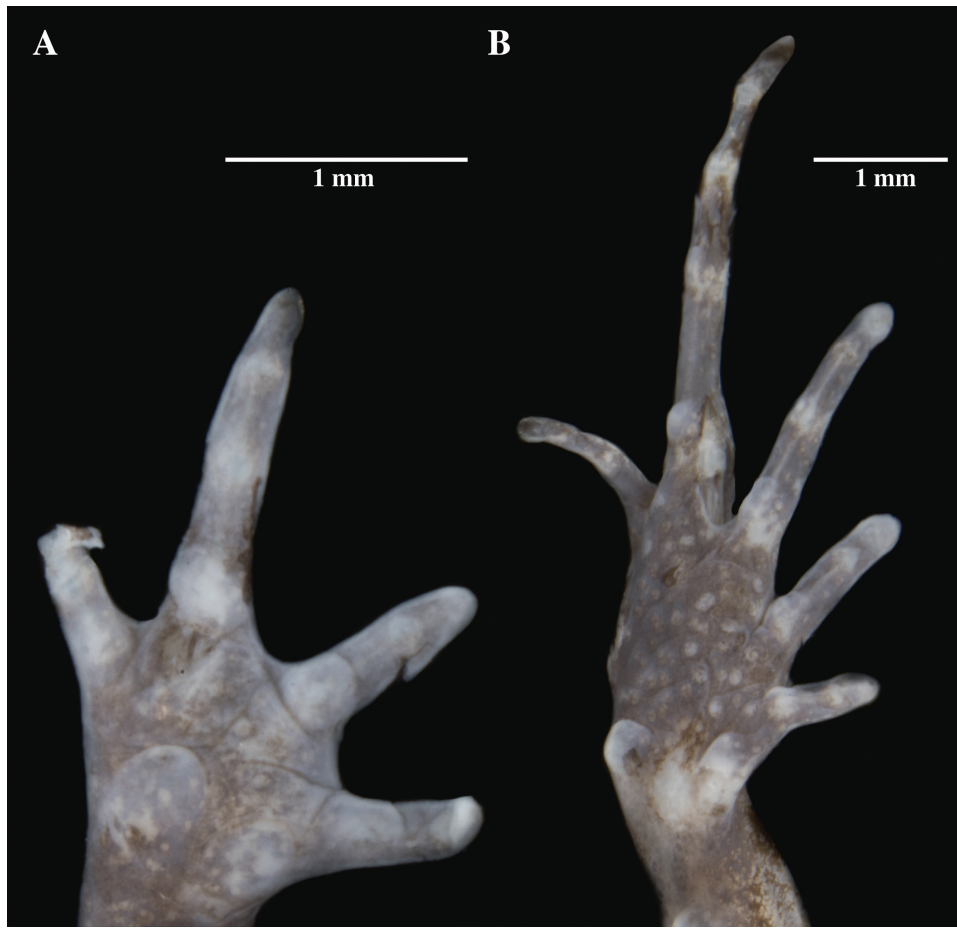


Figure 11. Palmar (A) and plantar (B) surfaces of *Phyllonastes cerrogolondrinus*. Photographs of right hand and right foot of the holotype QCAZ 66090. Finger IV of the hand shows some raised skin at the terminal end.

Table 4. Snout–vent length (SVL; in millimetres) and SD (in parentheses) for adult females and males. of *Phyllonastes* and *Urkuphryne* new species. The number of individuals is given in parentheses after the sex. For each group, minimum (Min) and maximum (Max) values are also shown.

Species	Sex	SVL average	SVL Min	SVL Max
<i>P. cerrogolondrinus</i>	Female (2)	13.7	13.6	13.8
<i>P. cerrogolondrinus</i>	Male (2)	11.5	10.9	12.2
<i>P. ecuadoriensis</i>	Female (2)	17.4	16.6	18.1
<i>P. ecuadoriensis</i>	Males (2)	14.2	13.6	14.8
<i>P. dicaprio</i>	Female (1)	15.2		
<i>P. dicaprio</i>	Male (6)	12.2 (1.7)	10.6	14.6
<i>P. macuma</i>	Female (1)	14.5		
<i>P. macuma</i>	Male (1)	11.9		
<i>P. plateadensis</i>	Female (1)	15.7		
<i>P. sardinayacu</i>	Female (2)	14.2	14.1	14.3
<i>U. merinoi</i>	Female (5)	19.7 (0.3)	19.4	20.1
<i>U. merinoi</i>	Male (3)	17.2 (1.8)	15.2	18.7

tubercles; broad dermal fringes on fingers, fingers not expanded distally, discs narrow, bearing round and inconspicuous pads, with an ill-defined circumferential groove; fingertips acuminate, without papillae; relative lengths of fingers is I < II < IV < III; phalangeal formula of hand is 2-2-3-2.

Hindlimbs robust; knee and heel without tubercles; tarsal folds (inner and outer) absent, outer tarsal tubercles absent; inner tarsal tubercle present, prominent and round; inner metatarsal tubercle present, elongate in ventral view and flat in lateral profile; well-defined, prominent and round outer metatarsal

tubercle; plantar surface with several rounded and conspicuous supernumerary tubercles; round subarticular tubercles ill defined, more conspicuous at the base of toes; toes slightly expanded distally, toes with narrow lateral fringes; basal webbing between toes; discs on toes ill defined, narrow, with acuminate tip, without papilla; ill-defined circumferential grooves; relative lengths of toes $I < II < V < III < IV$; toe III longer than toe V (toe III reaches the distal border of the second subarticular tubercle of toe IV; Toe V almost reaches half of the second tubercle of toe IV).

Colour of holotype in life (based on digital photographs) (Fig. 10): Dorsal surface light brown, with darker, scattered, and low tubercles and a darker hourglass-shaped blotch extending from the interorbital to the sacral region; circular dark brown sacral lateral patches well defined. Facial mask dark brown extending from the tip of snout to the midflank and delineated along its upper edge by a light brown line. Lips dark brown with irregular white flecks. Cloacal region dark brown surrounded by a paler stripe. Flanks light brown posteriorly and with the extension of the facial mask anteriorly. Upper arm dorsal surfaces yellowish brown, elbow and forearm light brown, becoming darker towards the hand. Dorsal surfaces of thighs and proximal half of shanks light brown; distal half of shanks and tarsus yellowish brown; dorsal surface of tarsus dark brown. Ventral surfaces of throat, chest, forearms, belly, and thighs dark brown (almost black) bearing irregular white flecks in greater quantity on the belly. Ventral surfaces of upper arms and distal half of shanks reddish brown. Distal half of shanks and heels bearing yellowish brown spots.

Colour of holotype in preservative (Fig. 10): Dorsal surface from the scapular region to the tip of snout dark brown, bearing cream blotches that become smaller and less abundant towards the snout. Dorsum cream from the scapular region to the vent. Dorsal surfaces of forearms, hands, thighs, and feet dark brown. Dorsal upper arms and shanks cream. Ventral surfaces dark brown; upper arms and shanks cream. Belly and ventral surfaces of thighs bearing cream irregular blotches. Cloacal region dark brown with a medial cream longitudinal stripe.

Variation (Fig. 10): In this section, traits refer to preserved individuals unless otherwise mentioned. Tympanic annulus can be differentiated beneath skin only anteriorly (e.g. QCAZ 66087) or be inconspicuous (i.e. QCAZ 66088–89); dorsal skin might be smooth (e.g. QCAZ 66087) or finely shagreen (e.g. QCAZ 66086); outer palmar tubercle can be elongate (e.g. QCAZ 66087). Snout is subacuminate in the only subadult male (QCAZ 66088). Dorsum might be completely dark brown (e.g. QCAZ 66087), dark brown bearing some cream blotches (e.g. QCAZ 66086), or cream with a dark brown snout (QCAZ 66088). Colour variation is shown in [Figure 10](#). Morphometric variation is detailed in [Table 4](#).

Distribution, natural history, and conservation status (Fig. 3): *Phyllonastes cerrogolondrinus* is known from the surroundings of Cerro Golondrinas Protective Forest from 2469 to 2554 m a.s.l. All individuals were collected in Eastern Montane Forest (1300–3600 m a.s.l.) at night, between 20:00 and 22:00 h. They were found on leaf litter near streams. Collections were made in

secondary *terra firme* forest. Because of the lack of information on population size and geographical range, we suggest assigning *P. cerrogolondrinus* to the Data Deficient Red List Category (based on [IUCN Standards and Petitions Committee 2023](#)); nevertheless, its presence in secondary forest suggests adaptability to anthropically modified environments.

Etymology: The specific epithet is a toponym in apposition, and it refers to the type locality. The Cerro Golondrinas Protective Forest is 1500 ha and is located within the Chocó Biogeographical Region in the province of Carchi, Ecuador. It is part of the Biological Corridor Chiles–Mataje. The Cerro Golondrinas Protective Forest is an important habitat for flora and fauna, with unique characteristics of richness and endemism. The forest is protected by the NGO Ecominga. *Phyllonastes cerrogolondrinus* is also a posthumous tribute to Jaime Levi, a naturalist who promoted the creation of the Cerro Golondrinas Protective Forest. This species name was chosen with the inhabitants of the communities of La Plata, Morán, and Golondrinas (Carchi Province) in an outreach effort to empower local communities in favour of environmental education and conservation.

Phyllonastes ecuadoriensis sp. nov.

LSID: urn:lsid:zoobank.org:act:2F984FAA-F04B-4623-9E30-7E29E32D659D

- Noblella lochites*—[Hedges et al. \(2008\)](#).
- Noblella lochites*—[Padial et al. \(2014\)](#).
- Noblella lochites*—[Catenazzi and Tito \(2016\)](#).
- Noblella lochites*—[Reyes-Puig et al. \(2019\)](#).
- Noblella lochites*—[Santa-Cruz et al. \(2019\)](#).
- Noblella lochites*—[Condori et al. \(2020\)](#).
- Noblella lochites*—[Reyes-Puig et al. \(2020\)](#).
- Noblella lochites*—[Catenazzi et al. \(2020\)](#).
- Noblella lochites*—[Motta et al. \(2021\)](#).
- Noblella lochites*—[Reyes-Puig et al. \(2021\)](#).
- Noblella lochites*—[Portik et al. \(2023\)](#).

Holotype (Figs 12, 13, 14A, 15A): QCAZ 57064 (field no. SC-PUCE 45767) adult female collected in Republic of Ecuador, province of Napo, Archidona canton, Pacto Sumaco parish, Wildsumaco Wildlife Sanctuary, Las Cascadas trail (0.6847°S, 77.6002°W), 1417 m a.s.l., by Fernando Ayala, Paloma Lima, Nadia Páez, Javier Pinto, and Santiago R. Ron on 3 April 2014.

Paratypes (N = 4; Fig. 12): All collected in Ecuador. Province of Napo: QCAZ 48916 subadult female, province of Napo, Wildsumaco Wildlife Sanctuary, Benavides trail (0.67744°S, 77.60133°W), 1465 m a.s.l., Jeffrey Camper and D. J. Zart, 15 July 2010; ZSFQ 346–347, adult females, ZSFQ 348, adult male, Archidona canton, Reserva Narupa (0.682°S, 77.74°W), 1150–1170 m a.s.l., David Brito-Zapata, Jose Vieira, Malki Bustos, 21 June 2018.

Proposed standard English name: Ecuadorian leaf litter frog.

Proposed standard Spanish name: Cutín de Hojarasca ecuatoriano.

Definition (Figs 12, 13, 14A, 15A; Tables 2 and 3): We assign the new species to the genus *Phyllonastes* based on its phylogenetic

relationships. The new species is characterized by: (1) skin on dorsum and flanks shagreen, dorsolateral folds absent, ventral surfaces smooth, discoidal fold present; (2) tympanic membrane and tympanic annulus distinct, supratympanic fold present, postrectal tubercles present or absent; (3) snout truncate in dorsal view and rounded in lateral view; (4) upper eyelid without tubercles, cranial crests absent; (5) vomerine teeth absent; (6) vocal slits present, nuptial pads absent; (7) fingers slightly expanded distally, with fingertips acuminate, bearing papillae, finger I shorter than finger II, supernumerary tubercles absent; (8) fingers without lateral fringes or circumferential grooves; (9) distal phalanges blunt or T-shaped, phalangeal formula of hand 2-2-3-2; (10) ulnar tubercles absent; (11) knees and heels without tubercles, outer edge of tarsus without tubercles, inner edge of tarsus bearing one subconical tubercle; (12) inner metatarsal tubercle large, elongate in ventral view and rounded in lateral view, bigger than knob of outer metatarsal tubercle; (13) toes expanded distally, with acuminate toe tips and bearing papillae, supernumerary tubercles present, toes bearing narrow lateral fringes, toe basal webbing absent, all toes bearing ill-defined pads and circumferential grooves, toe V shorter than toe III; (14) in life, dorsum brown, with faint dark marks and chevrons

in some specimens, throat brown, contrasting with paler belly, dark mask extending onto flanks; and (15) SVL in adult males 14.0 mm ($N = 1$) and SVL in adult females 16.76 mm ($N = 3$) (Table 4).

Diagnosis: *Phyllonastes ecuadoriensis* resembles the closely related *P. coloma* and *P. personinus* by the presence of a tympanic membrane and supratympanic fold, acuminate fingertips and toe tips, and dark brown mask. It differs from them by having only two phalanges in finger IV (*P. coloma* and *P. personinus* bear three phalanges in finger IV), truncate snout in dorsal view (round in *P. coloma* and *P. personinus*), fingers slightly expanded distally (fingers not expanded in *P. coloma* nor *P. personinus*), and toes expanded distally (toes slightly expanded in *P. coloma* nor *P. personinus*); by the absence of supernumerary palmar tubercles (present in *P. coloma* and *P. personinus*) and by the presence of supernumerary plantar tubercles (absent in *P. coloma* and *P. personinus*). *Phyllonastes ecuadoriensis* also differs from *P. coloma* by the presence of papillae on fingertips and toe tips (both absent in *P. coloma*), and from *P. personinus* by having dorsum and flanks shagreen (dorsum smooth with few low pustules and flanks smooth in *P. personinus*). For a comparison with other



Figure 12. Live and preserved specimens of *Phyllonastes ecuadoriensis*. Lateral, dorsal, and ventral views of: A, B, holotype QCAZ 57064, adult female, SVL = 18.07 mm; and C, paratype QCAZ 48916, subadult female. A, in life. B, C, in preservative. A scale bar is given only for preserved adults. The depigmentation visible in both specimens is attributable to preservation defects.



Figure 13. Palmar (A) and plantar (B) surfaces of *Phyllonastes ecuadoriensis*. Photographs of left hand and right foot of the holotype QCAZ 57064.

Phyllonastes species that are more phylogenetically distant, see [Tables 2](#) and [3](#).

Description of holotype (Figs 12, 13): Adult female (QCAZ 57064). Measurements (in millimetres): SVL, 18.1; tibia length, 9.3; foot length, 8.1; head length, 5.8; head width, 6.2; eye diameter, 2.2; tympanum diameter, 1.3; interorbital distance, 2.7; upper eyelid width, 1.5; internarial distance, 2.09; eye–nostril distance, 1.6.

Body robust, head is not distinct from body, head slightly wider than long. Snout truncate in dorsal view and rounded in lateral view, without rostral papilla; canthus rostralis slightly concave; interorbital space flat, with no cranial crests; tympanic membrane distinct, tympanic annulus prominent on anterior and ventral borders, and a broad and low supratympanic fold resembling a bulge is present dorsally; postriotal tubercles absent; vomerine teeth absent; tongue large, lanceolate, and with a straight posterior border; vocal slits and nuptial pads absent; lips are not flared; nostrils are elongate and slightly protuberant.

Skin of dorsum and flanks shagreen, top of the head and upper eyelid smooth; dorsolateral folds absent; ventral surfaces smooth; skin in cloacal region areolate; discoidal fold present. Ulnar tubercles absent, palmar tubercles distinct, low; outer palmar tubercle elongate, proximally wider and about twice the size of the elongate thenar tubercle; subarticular tubercles

ill-defined, elongate, and low; supernumerary tubercles absent; dermal fringes on fingers absent; discs narrow, bearing round and inconspicuous pads without circumferential grooves. Phalangeal formula is 2-2-3-2 and relative length of fingers is $I < II < IV < III$. Fingers are slightly expanded distally, with acuminate tips that are dorsoventrally flattened, papilla present, and antebrachial ornamentation absent.

Hindlimbs robust; knee and heel without tubercles; tarsal folds (inner and outer) absent. Outer tarsal tubercles absent; inner tarsal tubercle present, prominent, round in ventral view and subconical in lateral view, and about half the size of the outer metatarsal tubercle and in line with the inner metatarsal tubercle. Inner metatarsal tubercle elongate, $\sim 1.5 \times$ length of outer metatarsal tubercle. The latter is knob like and protrudes posteriorly. Subarticular tubercles low and rounded, supernumerary tubercles minute and ill defined. Toes with narrow lateral dermal fringes; basal webbing between toes absent; discs on toes ill defined, toes expanded distally bearing papilla; ill-defined circumferential grooves; relative lengths of toes $I < II < V < III < IV$; toe III longer than toe V (toe III reaches the distal border of the second subarticular tubercle of toe IV; toe V almost reaches the half of the second tubercle of toe IV).

Colour of holotype in life (based on digital photographs) (Fig. 12): Dorsum is light greyish orange, becoming more orange towards

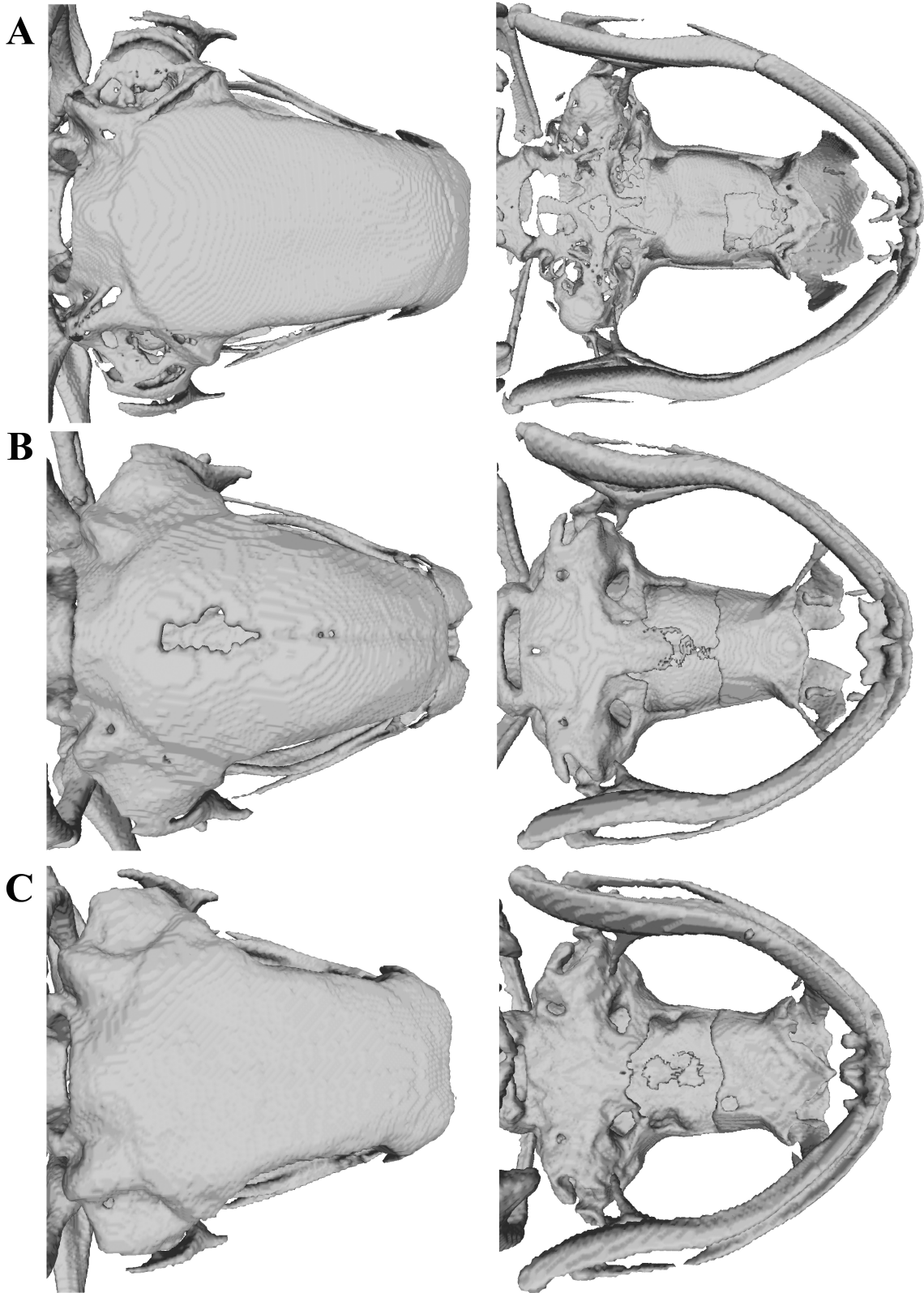


Figure 14. Skulls of *Phyllonastes* species. A, *Phyllonastes ecuadoriensis* QCAZ 57064. B, *Phyllonastes heyeri* QCAZ 24875. C, *Phyllonastes macuma* QCAZ 40180.

the cloacal region, bearing dark brown blotches fading posteriorly and a pair of dark sacral lateral patches that do not touch medially. Facial mask dark brown, almost black; the mask extends posteriorly on the flanks halfway to the hindlimb insertion; the dark

facial pigment extends dorsally to the eyelid; posterior to the mask extension, flanks are medium brown with light flecking. Lips dark brown, with few irregular white flecks. Forearms are brown, with two pale bands on the left and 1.5 on the right. Dorsal surfaces

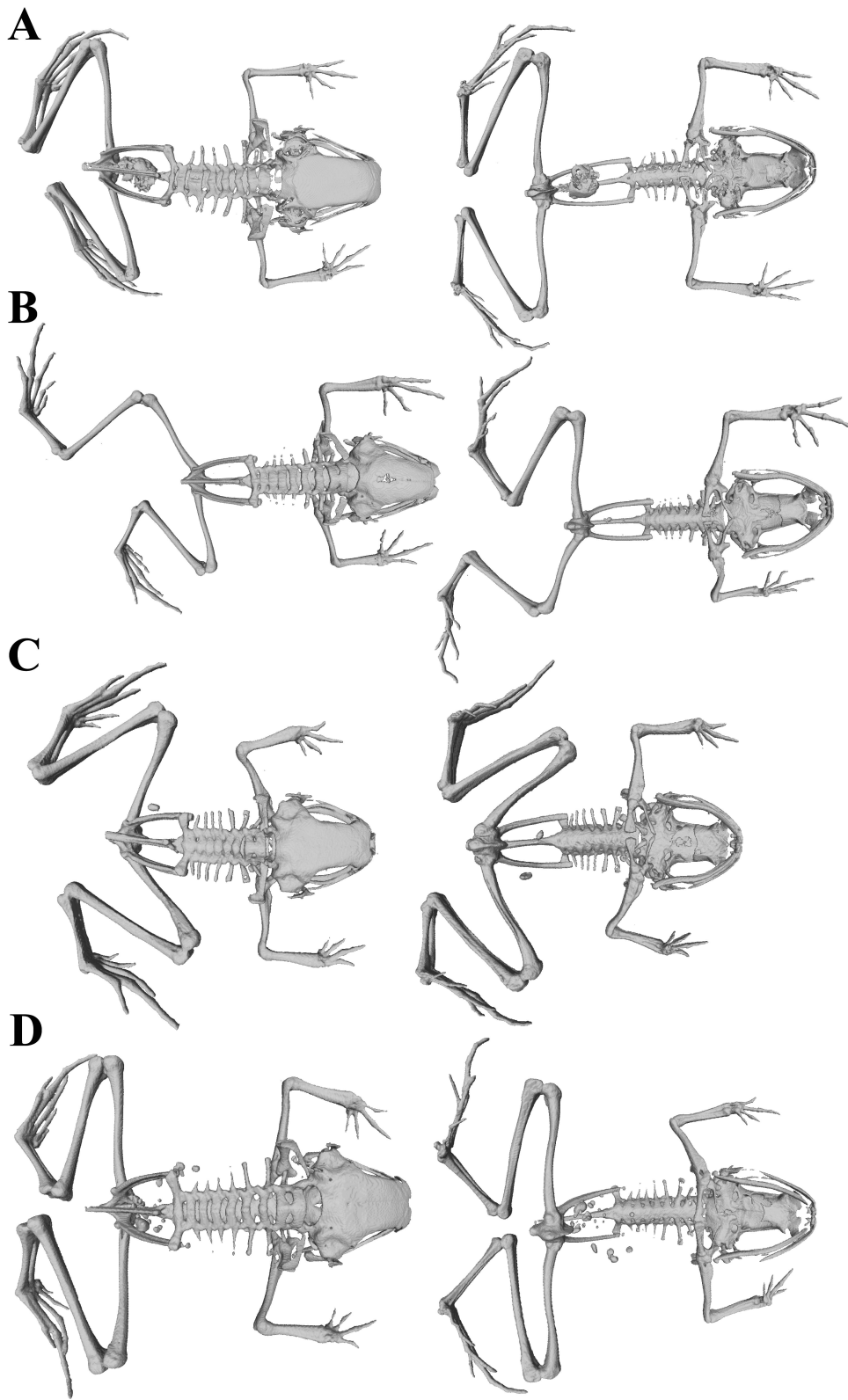


Figure 15. Skeletons of *Phyllonastes* species. A, *Phyllonastes ecuadoriensis* QCAZ 57064, SVL = 18.07 mm. B, *Phyllonastes heyeri* QCAZ 24875, SVL = 14.11 mm. C, *Phyllonastes macuma* QCAZ 40180, SVL = 11.92 mm. D, *Phyllonastes myrmecoides* QCAZ 53583, SVL = 11.13 mm.

of hindlimbs orange–brown, with dark brown transversal bars bordered by lighter colour. Throat uniformly dark brown, with an orange flecking anteriorly. Ventral surfaces of upper arms, thighs,

and belly bright orange, with scattered dark brown flecks. Ventral surfaces of forearms and shanks dark brown, with small bright orange blotches. Cloacal region dark brown.

Colour of holotype in preservative (Fig. 12): Dorsal surfaces dark brown; dorsum bearing a pair of darker sacral lateral patches; limbs with darker transversal bars. Throat, ventral surfaces of forearms, shanks, and feet dark brown, bearing cream flecks densely grouped on the posterior half of shanks. Chest, belly, and ventral surfaces of upper arms and thighs cream, with faint dark brown flecks. Posterior surfaces of thighs dark brown. Cloacal region dark brown, almost black.

Variation (Fig. 12): In this section, traits refer to preserved individuals unless otherwise mentioned. Tympanic annulus can be completely differentiated as in QCAZ 48916. The same specimen also presents an inconspicuous supratympanic fold (might be a preservation effect), dorsal surfaces dark brown, with white big irregular blotches in the lower back (might be only an effect of preservation of the individual), limbs without differentiated transversal bars, ventral surfaces of forearms, shanks, and posterior surfaces of thighs cream, bearing dark brown flecks densely grouped. Three specimens have a row of postrictal tubercles (ZSFQ 346–48). One male (ZSFQ 348) has a much paler throat, similar in colour to the venter. Three specimens have the suprainguinal spots elongated (ZSFQ 346–48), two of them merging into an hourglass-shaped large mark on dorsum (ZSFQ 347–48). One specimen (ZSFQ 347) has short papillae on most fingers, except for fingers III and IV on the left hand, which show long papillae. Two specimens (ZSFQ 346 and 348) have short papillae in all their fingers, sometimes ill defined. The male (ZSFQ 348) has vocal slits. Morphometric variation is detailed in Table 4.

Distribution, natural history, and conservation status (Fig. 3): *Phyllonastes ecuadoriensis* is known from three localities on the eastern slopes of the Andes, in the provinces of Napo and Pastaza, between 1150 and 1465 m a.s.l. in Eastern Foothill Forest. Individuals were collected at night (20:00–00:45 h) on leaf litter in *terra firme* forest. We propose assigning *P. ecuadoriensis* to the Data Deficient IUCN Red List Category owing to the lack of information about its population size and geographical range.

Etymology: The specific epithet refers to the country where the species is distributed, *ecuadoriensis*, meaning from Ecuador, and is masculine in gender.

Remarks: The identification of *P. lochites* in our study is based on the redescription provided by Harvey et al. (2013). Our phylogeny includes specimens from that publication (QCAZ51766/MEPN14255 and QCAZ51767/MEPN14253). According to Harvey's work and our phylogenetic results, the specimen KU177356, previously identified as *P. lochites* (e.g. Hedges et al. 2008, Catenazzi and Tito 2016, Reyes-Puig et al. 2019, 2020, 2021, Santa-Cruz et al. 2019, Catenazzi et al. 2020, Condori et al. 2020, Portik et al. 2023), is, in fact, *P. ecuadoriensis*.

Phyllonastes dicaprio sp. nov.

LSID:urn:lsid:zoobank.org:act:6BB7F9AC-DD71-4FA4-8251-0184D8991FCE

Noblella heyeri—Garzón-Santomaro et al. (2019).

Holotype (Figs 16, 17): DHMECN 13729 (field no. SRJ 2017-364), adult male from República del Ecuador, province of El

Oro, El Retiro (3.206528°S, 79.67977°W, 1705 m a.s.l.), collected by Filemón Benítez and Miguel Urgilés on 3 July 2017.

Paratypes (N = 9; Fig. 16): All from Ecuador, El Oro Province: El Retiro, DHMECN 13723, DHMECN 13730 adult females; DHMECN 13724–26, DHMECN 13728 adult males; collected with the holotype. Sinsao, DHMECN 12524–25 adult males; DHMECN 12527 female (3.61847°S, 79.58072°W) 1330 m a.s.l.

Proposed standard English name: DiCaprio's leaf litter frog.

Proposed standard Spanish name: Cutín de Hojarasca de DiCaprio.

Definition (Figs 16, 17; Tables 2 and 3): We assign the new species to the genus *Phyllonastes* based on its phylogenetic relationships. The new species is characterized by: (1) skin on head, dorsum and flanks shagreen, dorsolateral folds absent, dorsal limb skin smooth with dispersed low warts, ventral skin and posterior surface of legs areolate, discoidal fold present; (2) tympanic membrane undifferentiated, tympanic annulus present but weakly defined, small supratympanic fold present, row of postrictal tubercles present; (3) snout rounded in dorsal and lateral views; (4) upper eyelid without tubercles, cranial crests absent; (5) vomerine teeth absent; (6) vocal slits and nuptial pads absent; (7) fingers not expanded distally, finger tips acuminate without papillae, finger I shorter than finger II, supernumerary tubercles present; (8) fingers bearing narrow lateral fringes, well-defined pads without circumferential grooves; (9) distal phalanges blunt or T-shaped, phalangeal formula of hand 2-2-3-3; (10) ulnar tubercles usually present; (11) knees and heels without tubercles, outer edge of tarsus without tubercles, inner edge of tarsus bearing one conical tubercle; (12) inner metatarsal tubercle large, elongate in ventral view and rounded in lateral view, bigger than conical outer metatarsal tubercle; (13) toes expanded distally, with acuminate toe tips and lacking papillae; supernumerary tubercles, lateral fringes, and toe basal webbing absent; all toes bearing ill-defined circumferential grooves, toe V shorter than toe III; (14) in life, dorsum brown, with two suprainguinal spots, dark or light middorsal stripe and dark marks and chevrons in some specimens; dark mask (but faint in some specimens), extending onto darker flanks; arms brown, with dark marks usually forming bands; ventral surfaces of body and legs light brown, with small cream flecks and dots; and (15) SVL in adult males 12.62 mm ($N = 7$) and SVL in adult females 12.93 mm ($N = 3$) (Table 4).

Diagnosis: *Phyllonastes dicaprio* resembles the other *Phyllonastes* from the western foothills of Ecuadorian Andes, *P. cerrogolondrinas*, *P. coloma*, *P. mindo*, and *P. worleyae*, by having a tympanic annulus, supernumerary palmar tubercles, fingers not expanded distally, and circumferential grooves on toes. It differs from all of them by lacking vocal slits. Besides, *P. dicaprio* differs from *P. cerrogolondrinas* by having a round snout in dorsal view (snout truncate in dorsal view in *P. cerrogolondrinas*), by having a supratympanic fold (absent in *P. cerrogolondrinas*) and three phalanges in finger IV (finger IV with two phalanges in *P. cerrogolondrinas*), and by the absence of circumferential grooves in fingers and supernumerary plantar tubercles (both present

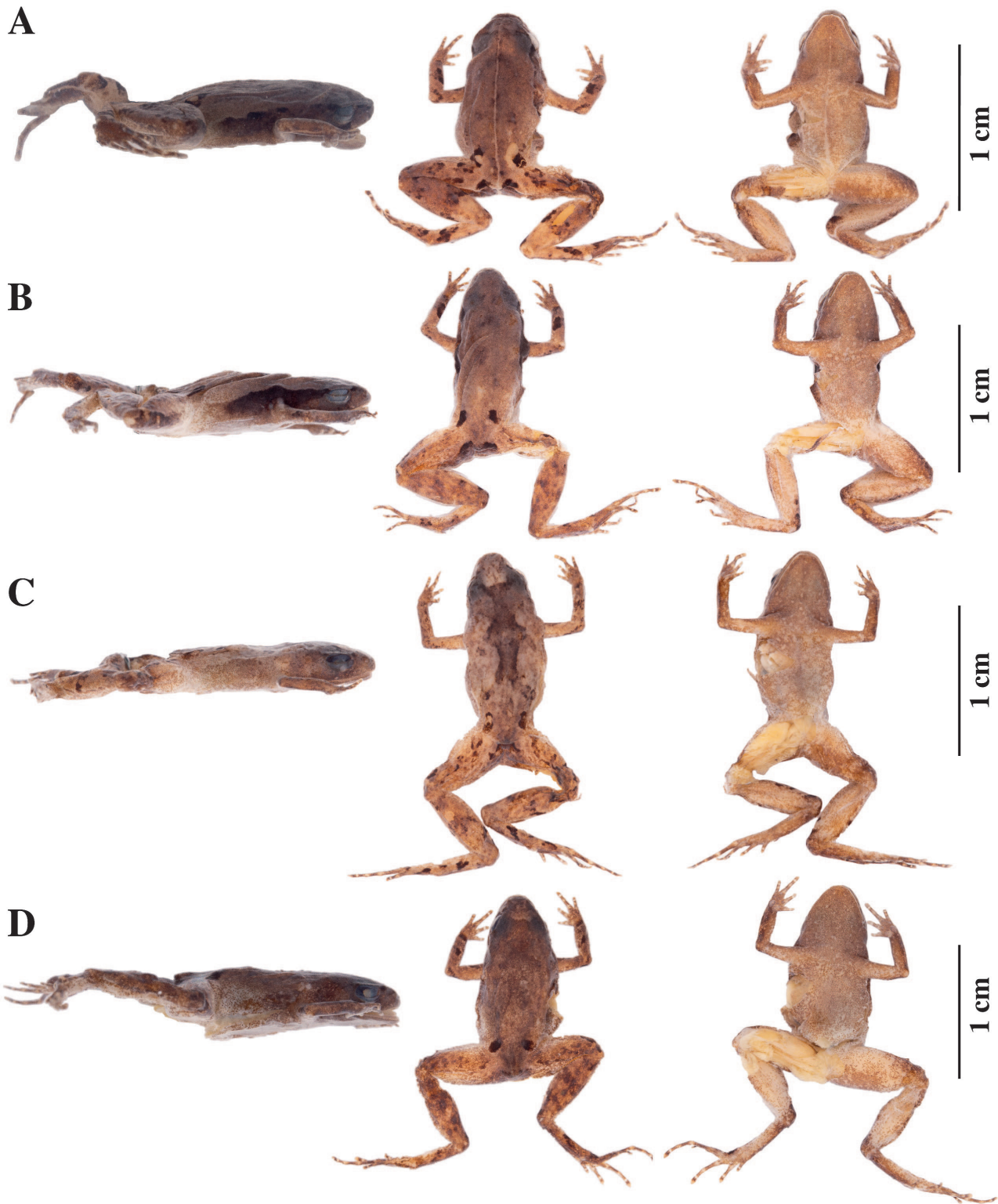


Figure 16. Preserved specimens of *Phyllonastes dicaprioi*. Lateral, dorsal, and ventral views of: A, holotype DHMECN 13729, adult male, SVL = 10.7 mm; B, paratype DHMECN 13723, adult female, SVL = 12.84 mm; C, paratype DHMECN 13725, adult male, SVL = 12.85 mm; and D, paratype DHMECN 13730, adult female, SVL = 13.56 mm.

in *P. cerrogolondrinas*). *Pristimantis dicaprioi* also differs from *P. coloma* by having toes distally expanded (slightly expanded in *P. coloma*); from *P. mindo* by having acuminate toe tips (rounded in *P. mindo*), and from *P. worleyae* by the absence supernumerary

plantar tubercles (present in *P. worleyae*) and by the mask extending to the groins (mask extending to flank half in *P. worleyae*). For a comparison with other *Phyllonastes* species that are more phylogenetically distant, see [Tables 2 and 3](#).

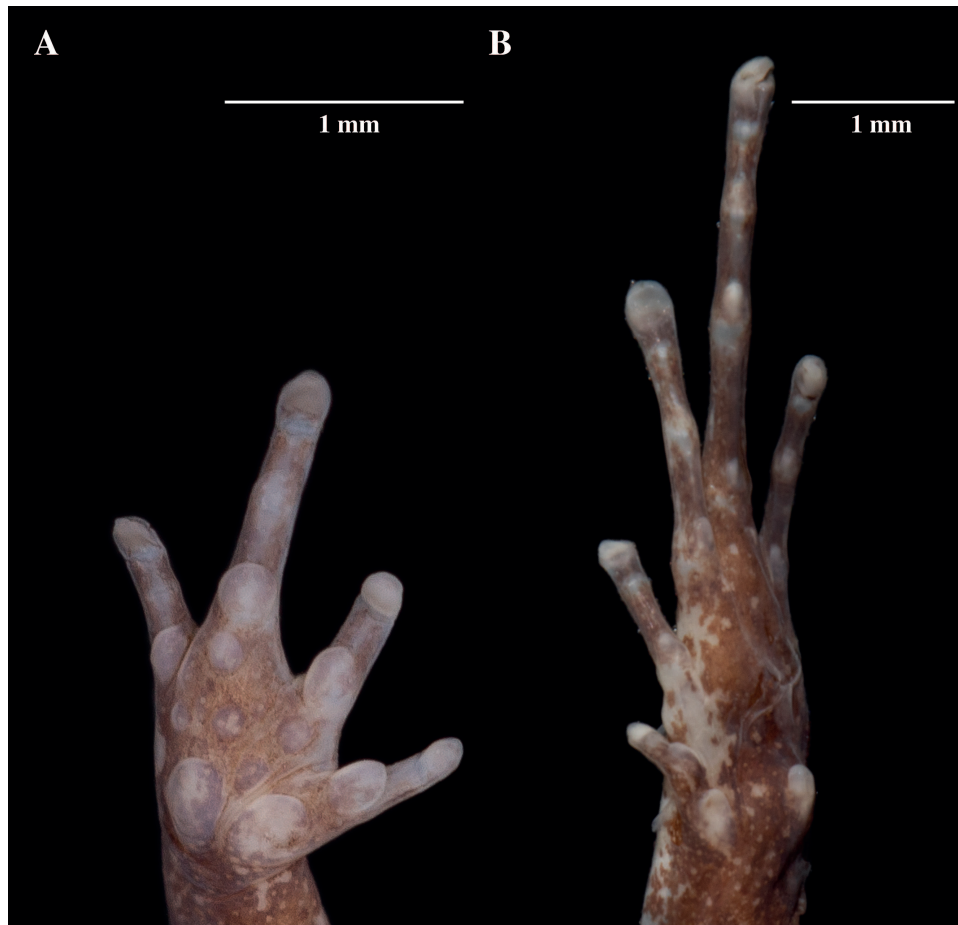


Figure 17. Palmar (A) and plantar (B) surfaces of *Phyllonastes dicaprioi*. Photographs of right hand and left foot of the holotype DHMECN 13729.

Description of holotype (Figs 16, 17): Adult male (DHMECN 13729). Measurements (in millimetres): SVL, 12.9; tibia length, 5.5; foot length, 4.9; head length, 3.0; head width, 3.5; eye diameter, 1.5; tympanum diameter, 0.5; interorbital distance, 1.3; upper eyelid width, 0.8; internarial distance, 1.3; eye–nostril distance 0.8.

Head wider than long, head slightly narrower than body; canthus rostralis weakly defined; loreal region slightly concave in dorsal view; cranial crests absent; upper eyelid bearing no tubercles. Tympanic annulus weakly defined, differentiated in its anterior and inferior portions; tympanic membrane undifferentiated from the surrounding skin; small supratympanic fold present; postrictal tubercles present. Snout round in dorsal and lateral views, without rostral papilla. Vomerine teeth absent; vocal slits and nuptial pads absent.

Skin on head, dorsum, and flanks shagreen, limbs smooth dorsally, with dispersed low warts; skin on posterior surfaces of legs and venter areolate; dorsolateral folds absent; discoidal fold present. Ulnar tubercle small and low; palmar tubercles prominent, outer palmar tubercle slightly elongate, thenar tubercle large and elongate, both rounded in lateral view; subarticular tubercles well defined, round in ventral and lateral views; distal subarticular tubercles not visible; supernumerary tubercles visible; thin lateral dermal fringes present, discs bearing well-defined pads without circumferential grooves, fingers not expanded distally,

tip of fingers acuminate, without papillae; relative length of fingers $I < II < IV < III$; phalangeal formula of 2-2-3-3.

Hindlimbs robust; heel and knee without tubercles; tarsal folds (inner and outer) absent, outer tarsal tubercles absent; inner tarsal tubercle present, prominent, and conical; inner metatarsal tubercle large, elongate in ventral view, rounded in lateral view; outer metatarsal tubercle small, well defined, prominent, rounded in ventral view, conical in lateral view; supernumerary plantar tubercles absent; subarticular tubercles well defined, round and prominent in dorsal view, toes without lateral fringes; basal webbing absent; discs rounded and bearing well-defined rounded pads; circumferential grooves present, ill defined; toes expanded distally, tip of toes acuminate without papillae; relative length of toes is $I < II < V < III < IV$; toe III longer than toe V (toe III surpasses the distal border of the second subarticular tubercle of toe IV; toe V reaches the proximal border of the second tubercle of toe IV).

Colour of holotype in life: Dorsum brown, with darker, scattered marks and chevrons, two suprainguinal spots and a middorsal cream stripe extending to the vent. Cloacal region dark brown, with a cream stripe extending towards each hindlimb along the posterior surface of the thigh, ventral surface of shank, and posterior surface of pes, ending at the inner metatarsal tubercle. Faint dark mask present, extending from the tip of the snout to the groins, bordering dorsally dark flanks. Lips with dark vertical bars.

Arms and legs brown, with dark marks usually forming bands. Ventral surfaces of body and legs light brown, with small cream flecks and dots. A mid-ventral pale stripe extends from the throat to the vent; a pale stripe extends ventrally along each hindlimb, joining the midventral pale stripe to form a cross on the chest.

Colour of holotype in preservative: Similar to coloration in life but paler.

Variation (Fig. 16): Four specimens have an almost unnoticeable tympanic membrane and annulus, on one or both sides (DHMECN 12524–5 and 13724–25). Ulnar tubercles absent in all paratypes. Three specimens have the dorsum paler than the holotype, without dark marks except for suprainguinal spots (DHMECN 13723, 13726, and 12524). One individual is similar to the holotype in having a pale mid-dorsal stripe but lacks dark marks, except for suprainguinal spots. Two specimens have a darker brown dorsum than the holotype and a faint dark mid-dorsal stripe and inverted-V chevrons (DHMECN 12527 and 13720). One specimen has a dark hourglass-shaped large mark on the dorsum DHMECN 13725. One specimen has a faint midventral pale stripe, but no stripes on ventral surfaces of the arms (DHMECN 13728). Two specimens have faint pale stripes along hindlegs (DHMECN 13724 and 13728). Midventral and hindleg stripes are absent in all paratypes. Morphometric variation is detailed in Table 4.

Distribution, natural history, and conservation status (Fig. 3): *Phyllonastes dicaprio* is known from the Western Montane Forest of the province El Oro, Ecuador, between 1330 and 1705 m a.s.l. Individuals were collected at night on the ground, buried in leaf litter. Because of the lack of information on population size and geographical range, we suggest assigning *P. dicaprio* to the Data Deficient IUCN Red List Category (based on IUCN Standards and Petitions Committee 2023).

Etymology: The specific name *dicaprio* is a patronym honouring Leonardo DiCaprio, actor, film producer, and conservationist. He has voiced his support for several conservation initiatives in Ecuador; and in 2021, he pledged funds for the conservation and ecosystem restoration of the Galapagos Islands, Ecuador.

Phyllonastes macuma sp. nov.

LSID: urn:lsid:zoobank.org:act:B8D4C8B8-DED1-4475-8400-482B0FBCB719

Holotype (Figs 14C, 15C, 18, 19): QCAZ 40180 (field no. SC-PUCE 24877) adult male from Ecuador, Morona Santiago Province, Canton Macas, Macuma Parish, Cordillera del Kutuku, Wisiu (2.0901°S, 77.7661°W), 1361 m a.s.l. Collected by Octavio Jiménez Robles on 30 December 2008.

Paratypes (N = 2; Fig. 18): All from Ecuador, Morona Santiago Province, Canton Macas, Macuma Parish, Cordillera del Kutuku, Wisiu: QCAZ 40181 subadult female (2.1066°S, 77.7627°W) 955 m a.s.l., collected by Octavio Jiménez Robles on 18 December 2008; QCAZ 46352 adult female (2.1111°S, 77.7391°W) 650 m a.s.l., collected by Ignacio de la Riva and Octavio Jiménez on 7 December 2009.

Proposed standard English name: Macuma leaf litter frog.

Proposed standard Spanish name: Cutín de Hojarasca de Macuma.

Definition (Figs 14C, 15C, 18, 19; Tables 2 and 3): We assign the new species to the genus *Phyllonastes* based on its phylogenetic relationships. The new species is characterized by: (1) skin on dorsum smooth to finely shagreen, dorsolateral folds absent, ventral surfaces smooth to weakly areolate, discoidal fold present, skin on flanks finely shagreen; (2) tympanic membrane and tympanic annulus present, supratympanic fold absent, postrictal tubercle ill defined; (3) snout broadly rounded in dorsal view and rounded in lateral view; (4) upper eyelid without tubercles, cranial crests absent; (5) vomerine teeth absent; (6) vocal slits present, nuptial pads absent; (7) fingers not expanded distally, finger tips acuminate, without papillae, finger I shorter than finger II, supernumerary tubercles present; (8) fingers bearing narrow lateral fringes, ill-defined pads lacking circumferential grooves; (9) distal phalanges blunt to T-shaped, phalangeal formula of hand 2-2-3-3; (10) ulnar tubercles absent; (11) knees and heels without tubercles, outer edge of tarsus without tubercles, inner edge of tarsus bearing one rounded tubercle; (12) inner metatarsal tubercle elongate in ventral view and rounded in lateral view, bigger than rounded outer metatarsal tubercle; (13) toes expanded distally, with acuminate toe tips and bearing papillae, supernumerary tubercles ill defined, narrow lateral fringes on toes, toe basal webbing present between toes I and II, all toes bearing well-defined circumferential grooves, toe V shorter than toe III; (14) in preserved specimens, dorsum cream bearing dark brown flecks, back with two ill-defined chevrons of anterior vertex, dark brown blotches at the level of the sacrum, facial mask dark brown extending from the tip of snout up to halfway down the flanks, cream ventral surfaces; (15) SVL in adult males 11.92 mm ($N = 1$) and in adult females 14.49 mm ($N = 1$) (Table 4).

Diagnosis: *Phyllonastes macuma* resembles its closest species, *P. lochites*, *P. myrmecoides*, and *P. sardinayacu*, by having a tympanic annulus, tympanic membrane, fingers not expanded, and acuminate toe tips. It differs from all of them by having broadly rounded snout in dorsal view (rounded in *P. lochites*, truncate in *P. myrmecoides*) and rounded inner tarsal tubercle (conical in *P. lochites* and *P. myrmecoides*, and subconical in *P. sardinayacu*). It also differs from *P. sardinayacu* by having papillae on toe tips (absent in *P. sardinayacu*). It differs from *P. lochites* and *P. myrmecoides* by having three phalanges in finger IV (only two phalanges on finger IV in *P. lochites* and *P. myrmecoides*), vocal slits (absent in *P. lochites* and *P. myrmecoides*), supernumerary plantar tubercles (absent in *P. myrmecoides*), and by the absence of papillae on fingertips (present in *P. myrmecoides*). For a comparison with other *Phyllonastes* species that are more phylogenetically distant, see Tables 2 and 3.

Description of the holotype (Figs 18, 19): Adult male (QCAZ 40180). Measurements (in millimetres): SVL, 11.92; tibia length, 6.09; foot length, 5.08; head length, 3.64; head width, 4.20; eye diameter, 1.43; tympanum diameter, 0.73; interorbital distance, 1.67; upper eyelid width, 1.04; internarial distance, 1.59; eye–nostril distance, 0.89.



Figure 18. Preserved specimens of *Phyllonastes macuma*. Lateral, dorsal, and ventral views of: A, holotype QCAZ 40180, adult male, SVL = 11.92 mm; B, paratype QCAZ 46352, adult female, SVL = 14.49 mm; and C, paratype QCAZ 40181, juvenile. Scale bars are given only for preserved adults. Paratype QCAZ 46352 has a missing shank and foot.

Head wider than long, head wider than body; canthus rostralis slightly convex in lateral view; loreal region straight in dorsal view; cranial crests absent; upper eyelid bearing no tubercles. Tympanic annulus visible; tympanic membrane present; supratympanic fold absent; postrictal tubercle ill defined on right side (probably lost on left side as a preservation effect). Snout broadly rounded in dorsal view and rounded in lateral view, without rostral papilla. Vomerine teeth absent, vocal slits present, and nuptial pads absent.

Skin on dorsum smooth and finely shagreen on flanks; dorso-lateral folds absent; throat areolate, belly and ventral surface of limbs smooth; skin on cloacal region areolate; discoidal fold not differentiated, probably as a preservation artefact. Ulnar tubercles absent, palmar tubercles prominent, outer palmar tubercle almost twice the size of the thenar tubercle, drop-shaped, with the tip pointing towards the palm and the base towards the wrist; thenar tubercle rounded; subarticular tubercles round in ventral and lateral views, visible only at the base of fingers; supernumerary tubercles present, narrow lateral dermal fringes on fingers, discs not expanded, bearing round and inconspicuous pads (conspicuous only on fingers III), circumferential groove not visible; acuminate fingertips, especially on the third finger,

without papilla; relative length of fingers is $I < IV < II < III$; phalangeal formula of hand is 2-2-3-3.

Hindlimbs not robust; heel and knee without tubercles; tarsal folds (inner and outer) absent, outer tarsal tubercles absent; inner tarsal tubercle present, small, prominent, and round; inner metatarsal tubercle prominent, elongated in ventral view and rounded in lateral view; outer metatarsal tubercle well defined and round, more prominent than the inner one; plantar surface bearing rounded, small, and ill-defined supernumerary tubercles; round subarticular tubercles well defined and rounded; toes with narrow lateral dermal fringes; basal webbing only between toes I and II; discs on toes well defined, expanded with acuminate tip, papilla on tip visible on toes III–V; well-defined circumferential grooves; relative lengths of toes $I < II < V < III < IV$; toe III longer than toe V (toe III reaches the distal border of the second subarticular tubercle of toe IV; toe V almost reaches the proximal border of the second tubercle of toe IV).

Colour of holotype in life: Unknown.

Colour of holotype in preservative (Fig. 18): Dorsum cream, darkening anteriorly, and bearing dark brown flecks. Back with



Figure 19. Palmar (A) and plantar (B) surfaces of *Phyllonastes macuma*. Photographs of left hand and left foot of the holotype QCAZ 40180.

two chevrons of anterior vertex, poorly defined and dark brown. Dark brown irregular blotches at the level of the sacrum. Dorsal surfaces of limbs cream coloured, with some dark brown spots. The spots are condensed on the elbows and knees. Dark, poorly defined transverse bars on the dorsal surfaces of the limbs. Facial mask dark brown, extending from the tip of snout up to halfway down the flanks. Cream-coloured flanks with brown flecks. Cream ventral surfaces with small dark brown dots that condense towards the throat, making it appear uniformly dark brown. Ventral surfaces of the extremities cream coloured. Thighs and legs with small dark brown dots condensed towards the knees. Dark brown knees and heels. Cloacal region dark brown, much darker dorsally.

Variation (Fig. 18): In this section, traits refer to preserved individuals. Adult female (QCAZ 46352) is much larger (SVL = 14.49 mm). This specimen differs from the holotype by having a tympanic annulus much more defined, in addition to the postrictal tubercles, dorsum finely shagreen, ventral surfaces weakly areolate, discoidal fold present and well defined, hindlimbs robust, basal webbing absent, paler throat, better-defined transverse bars on the extremities. Dorsal coloration in the sub-adult female (QCAZ 40181) is generally darker. Morphometric variation is detailed in Table 4.

Distribution, natural history, and conservation status (Fig. 3): *Phyllonastes macuma* is known only from the surroundings

of Macuma, Wisiu from 650 to 1361 m a.s.l., at the base of Cordillera de Kutuku. It was collected in Eastern Foothill Forest and Eastern Montane Forest. Owing to the lack of ecological and demographic information and uncertainty on its geographical range size, we assign *P. macuma* to the Data Deficient IUCN Red List Category (based on IUCN Standards and Petitions Committee 2023).

Etymology: The specific name *macuma* is a toponym used in apposition, and it refers to the locality where the species is found. The word 'macuma' belongs to the Shuar native American language and refers to a Shuar woman.

Phyllonastes plateadensis sp. nov.

LSID: urn:lsid:zoobank.org:act:73A895D9-46FE-4DA0-AF85-18FF11503A30

Holotype (Figs 20, 21, 22B, 23A): QCAZ 65015 (field no. SC-PUCE 56489) adult female from Ecuador, Zamora Chinchipe Province, Canton Palanda, La Canela Parish, Cerro Plateado Biological Reserve, surroundings of Camp 3, trail from Mirador to Camp 3 (4.6027°S, 78.8310°W), 2055 m a.s.l. Collected by Diego Almeida, Kunam Nusirquia, Fernando Ayala, Javier Pinto, Alex Áchig, and Malki Bustos on 23 September 2016.

Paratypes (N = 1; Fig. 20): QCAZ 65016 juvenile from Ecuador, Zamora Chinchipe Province, Canton Palanda, La Canela Parish,

Biological Reserve Cerro Plateado, surroundings of Camp 3, trail of the upper section of Río Negro (4.5993°S, 78.8350°W) 1980 m a.s.l. Collected by Diego Almeida, Kunam Nusirquia, Fernando Ayala, Javier Pinto, Alex Áchig and Malki Bustos on 26 September 2016.

Proposed standard English name: Cerro Plateado leaf litter frog.

Proposed standard Spanish name: Cutín de Hojarasca de Cerro Plateado.

Definition (Figs 20, 21, 22B, 23A; Tables 2 and 3): We assign the new species to the genus *Phyllonastes* based on its phylogenetic relationships. The new species is characterized by: (1) skin on dorsum and flanks finely shagreen, dorsolateral folds absent, ventral surfaces weakly areolate, discoidal fold present; (2) tympanic membrane not differentiated, tympanic annulus present but inconspicuous, supratympanic fold and postrictal tubercles absent; (3) snout broadly rounded in dorsal view and rounded and lateral view; (4) upper eyelid without tubercles, cranial crests absent; (5) vomerine teeth absent; (6) vocal slits and nuptial pads unknown; (7) fingers not expanded distally, finger tips subacuminate, without papillae, finger I shorter than finger II, supernumerary tubercles present; (8) fingers bearing narrow lateral fringes, ill-defined pads and circumferential grooves; (9) distal phalanges blunt or T-shaped, phalangeal formula of hand 2-2-3-3; (10) ulnar tubercles absent; (11) knees and heels without tubercles, outer edge of tarsus without tubercles, inner edge of tarsus bearing one rounded tubercle; (12) inner metatarsal tubercle small, rounded in ventral view and very low in lateral view, smaller than rounded outer metatarsal tubercle; (13) toes slightly expanded distally, with acuminate toe tips and lacking papillae, supernumerary tubercles ill defined, narrow lateral fringes on toes, toe basal webbing absent, all toes bearing ill-defined circumferential grooves, toe V shorter than Toe III; (14) in life, dorsal surfaces light brown with scattered white dots; circular dark brown sacral lateral marks delineated by a paler line, cloacal region cream surrounded by a dark brown stripe, facial mask dark brown extending from tip of snout to groins, flanks brown, ventral surfaces brown with white spots; and (15) SVL in adult males unknown, adult female 19.35 mm ($N = 1$) (Table 4).

Diagnosis: *Phyllonastes plateadensis* resembles its closest species, *P. dicaprio* and *P. heyeri*, by having the snout rounded in lateral view, a tympanic annulus, supernumerary palmar tubercles, three phalanges in finger IV, and by the absence of papillae in fingers and toes. It differs from both by lacking a supratympanic fold (present in *P. dicaprio* and *P. heyeri*) and by having a broadly rounded snout in dorsal view (snout rounded in *P. dicaprio* and subacuminate in *P. heyeri*), rounded inner tarsal tubercle (inner tarsal tubercle conical in *P. dicaprio* and *P. heyeri*), and circumferential grooves of fingers (fingers without circumferential grooves in *P. dicaprio* and *P. heyeri*). For a comparison with other *Phyllonastes* species that are more phylogenetically distant, see Tables 2 and 3.

Description of the holotype (Figs 20, 21, 22B, 23A): Adult female (QCAZ 65015). Measurements (in millimetres): SVL,

19.35; tibia length, 7.79; foot length, 8.66; head length, 5.74; head width, 7.05; eye diameter, 2.14; tympanum diameter, 1.18; interorbital distance, 1.93; upper eyelid width, 1.31; internarial distance, 1.79; eye–nostril distance, 1.51.

Head wider than long, head wider than body; canthus rostralis straight in lateral view; loreal region slightly concave in dorsal view; cranial crests absent; upper eyelid lacking tubercles. Tympanic annulus inconspicuous but visible beneath skin; tympanic membrane not differentiated; supratympanic fold and postrictal tubercles absent. Vomerine teeth absent, vocal slits and nuptial pads absent. Snout broadly rounded in dorsal view and rounded in lateral view, without rostral papilla.

Skin on dorsum and flanks finely shagreen; dorsolateral folds absent; ventral surfaces weakly areolate; skin in cloacal region areolate; discoidal fold present. Ulnar tubercles absent; palmar tubercles low, outer palmar tubercle circular, larger than elongate thenar tubercle; subarticular tubercles ill defined, more conspicuous at the base of fingers, round in ventral and lateral view; three supernumerary tubercles present at the base of fingers; narrow lateral dermal fringes on fingers, fingers not expanded distally; discs narrow, bearing round and inconspicuous pads with an ill-defined circumferential groove; fingertips subacuminate lacking papillae; relative length of fingers is $I < IV < II < III$; phalangeal formula of hand is 2-2-3-3.

Hindlimbs robust; knees and heels without tubercles; tarsal folds (inner and outer) absent, outer tarsal tubercle absent; inner tarsal tubercle present, small and round; inner metatarsal tubercle small (ill defined in preservative), rounded in ventral and lateral views; well-defined and round outer metatarsal tubercle, bigger than the inner one; plantar surface with ill-defined supernumerary tubercles; round subarticular tubercles ill defined; toes with narrow dermal lateral fringes; webbing between toes absent; toes slightly expanded distally, discs on toes ill defined (ill defined in preservative), narrow with acuminate tip, papilla on tip not visible; ill-defined circumferential grooves; relative lengths of toes $I < II < V < III < IV$; toe III longer than toe V (toe III reaches the distal border of the second subarticular tubercle of toe IV; toe V almost reaches the proximal border of the second tubercle of toe IV).

Colour of holotype in life (based on digital photographs) (Fig. 20): Dorsal surfaces light brown, with some scattered white dots; circular dark brown sacral lateral patches well defined, delineated by a paler line. Cloacal region cream, surrounded by a dark brown stripe. Facial mask dark brown extending from tip of snout to groins and delineated along its dorsal edge by a light orange line, more conspicuous rostrally. Flanks light brown, bearing the dark brown mask extension. Lips bearing small and white spots. Forearms with two dark brown blotches delineated by a paler line; the proximal blotch is bigger than the distal one. Heels bearing a dark brown blotch with a paler border; tarsus bearing dark brown blotches surrounded by a paler border dorsally. Ventral surfaces brown with white spots that become bigger towards the cloacal region.

Colour of holotype in preservative (Fig. 20): Dorsal surfaces light brown, with dark brown sacral lateral circular blotches surrounded by a cream edge. Facial mask dark brown extending from tip of snout to near groins, limited on its upper side by a

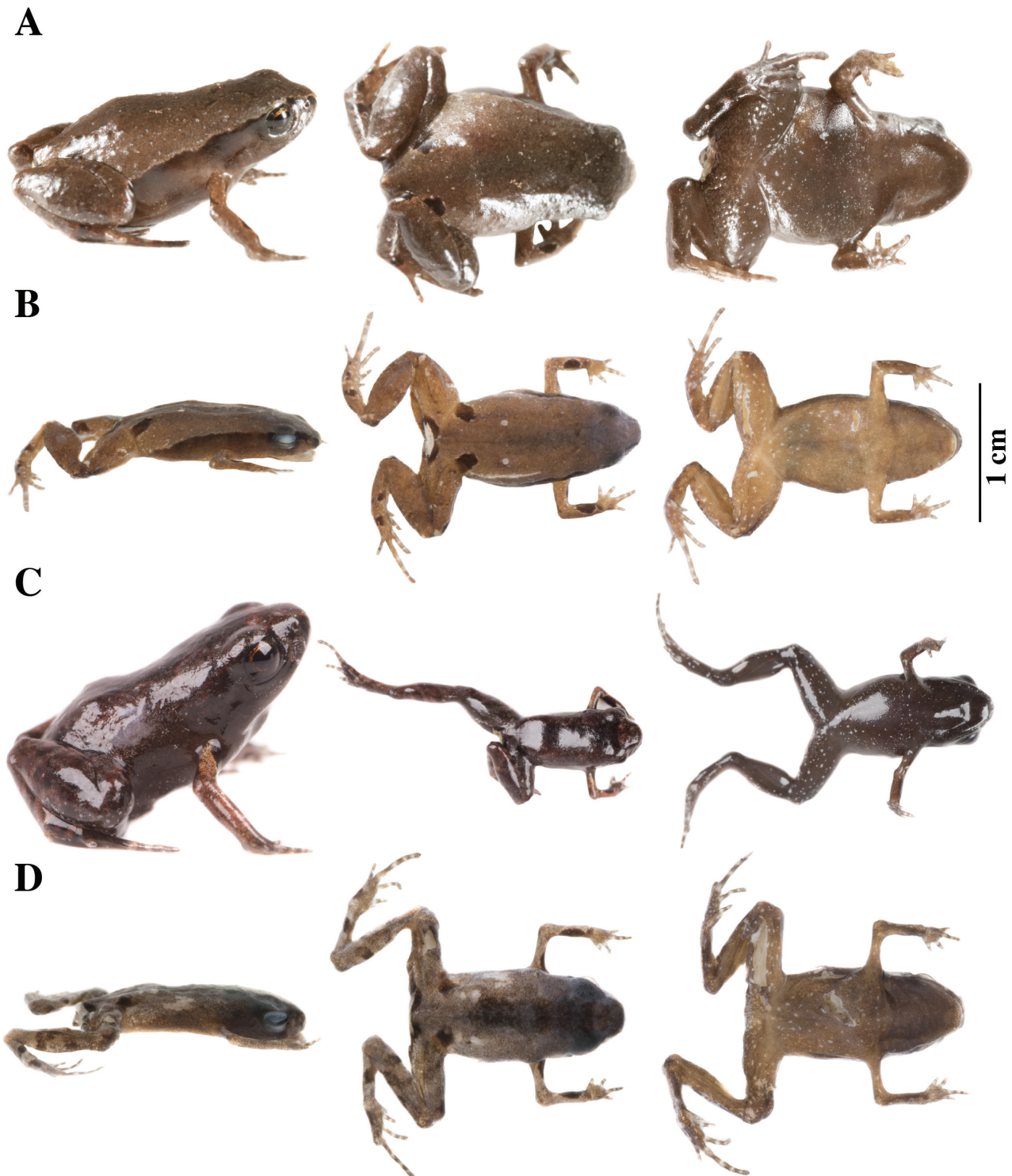


Figure 20. Live and preserved specimens of *Phyllonastes plateadensis*. Lateral, dorsal, and ventral views of: A, B, holotype QCAZ 65015, adult female, SVL = 15.70 mm; and C, D, paratype QCAZ 65016, juvenile, SVL = 9.27 mm. A, C, in life. B, D, in preservative. Scale bar is given only for preserved adults.

thin cream-coloured line. Ventral surfaces light brown, bearing ill-defined white spots that become bigger posteriorly. Posterior surfaces of thighs light brown. Cloacal region white, surrounded by a dark brown stripe, and bearing small and dispersed dark brown flecks. Forearms dorsally with two dark brown blotches

delineated by a paler line; the proximal blotch is bigger and better defined than the distal one.

Variation (Fig. 20): This section refers to living individuals unless otherwise mentioned. Juvenile QCAZ 65016 has more and



Figure 21. Palmar (A) and plantar (B) surfaces of *Phyllonastes plateadensis*. Photographs of right hand and right foot of the holotype QCAZ 65015.

better-defined dark brown circular marks on the tarsus. Facial mask can be ill defined and weakly contrasting, as in QCAZ 65016. Juvenile ventral coloration is darker than in adult, with a darker throat and white spots restricted to belly and thighs, as in QCAZ 65016. Tip of toes may be subacuminate, as in QCAZ 65016. Juvenile presents more inconspicuous palmar and plantar tubercles, round and lower than those in adults in lateral view. Morphometric variation is detailed in [Table 4](#).

Distribution, natural history, and conservation status (Fig. 3): *Phyllonastes plateadensis* is known from the surroundings of the Biological Reserve Cerro Plateado from 1980 to 2093 m a.s.l. Cerro Plateado is in Cordillera del Cóndor, a sub-Andean cordillera separate from the main Andean chain. Individuals were collected in primary Eastern Montane Forest, at night (22:00–23:00 h), on mossy soils and on leaf litter, at the edge of creeks next to water pools. Cerro Plateado is a sandstone formation. Forests in sandstone at Cordillera del Cóndor are characterized by dwarf trees with a canopy of ~5 m (Schulenberg and Awbrey 1997). Because of the lack of information related to population size and geographical range, we assign *P. plateadensis* to the Data Deficient IUCN Red List Category (based on [IUCN Standards and Petitions Committee 2023](#)).

Etymology: The specific epithet *plateadensis* is a toponym noun in apposition and it refers to the type locality.

Phyllonastes sardinayacu sp. nov.

LSID: urn:lsid:zoobank.org:act:B12C9470-F32C-4CEA-9A1B-E2DE6D0CDBA3

Holotype (Figs 22C, 23B, 24, 25): QCAZ 58822 (field no. SC-PUCE 49151) adult female from Ecuador, Morona Santiago Province, Canton Morona, Sináí Parish, Sangay National Park, Sardinayacu, trail to El Enmascarado Lagoon from refuge 3 (2.0500°S, 78.2196°W), 1798 m a.s.l. Collected by Javier Pinto, David Velalcázar, and Darwin Núñez on 23 January 2015.

Paratype (N = 1; Fig. 24): Same locality, collectors, and date as holotype, QCAZ 58821 adult female.

Proposed standard English name: Sardinayacu leaf litter frog.

Proposed standard Spanish name: Cutín de Hojarasca de Sardinayacu.

Definition (Figs 22C, 23B, 24, 25; Tables 2 and 3): We assign the new species to the genus *Phyllonastes* based on its phylogenetic relationships. The new species is characterized by: (1) skin on dorsum and flanks finely shagreen, dorsolateral folds absent, ventral surfaces smooth, discoidal fold present; (2) tympanic membrane and tympanic annulus present, supratympanic fold absent, postrictal tubercle absent; (3) snout rounded to truncate

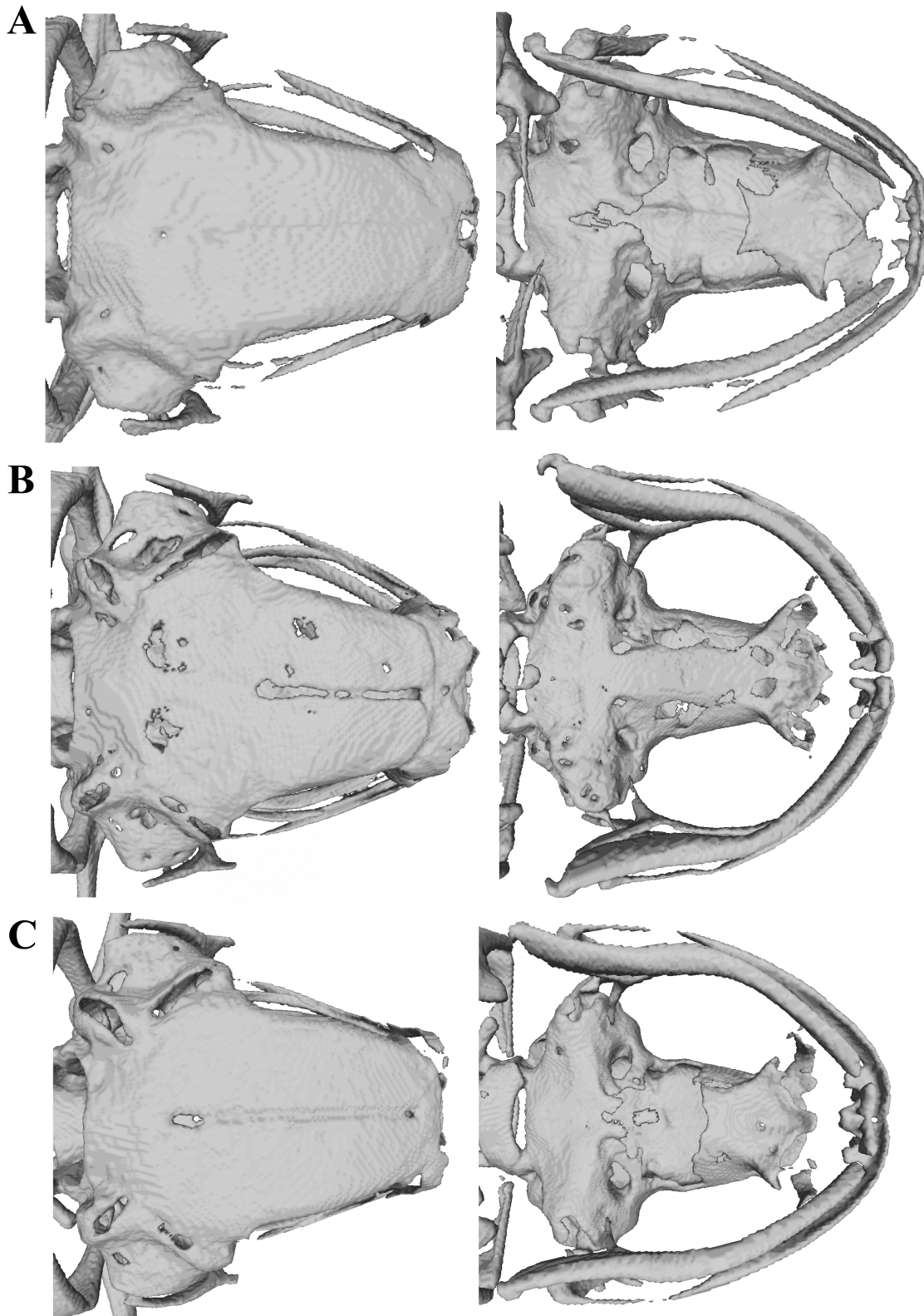


Figure 22. Skulls of *Phyllonastes* species. A, *Phyllonastes myrmecoides* QCAZ 53583. B, *Phyllonastes plateadensis* QCAZ 65015. C, *Phyllonastes sardinayacu*, QCAZ 58821.

in dorsal view and rounded in lateral view; (4) upper eyelid without tubercles, cranial crests absent; (5) vomerine teeth absent; (6) vocal slits and nuptial pads unknown; (7) fingers not expanded distally, finger tips subacuminate without papillae, finger I shorter than finger II, supernumerary tubercles present;

(8) fingers bearing narrow lateral fringes, ill-defined pads lacking circumferential grooves; (9) distal phalanges blunt to T-shaped, phalangeal formula of hand 2-2-3-3; (10) ulnar tubercles absent; (11) knees and heels without tubercles, outer edge of tarsus without tubercles, inner edge of tarsus bearing one subconical

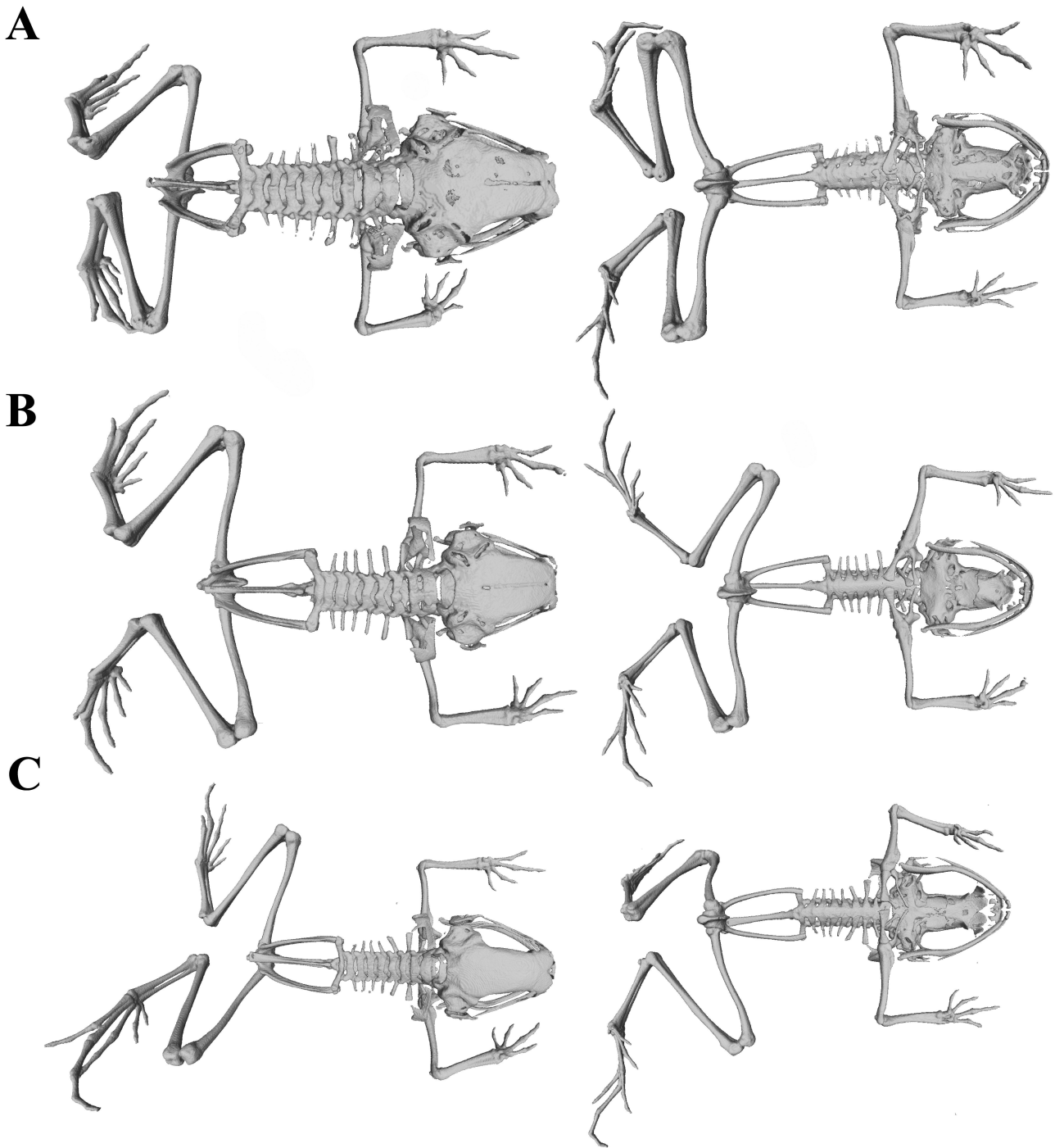


Figure 23. Skeletons of *Phyllonastes* species. A, *Phyllonastes plateadensis* QCAZ 65015, SVL = 15.70 mm. B, *Phyllonastes sardinayacu* QCAZ 58821, SVL = 14.32 mm. C, *Phyllonastes personinus* QCAZ 58818, SVL = 16.91 mm.

tubercle; (12) inner metatarsal tubercle elongated in ventral view and rounded in lateral view, bigger than rounded outer metatarsal tubercle; (13) toes slightly expanded distally, with acuminate toe tips and lacking papillae, supernumerary tubercles present, narrow lateral fringes on toes, toe webbing absent, all toes bearing ill-defined pads and circumferential grooves, toe V shorter than toe III; (14) in life, brown dorsum, with two dark brown sacral lateral patches with light brown border, triangular cloacal blotch dark brown with light brown border, ventral surfaces dark brown with scattered small white spots, facial mask

dark brown extending from tip of snout to groins, groins orange-brown; and (15) SVL in adult males unknown, SVL in adult females 14.21 mm ($N = 2$) (Table 4).

Diagnosis: *Phyllonastes sardinayacu* resembles its closest related species, *P. macuma*, *P. lochites*, and *P. myrmecoides*, by having a tympanic annulus, tympanic membrane, fingers not expanded distally, and acuminate toe tips. It differs from *P. macuma* by having subconical inner tarsal tubercle (rounded in *P. macuma*) and a mask extending to groins (mask extending



Figure 24. Live and preserved specimens of *Phyllonastes sardinayacu*. Lateral, dorsal, and ventral views of: A, B, holotype QCAZ 58822, adult female, SVL = 14.10 mm; and C, paratype QCAZ 58821, adult female, SVL = 14.32 mm. A, in life. B, C, in preservative. Scale bars are given for preserved adults.

to anterior half of flank in *P. macuma*), and by the absence of papillae in toe tips (present in *P. macuma*). *Phyllonastes sardinayacu* also differs from *P. lochites* and *P. myrmecoides* by having three phalanges in finger IV (two phalanges in finger IV in *P. lochites* and *P. myrmecoides*). It differs further from *P. lochites* by having a rounded snout in lateral view (subtruncate in *P. lochites*) and from *P. myrmecoides* by the absence of papillae in fingertips and toe tips (both present in *P. myrmecoides*) and by the presence of supernumerary plantar tubercles (absent in *P. myrmecoides*). For a comparison with other *Phyllonastes* species that are more phylogenetically distant, see [Tables 2 and 3](#).

Description of the holotype (Figs 24, 25): Adult female (QCAZ 58822). Measurements (in millimetres): SVL, 14.10; tibia length, 6.53; foot length, 6.39; head length, 3.77; head width, 4.33; eye diameter, 1.66; tympanum diameter, 0.78; interorbital distance, 1.87; upper eyelid width, 1.26; internarial distance, 1.68; eye–nostril distance, 0.92.

Head wider than long, head wider than body; canthus rostralis slightly convex in lateral view; loreal region straight in dorsal view; cranial crests absent; upper eyelid lacking tubercles.

Tympanic annulus beneath skin; tympanic membrane present; supratympanic fold and postrictal tubercles absent. Vomerine teeth absent, vocal slits and nuptial pads absent. Snout short and round in dorsal and lateral views, without rostral papilla.

Skin on dorsum and flanks finely shagreen; dorsolateral folds absent; ventral surfaces smooth; skin on cloacal region areolate; discoidal fold present. Ulnar tubercles absent, palmar tubercles low, outer palmar tubercle rounded, with a small extension pointing towards the centre of the palm, larger than elongate thenar tubercle; subarticular tubercles visible only at base of fingers, round in ventral and lateral view; supernumerary tubercles present; narrow lateral dermal fringes on fingers; discs narrow, bearing round and inconspicuous pads; fingers not expanded distally, tip of fingers subacuminate; circumferential grooves not visible; relative length of fingers is I < IV < II < III; phalangeal formula of hand is 2-2-3-3.

Hindlimbs robust; heels and knees without tubercles; tarsal folds (inner and outer) absent, outer tarsal tubercles absent; inner tarsal tubercle present, small, subconical, and prominent; inner metatarsal tubercle small (ill defined in preservative), elongated in ventral view and rounded in lateral view; round outer metatarsal tubercle well defined and prominent; plantar



Figure 25. Palmar (A) and plantar (B) surfaces of *Phyllonastes sardinayacu*. Photographs of left hand and left foot of the holotype QCAZ 58822.

surface with supernumerary tubercles; round subarticular tubercles, ill defined, visible only at base of toes; toes with narrow lateral dermal fringes; webbing between toes absent; discs on toes ill defined (ill defined in preservative), slightly expanded, with acuminate tip (specially on toe III), papilla on tip absent; ill-defined pads and circumferential grooves; relative lengths of toes $I < II < V < III < IV$; toe III longer than toe V.

Colour of holotype in life (based on digital photographs) (Fig. 24): Brown dorsum, slightly darker anteriorly, with two lateral, dark brown circular spots with a light brown border at sacrum level. Triangular cloacal blotch dark brown with light brown border. Ventral surfaces dark brown with scattered small white spots. Ventral surfaces of thighs and lower abdomen with irregular orange–brown blotches. Facial mask dark brown extending from tip of snout to groins and delineated dorsally by a light line. Flanks brown, with dark brown band along anterior half, connecting anteriorly with dark brown face mask. Groins brownish orange. Lips bearing small and white spots. Forearms, elbows, and knees with dark brown blotches delineated by a paler line.

Colour of holotype in preservative (Fig. 24): Dorsal surfaces brown. Head slightly darker than dorsum. Sacral lateral patches dark brown, with slightly lighter border. Cloacal triangle, spots

on knees, and elbows dark brown with lighter margins. Ventral surfaces brown, becoming darker towards the throat. Scattered cream spots on ventral surfaces, more marked posteriorly and on hindlimbs.

Variation (Fig. 24): This section refers to preserved individuals, unless otherwise mentioned. The only paratype, QCAZ 58821 (adult female), differs from the holotype in having a truncate snout in dorsal view and darker coloration. Morphometric variation is detailed in Table 4.

Distribution, natural history, and conservation status (Fig. 3): *Phyllonastes sardinayacu* is known from a single locality in Sangay National Park, near Sardinayacu, 1700 m a.s.l. Individuals were collected in Eastern Montane Forest at night (22:00–23:00 h) on leaf litter in primary and *terra firme* forest. Because of the lack of information on population size and geographical range, we suggest assigning *P. sardinayacu* to the Data Deficient IUCN Red List Category (based on IUCN Standards and Petitions Committee 2023).

Etymology: The specific name *sardinayacu* is a toponym used in apposition and it refers to a river at the species type locality. Sardinayacu is a compound word of Kichua origin, ‘sardina’ meaning sardine and ‘yaku’ meaning water.

Phyllonastes personinus Harvey, Almendáriz,
Brito & Batallas, 2013

(Figs 26, 27)

Notes about external morphology (Fig. 26): Comparing the original description of *P. personinus* with the Kutuku and Sumaco populations, we found a wider morphological variation than previously documented: in the type series, the dorsal skin was described as smooth with pustules, whereas in the Kutuku and Sumaco populations the dorsal skin is finely shagreened. Ventral skin was described as smooth, but in Kutuku it is areolate, and in Sumaco it is weakly areolate. The snout was described as rounded in dorsal view and subtruncate in lateral view; in Kutuku and Sumaco the snout is acuminate in both views. The inner tarsal tubercle is round in lateral view in the original description; however, it is conical in Kutuku and Sumaco. According to the original description, *P. personinus* lacks supernumerary plantar tubercles, but the Sumaco population does have them. Finally, the characteristic dark mask of *P. personinus* was described as short and extending only to the anterior third of the flank; in Kutuku, the mask extends to the groins. These morphological differences could indicate the existence of more than one species within *P. personinus* (see ‘Remarks’ section).

Distribution and natural history (Fig. 3): *Phyllonastes personinus* was known only from the type locality region (Ecuador, Morona Santiago Province, Canton Morona, Sinaí Parish, Sardinayacu Lake Complex) between 1647 and 1916 m a.s.l. (Harvey *et al.* 2013), the Sangay-Llanganates Ecological Corridor (Instituto Nacional de Biodiversidad 2023), and the Cordillera del Cóndor mountain range (Valencia *et al.* 2023). The species had been reported only in primary rainforest in swampy, densely vegetated areas along the edge of lakes. In this study, we report four more Ecuadorian populations. First, Morona Santiago Province, Canton Santiago de Méndez, San Francisco de Chinimbimi Parish, Kutuku mountain range and Contrafuerte de Tzunatza between 1355 and 1407 m a.s.l. (Fig. 26B; for the specimen list, see Table S1). Most of these individuals were collected at night between 20:00 and 00:30 h in primary *terra firme* forest. They were found on the ground, on moss, or under logs or dry or wet leaf litter, and on bromeliads 15 cm above the ground, often near creeks with small streams (1 or 2 m wide) of clear water. Individuals QCAZ 71452 and QCAZ 71453 were found amplexed on leaf litter on the ground. Three individuals (QCAZ 71454–56) were collected in secondary forest near grasslands on the ground on leaf litter and near small streams. One individual (QCAZ 71455) was collected in the afternoon ~15:40 h and was found on wet leaf litter on a creek slope. Second, Napo Province, Pacto Sumaco, surroundings of Sumaco National Park, 1500 m a.s.l. (Fig. 26C; for the specimen list, see Supporting Information, Table S1). Third, Morona Santiago Province, Canton Morona, Sinaí Parish, between 1345 and 1874 m a.s.l. (for the specimen list, see Supporting Information, Table S1). Specimens were collected in leaf litter or perching on leaves 5 cm above the ground, at night between 19:00 and 23:40 h; one specimen (QCAZ 58820) was collected at 14:30 h. The collection localities were in primary forest, and some were near the Jurumbuno River, Volcan River, and Cormoran Lagoon. Fourth,

Pastaza Province, Canton Mera, Mera Parish, Llanganates National Park, Zarentza Community, between 1331 and 1419 m a.s.l. (for the specimen list, see Supporting Information, Table S1). Specimens were collected at night between 21:00 and 01:15 h, in leaf litter or perching on leaves 15–100 cm above the ground in primary dryland forest near streams and small creeks.

Remarks: We report notable morphological differences between populations that could indicate the existence of one or two unnamed species within ‘*P. personinus*’. One species would be in the Kutuku mountain range, Morona Santiago Province, and the other in the Sumaco National Park, Napo Province. This hypothesis is supported by relatively high uncorrected p-genetic distances for 16S ($\leq 3.6\%$; Supporting Information, Table S7) and 12S ($\leq 2.0\%$; Supporting Information, Table S9).

***Urkuphryne* gen. nov.**

(Fig. 4)

LSID: urn:lsid:zoobank.org:act:95EC41FF-368A-4DAC-82D7-BB4F3462B89F

Order: Anura [Oppel, 1811](#).

Superfamily: Brachycephaloidea [Günther, 1858](#).

Family: Strabomantidae [Hedges *et al.*, 2008](#).

Subfamily: Holoadeninae [Hedges *et al.*, 2008](#).

Genus: *Urkuphryne* gen. nov.

Type species: *Urkuphryne merinoi* sp. nov. (described below).

Definition (Tables 2 and 3): (1) Larger than its sister genus, *Phyllonastes* (average adult female SVL = 19.7 mm, adult male = 17.2 mm, Table 4); (2) head wider than long, narrower than body, body robust; (3) columella, tympanic annulus and tympanic membrane present; (4) cranial crest absent; (5) finger I < finger II; (6) distal phalanges of fingers and toes rounded; (7) knees and heels without tubercles; (8) presence of inner tarsal fold; (9) fingers and toes lacking circumferential grooves and lateral dermal fringes; (10) toe V < toe III; (11) hand phalangeal formula 2-2-3-3; foot phalangeal formula 2-2-3-4-3; (12) dark facial mask extending to the groins, triangular cloacal blotch present; (13) thin frontoparietals, longer than wide, big orbital fossae; (14) very prominent premaxillary and maxillary teeth present; (15) large nasal bones, almost in contact with maxilla; (16) zygomatic branch of squamosal shorter than otic branch; (17) large vomers with protruding vomerine teeth; (18) occipital condyles widely separated from each other; (19) prominent medial ridges present in all presacral and sacral vertebrae; (20) urostyle crest very prominent; (21) broadly expanded sacral diapophyses; (22) very large prepollex and prehallux present.

Remarks: Autapomorphies for this genus are the reduction of the distal expansion of the phalanges of fingers and toes (Figs 7D, 8), the absence of supernumerary plantar tubercles (Supporting Information, Fig. S20), and protruding vomerine teeth (see ‘Diagnosis’).

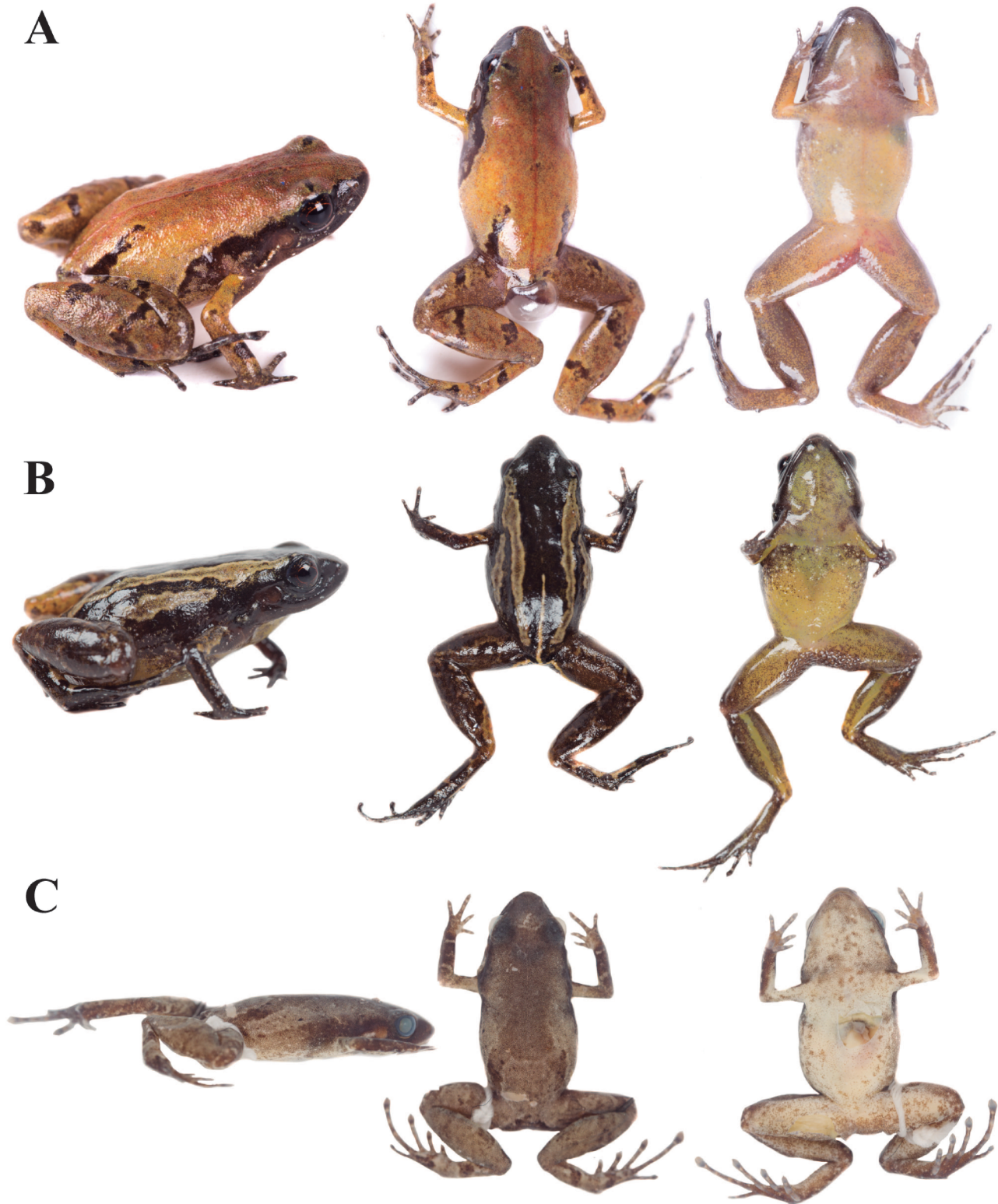


Figure 26. Live and preserved specimens of *Phyllonastes personinus*. A, QCAZ 59437. B, QCAZ 71453. C, QCAZ 31118. A, B, in life. C, in preservative.

Diagnosis: *Urkuphryne* can be distinguished easily from its sister clade, the genus *Phyllonastes* by (characteristics of *Phyllonastes* shown in parentheses): (1) tips of fingers and toes subacuminate and rounded (tips pointed); (2) vomerine teeth present (vomerine teeth absent), and (3) larger size (Table 4).

Osteologically, *Urkuphryne* differs from *Phyllonastes* by having a shorter skull and a slightly broader maxilla, with a broader space between angulosplenials, thinner frontoparietals and larger orbital fossae (broader frontoparietals with smaller orbital fossae), bigger and more conspicuous premaxillary and maxillary teeth

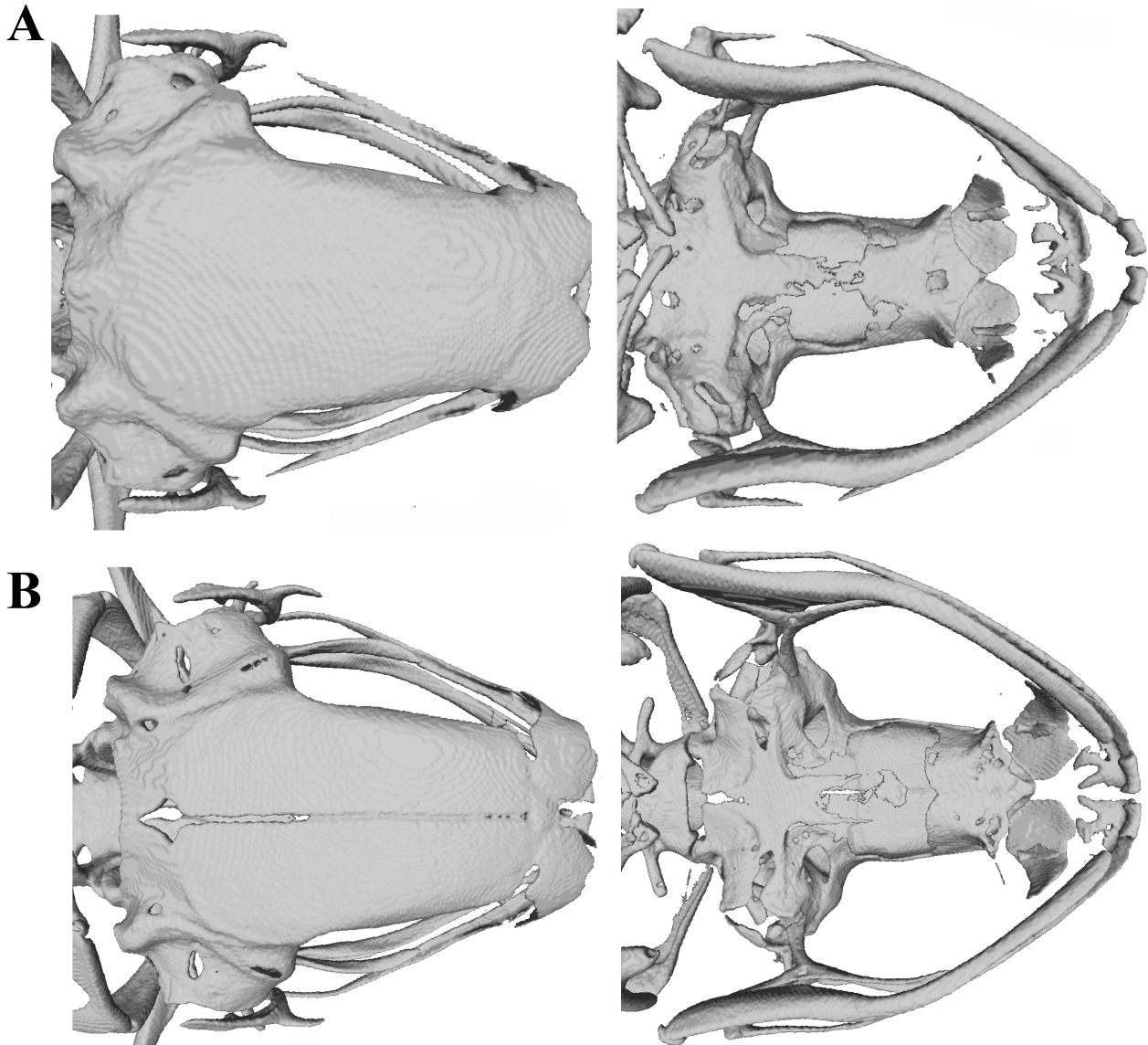


Figure 27. Skeletons of *Phyllonastes personinus*. A, QCAZ 58818. B, QCAZ 31115.

(premaxillary and maxillary teeth present but smaller), broader nasal bones almost in contact with the maxilla (nasal bones small, broadly separate from maxilla), vomers large and prominent, bearing protruding teeth (vomeres reduced, broadly separated from each other, vomerine teeth absent), prominent medial ridges present on all presacral and sacral vertebrae (low medial ridges present only on presacral vertebrae), very prominent prepollex and prehallux (small prepollex and prehallux), and terminal phalanges rounded in fingers and toes (terminal phalanges expanded in fingers and toes).

Urkuphryne differs from *Barycholos* by the absence of dorsolateral folds (dorsolateral folds present), by the reduction of the distal expansion of the phalanges of fingers and toes, and by the arrangement of the vomerine teeth (small, oblique, broadly separated, and posteromedial to choanae in *Urkuphryne*; and in two long arcuate series extending beyond the choana in *Barycholos*). *Urkuphryne* can be distinguished from *Bahius* by the absence of circumferential grooves of fingers and toes (both present

in *Bahius*) and by the presence of an inconspicuous and thin inner tarsal fold (conspicuous, short, tubercle-like inner tarsal fold present in *Bahius*). The presence of a tympanic membrane, tympanic annulus, and inner tarsal tubercle differentiates *Urkuphryne* from *Euparkerella* and *Holoaden* (tympanic membrane, tympanic annulus, and tarsal tubercle absent), two genera sequentially sister to *Urkuphryne* + *Phyllonastes* + *Barycholos* + *Bahius*.

Content: One species, *Urkuphryne merinoi* sp. nov.

Etymology: The name refers to the type locality of the type species, 'Cerro Golondrinas protective forest' (Golondrinas hill). *Urkuphryne* is a compound word: *Urku* means 'hill' in the Native American Quichua language, and *phryne* means 'frog'.

Distribution: Pacific Basin of Northern Ecuador, western Andean slopes at elevations 2500–2800 m a.s.l.



Figure 28. Holotype of *Urkuphryne merinoi*. Lateral, dorsal, and ventral views of holotype, QCAZ 66078, adult female, SVL = 19.53 mm. A, in life. B, in preservative. Scale bar is given only for specimen in preservative. The depigmentation visible in the specimen is attributable to preservation defects.

***Urkuphryne merinoi* sp. nov.**

LSID: urn:lsid:zoobank.org:act:FD715F02-0CB4-4A5F-93C2-BFD649C05240

Holotype (Figs 28, 29): QCAZ 66078 (field no. SC-PUCE 48592) adult female from Ecuador, Carchi Province, Canton Espejo, El Goaltal Parish, protective forest Cerro Golondrinas, trail from the Heliconia Cabin to the Cortadera (0.8204°N, 78.0944°W), 2600 m a.s.l. Collected by Diego Almeida, Kunam Nusirquia, Darwin Núñez, Fernando Ayala, David Mantilla, Santiago Recalde, Carlos Castro, and Polibio Malte on 12 October 2016.

Paratypes ($N = 8$; Fig. 30): All collected in Ecuador, Carchi Province. QCAZ 66080 juvenile, QCAZ 66081–82 adult males, QCAZ 66079, QCAZ 66083, and QCAZ 66091 adult females, same locality as holotype; QCAZ 66085 adult male from protective forest Cerro Golondrinas, Waterfall trail to Las Juntas (0.8217°N, 78.0951°W), 2544 m a.s.l.; collected by Diego Almeida, Kunam Nusirquia, Darwin Núñez, Fernando Ayala, David Mantilla, Santiago Recalde, Carlos Castro, and Polibio Malte on 12 October 2016. QCAZ 41813 adult female from Ecuador, Carchi Province, La Comadre waterfall (0.8233°N, 78.0232°W), 2740 m a.s.l. Collected by Juan Fernando Dueñas and Ítalo Tapia on 18 September 2008.

Proposed standard English name: Merino leaf litter frog.

Proposed standard Spanish name: Cutín de hojarasca de Merino.

Definition (Figs 28–33; Tables 2 and 3): We assign the new species to the genus *Urkuphryne* based on its phylogenetic relationships. The new species is characterized by: (1) skin on dorsum smooth to finely shagreen, dorsolateral folds absent, dorsal surfaces of thighs smooth, finely shagreen or shagreen, skin on throat, chest and belly smooth, discoidal fold present, ventral surfaces of thighs finely shagreen, skin on flanks shagreen to weakly areolate; (2) tympanic membrane, tympanic annulus, supratympanic fold, and postrectal tubercle present; (3) snout rounded to broadly rounded in dorsal and lateral views; (4) upper eyelid without tubercles, cranial crests absent; (5) vomerine teeth present; (6) vocal slits present, nuptial pads absent; (7) fingers not expanded distally, finger tips rounded to subacuminate, lacking papillae, finger I shorter than finger II, supernumerary tubercles present; (8) fingers lacking lateral fringes, pads present, lacking circumferential grooves; (9) distal phalanges of all toes and fingers narrower distally, with the tip pointed; phalangeal formula of hand 2-2-3-3; (10) ulnar tubercles absent; (11) knees and heels without tubercles, outer edge of tarsus without tubercles, inner edge of tarsus bearing an inconspicuous fold; (12) inner metatarsal tubercle elongate in ventral view and rounded in lateral view, bigger than rounded outer metatarsal tubercle; (13) toes not expanded distally, with rounded to subacuminate toe tips, lacking papillae, supernumerary tubercles absent, lateral fringes on toes absent, toe basal webbing present, all toes bearing well-defined pads lacking circumferential grooves, toe V shorter than toe III; (14) in life, dorsal surfaces dark brown,

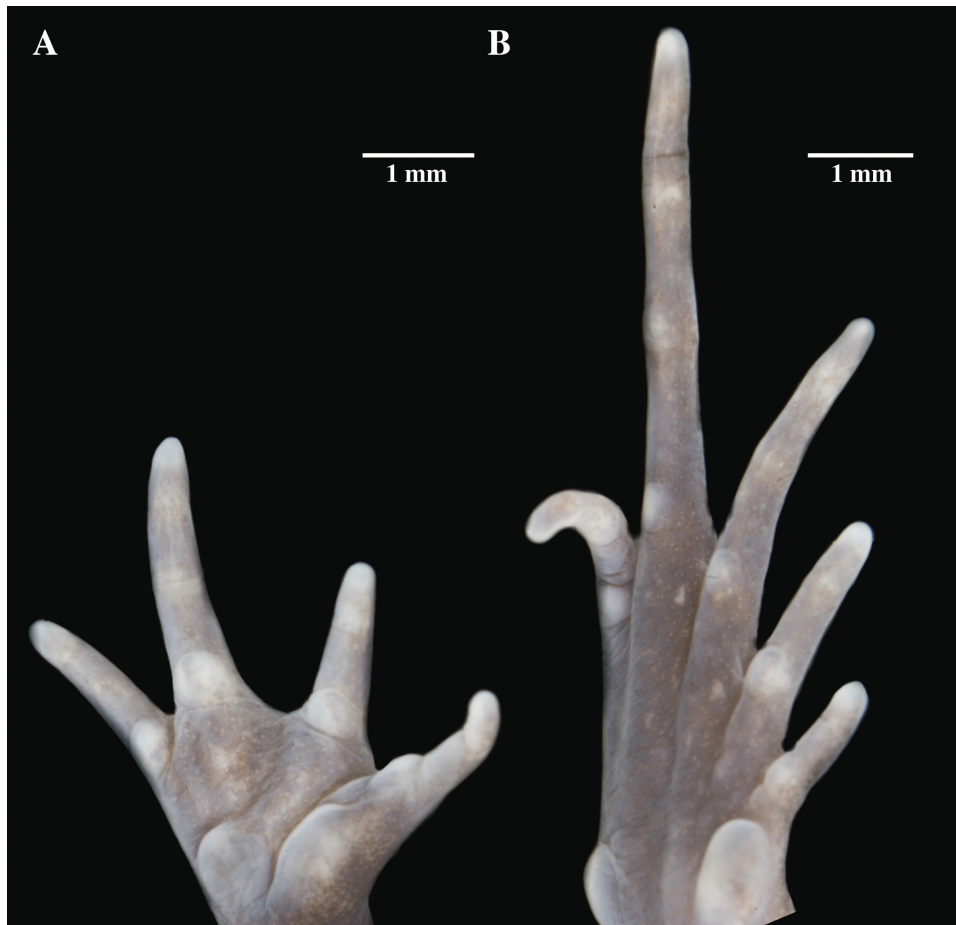


Figure 29. Palmar (A) and plantar (B) surfaces *Urkuphryne merinoi*. Photographs of right hand and right foot of the holotype QCAZ 66078.

bearing darker circular sacral lateral patches delineated by an orange line; dark brown facial mask from the tip of snout to near the groins, bordered dorsally by an orange line; throat dark brown or cream in females and almost black in males; ventral surfaces light brown or brown, bearing white spots; and (15) SVL in adult males 17.22 mm ($N = 3$) and SVL in adult females 19.69 mm ($N = 5$) (Table 4).

Diagnosis (Tables 2 and 3): *Urkuphryne merinoi* resembles species of the genus *Phyllonastes* but can be distinguished from them by the presence of vomerine teeth (absence of vomerine teeth is a synapomorphy of *Phyllonastes*) and by the absence of circumferential grooves on toes (present in all *Phyllonastes* species). *Urkuphryne merinoi* can be differentiated easily from *Barycholos pulcher* (Boulenger, 1898) by the presence of vomerine teeth in two small rows, oblique, broadly separated, and posteromedial to choanae (vomerine teeth in two long transverse rows posterior to the level of choana, narrowly separated in *Barycholos pulcher*).

Description of the holotype (Figs 28 and 29): Adult female (QCAZ 66078). Measurements (in millimetres): SVL, 19.53; tibia length, 7.79; foot length, 8.66; head length, 5.74; head width, 7.05; eye diameter, 2.14; tympanum diameter, 1.18; interorbital distance, 1.93; upper eyelid width, 1.31; internarial distance, 1.79; eye–nostril distance, 1.51.

Head wider than long, head wider than body; canthus rostralis slightly convex in lateral view; loreal region slightly concave in dorsal view; cranial crests absent; upper eyelids bearing no tubercles. Tympanic annulus weakly defined, differentiated only at its lower half; tympanic membrane present; small supratympanic fold present; poststrictal tubercle present. Snout rounded in dorsal and lateral views, without rostral papilla. Vomerine teeth present, small, oblique, broadly separated, posteromedial to choanae; each vomer bearing small teeth; vocal slits and nuptial pads absent, 30 teeth visible in the upper maxilla.

Skin on dorsum smooth, skin on flanks shagreen; dorsolateral folds present; skin on throat, chest, and belly smooth; ventral surfaces of thighs finely shagreen; discoidal fold absent; skin in ventral cloacal region areolate. Ulnar tubercles absent; palmar tubercles prominent, outer palmar tubercle circular on right hand and slightly elongate on left hand, thenar tubercle large and elongate; proximal subarticular tubercles well defined, round in ventral and lateral view; distal subarticular tubercles not visible; minute and round supernumerary tubercles all over palmar surface; lateral dermal fringes absent; discs narrow, rounded, and bearing well-defined rounded pads without circumferential grooves; fingers not expanded distally, tip of fingers rounded without papillae; phalangeal formula of 2-2-3-3; relative length of fingers is $I < II < IV < III$.

Hindlimbs robust; dorsal surface of hindlimbs smooth; posterior and ventral surfaces of thighs shagreen; heel and knee

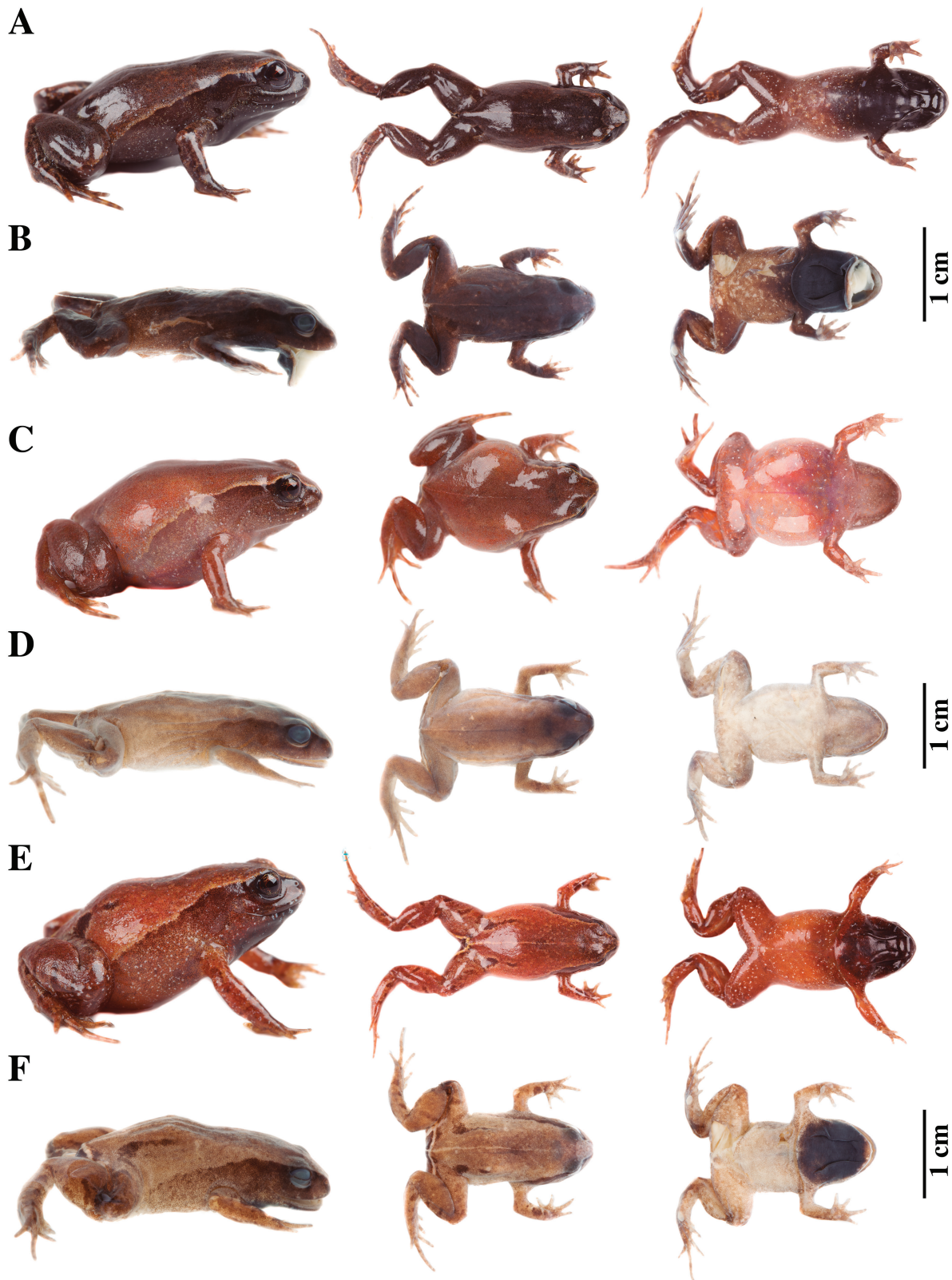


Figure 30. Live and preserved specimens of *Urkuphryne merinoi*. Lateral, dorsal, and ventral views of: A, B, QCAZ 66082, adult male, SVL = 18.33 mm; C, D, QCAZ 66083, adult female, SVL = 19.40 mm; and E, F, QCAZ 66085, adult male, SVL = 18.16 mm. A, C, E, in life. B, D, F, in preservative. Scale bars are given only for preserved adults.

without tubercles; outer tarsal folds absent; inner tarsal fold present, inconspicuous and thin; outer tarsal tubercles absent; inner tarsal tubercle absent; inner metatarsal tubercle

small (1.08 mm), prominent, elongate in ventral view and rounded in lateral view, 1.86 × longer than rounded; outer metatarsal tubercle small (0.75 mm), well defined, rounded,

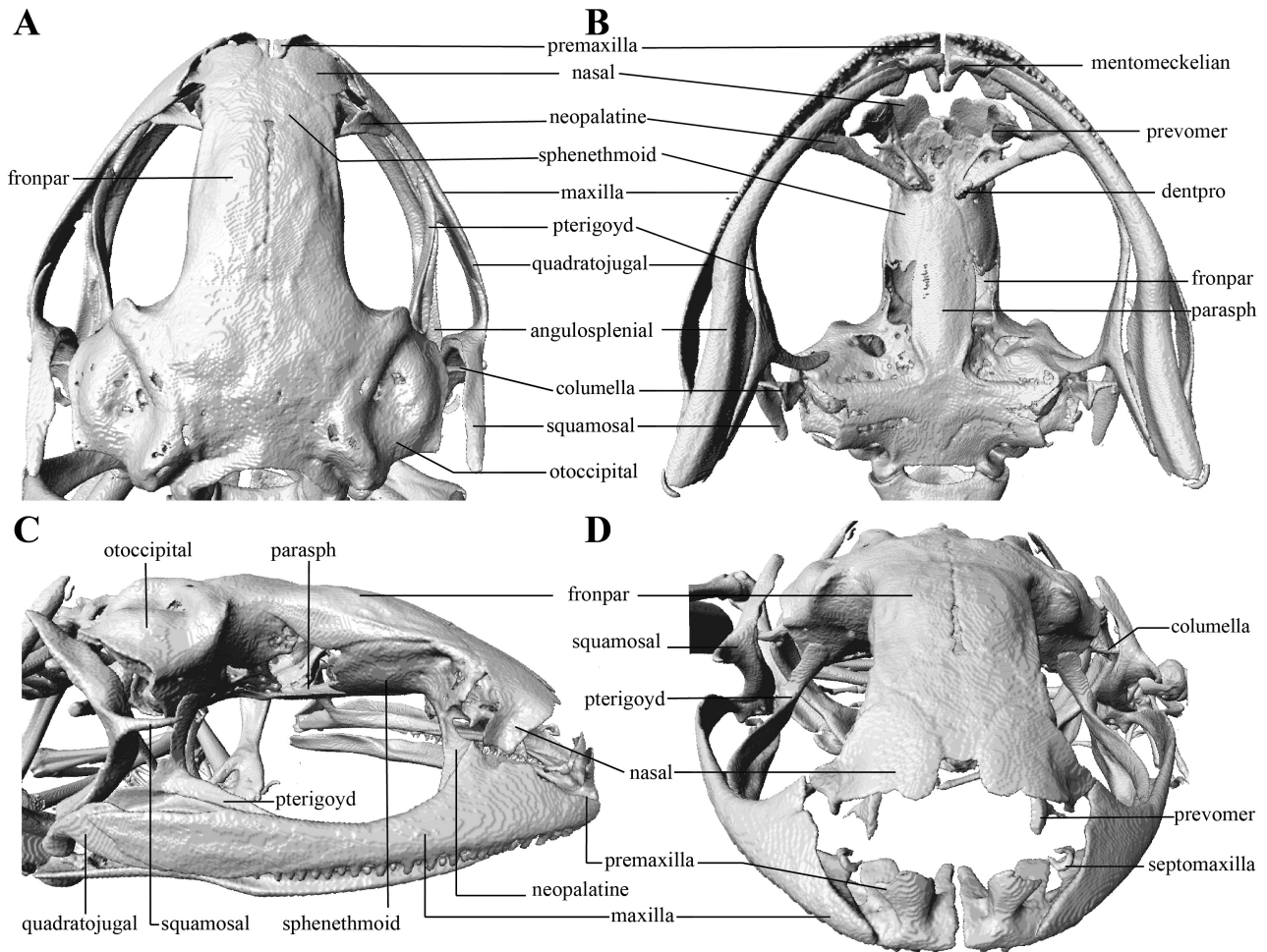


Figure 31. Skull of *Urkuphryne merinoi* holotype QCAZ 66078. The skull is shown in dorsal (A), ventral (B), lateral (C), and frontal (D) views.

and prominent; plantar surface without supernumerary tubercles; basal subarticular tubercles well defined, round in dorsal view; distal subarticular tubercles not visible; toes without lateral dermal fringes; basal webbing between toes present; discs narrow, rounded and bearing well-defined rounded pads without circumferential grooves; toes not expanded distally, tip of toes rounded without papillae; relative length of toes is $I < II < V < III < IV$; toe III longer than toe V (toe III surpasses the distal border of the second subarticular tubercle of toe IV; toe V reaches the proximal border of the second tubercle of toe IV).

Colour of holotype in life (based on digital photographs) (Fig. 28): The dorsal surface is dark brown, with a few scattered white and low tubercles, and covered by small orange dots that group in two conspicuous lateral lines (one on each side) from the arm insertion to the tip of the snout through the upper eyelids. Posteriorly, the dorsum bears two dark brown circular sacral lateral patches, with a few orange flecks and delineated by an orange line formed by the aggregation of the same orange dots, more densely grouped medially at the level of the sacrum. The dorsal surface of limbs is dark brown, covered with white and orange flecks; it bears a few irregular dark brown blotches

delineated by aligned orange dots. Dorsal feet surface dark brown, covered by orange and yellowish brown flecks and with irregular dark brown blotches with yellowish brown borders formed by the alignment of the flecks. Laterally, a dark brown facial mask extends as a dark band from the tip of snout to near the groins. The facial mask bears irregular white marks and orange and yellowish brown flecks more conspicuous rostrally. The flecks form ill-defined bars in the upper lip, with white marks. Along its path, the mask is bordered dorsally by orange spots, longitudinally aligned. Groins are dark brown, uniformly covered by small orange dots and with some scattered white marks. Throat uniformly dark brown, darker than belly and limb ventral surfaces, with white scattered marks. Belly and limb ventral surfaces with dark brown flecks densely aggregated in many irregular patches alternated with yellowish brown irregular blotches, with fewer dark brown flecks. Posterior surfaces of thighs dark brown with orange flecks; flecks form an orange stripe in the upper cloacal region that extends over the thighs.

Colour of holotype in preservative (Fig. 28): Dorsal surfaces dark brown, with darker sacral lateral circular patches surrounded by a poorly defined cream edge. Facial mask dark brown (darker than

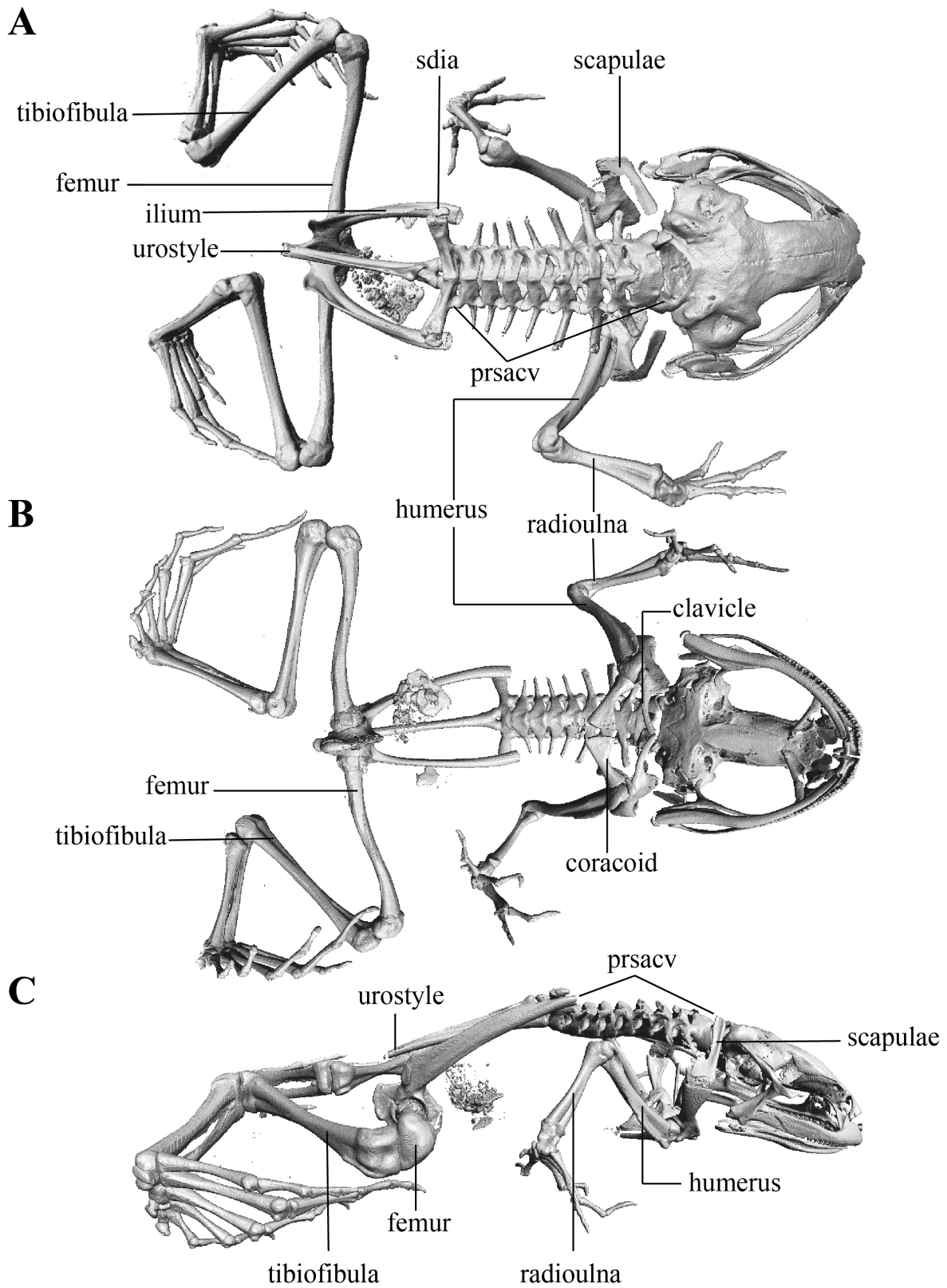


Figure 32. Computed tomography scan images of the skeleton of *Urkuphryne merinoi* holotype QCAZ 66078, SVL = 19.53 mm, in dorsal (A), ventral (B), and lateral (C) views.

dorsal surface) to black extending from the tip of snout to near the groins, delimited dorsally by a thin cream line. Throat dark brown, belly and ventral surfaces of limbs with a mosaic of cream

and dark brown blotches bearing dark brown flecks. Posterior surfaces of thighs dark brown, with a darker triangular blotch in the cloacal region limited on its upper side by a thin cream line.

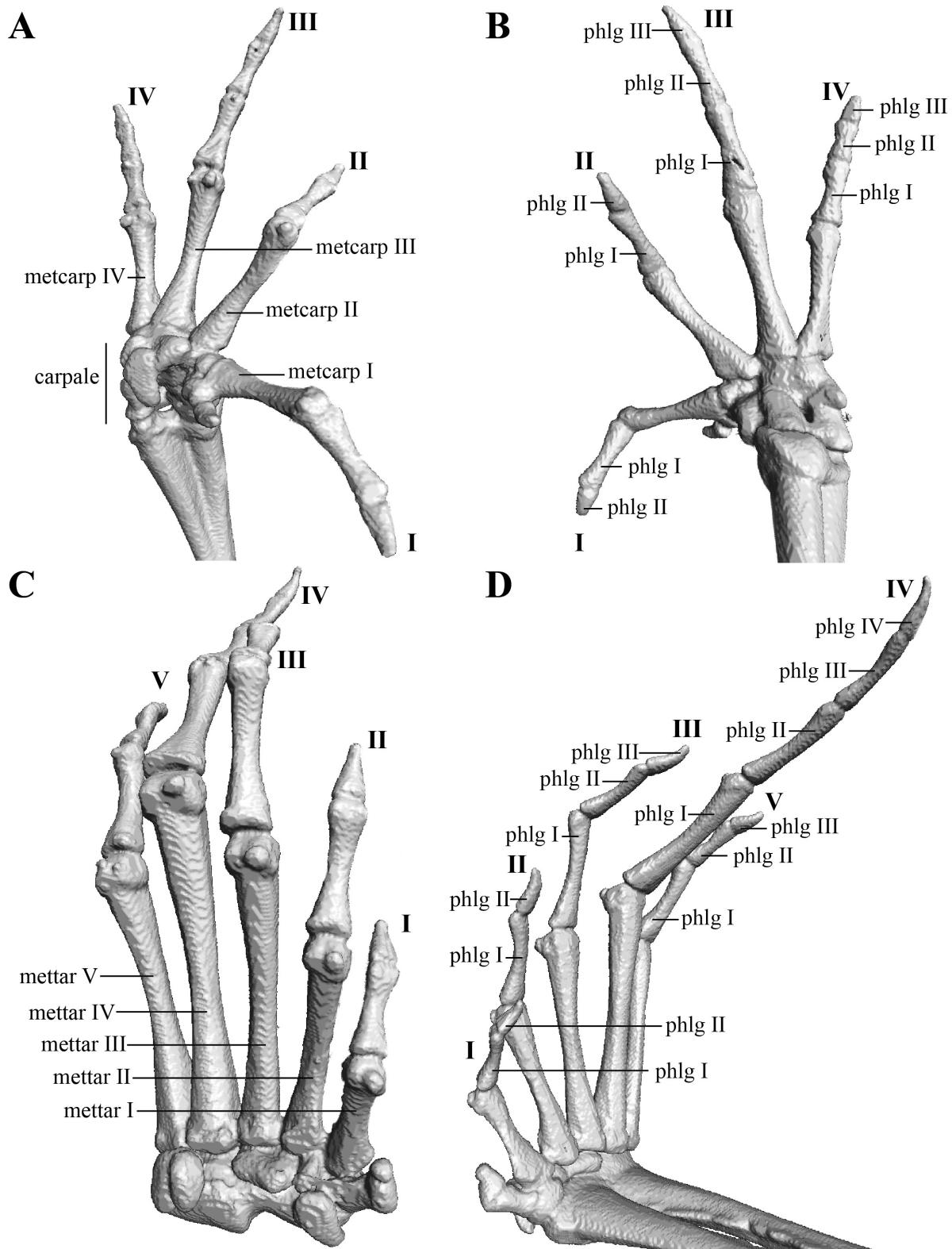


Figure 33. Computed tomography scan images of the hand and foot osteology of *Urkuphryne merinoi* holotype QCAZ 66078. The right hand is shown in ventral (A) and dorsal (B) views. The left foot is shown in ventral (plantar) (C) and dorsal (D) views.

Variation (Fig. 30): Vocal slits are present in adult males (e.g. QCAZ 66085); dorsum skin might be finely shagreened (e.g. QCAZ 66079 and QCAZ 66083) and on flanks (e.g.

QCAZ 41813); the latter can also be weakly areolate (QCAZ 66083). Snout might be broadly rounded (QCAZ 66083). Supernumerary palmar tubercles might be inconspicuous

(e.g. QCAZ 66091); tip of fingers might be subacuminate (e.g. QCAZ 66081). Dorsal surfaces of limbs might be weakly shagreened (e.g. QCAZ 66085 and QCAZ 66091) or shagreen (e.g. QCAZ 41813); toe III might be subacuminate (QCAZ 66082). Live individuals might have dark brown, almost black (e.g. 66082), or cream (e.g. QCAZ 66091) throat and chest; the round sacral lateral patch might expand anteriorly to the iliac region (e.g. QCAZ 66085) or be inconspicuous (QCAZ 66083); belly and dorsal surfaces might be light brown (e.g. QCAZ 66085); the entire coloration can be lighter (e.g. QCAZ 66083 and QCAZ 66091). Morphometric variation is detailed in Table 4.

Osteology

The osteological description is based on micro-CT images of the holotype (adult female QCAZ 66078) and paratypes (adult females QCAZ 41813 and QCAZ 66091).

Skull (Fig. 31): The skull is slightly wider than long; the widest section is at the quadratojugal–maxillary joint. The longest part of the skull, measured from the anterior face of the premaxilla to posterior border of the exoccipital, is 92.5% of its widest section. The rostrum is short, with a distance from the anterior edge of the frontoparietals to the anterior face of the premaxilla of ~32.2% of the skull length (measured from the anterior face of the premaxilla to posterior face of the exoccipital). At the level of the anterior edge of orbits, skull is ~62.2% of the maximum skull width and reaches ~88.5% of the maximum skull width at the level of midorbit. The posterior edge of orbits reaches 99.2% of the maximum skull width and is located posterior to it.

The braincase contains well-ossified elements. The frontoparietals are well-developed bones, markedly longer than wide and slightly narrower anteriorly than posteriorly; frontoparietals are ossified and sutured along their entire length, but they leave a thin, short, unossified fontanel at their anterior end. At their posterior end, the frontoparietals are completely sutured with the otoccipitals, together forming prominent ridges on each side and a completely closed braincase. The ridges formed have very small unossified patches. The otoccipitals are formed by well-fused prootic and exoccipital, with small unossified patches in the crests they formed when fused. Ridges formed between frontoparietals + otoccipitals and prootic + exoccipitals form a continuous V-shaped ridge, with the anterior ramus (frontoparietals + otoccipitals) more prolonged (posterior ramus is 61.96% of the anterior ramus). The apex between rami is medial and angled at slightly $>90^\circ$. At their anterior and lateral end, the frontoparietals fuse with the sphenethmoids. The latter have complete ossification and are fused ventrally with the anterior portion of the cultriform process of the parasphenoid. Ventrally and posteriorly, the sphenethmoids surpass the midpoint of the orbits.

The cultriform process of the parasphenoid is complete and well ossified, with a biconvex shape, with anterior and posterior ends pointed and thinner than its medial segment; at its base (at the anterior border of the alar processes of the parasphenoid) is ~8.21% of the maximum skull width and reaches its maximum thickness at its midpoint (24.09% of the maximum skull width). It is important to mention that the alar processes do not emerge from the posterior end of the cultriform process, but a few

millimetres anteriorly, hence the posterior tip of the cultriform process protrudes posteriorly. Fenestra vestibule (parasphenoid alar processes + otoccipitals) is poorly ossified, and their shape cannot be detailed.

The neopalatines are thin and separated from one another. They articulate with the ventral face of the sphenethmoid by their upper tip and with the internal face of the maxilla in its anterior third, by their lower end forming the anteroventral corner of the orbit. The septomaxilla is small and horseshoe shaped, with a medial and slightly posterior opening; both ends are pointed, and the centre is widened and flattened laterally; both ends are free and do not articulate with any bone. The prevomers are large, located medial, superior, and posterior to the septomaxilla; they are broadly separated from one another medially; the separation is greater rostrally. The dentigerous processes are conspicuous, more visible ventrally, in the left prevomer. The columella (or stapes) is large and well ossified. The nasals are thin and posterolaterally expanded. They are ossified only in their posterior portion, hence they are completely distant from the alar processes of the premaxilla. Posteroventrally they are fused with the sphenethmoids and posteriorly with the anterior border of the frontoparietals; their posterolateral expansion is close but not fused to the neopalatine + maxillary joint.

The maxillary arch bears many small and moderately sized teeth on the maxillae and on the transversal section of the premaxillae. The premaxillae are partly separated medially, and their rostral alary processes rise divergent from the midline. Alary processes of the premaxillae are prominent and widened in the opposite direction to their base, rising perpendicular to the cross-section of the premaxillae. They are separated ventrally from each other. The short premaxilla and maxilla are in lateral contact by juxtaposed articulation. The maxilla becomes narrow posteriorly, reaching an acuminate caudal end, which is in contact, on its inner side, with the quadratojugals. The triradiate pterygoid bears a long, curved rostral ramus oriented anterolaterally that fuses with the internal face of the maxilla near its midpoint; this ramus is the longest of the three, it is flattened laterally, and its anterior end is thinner than the posterior one. The caudal ramus is shorter than the rostral one and as wide as the latter in its initial portion, and likewise, it sharpens towards the tip (posterior end), which merges with the posterior tip of the angulosplenic; this ramus is also flattened laterally. The medial ramus has the same length as the caudal, is widened in its terminal portion and flattened anteroposteriorly; on its posterior face it articulates with the anterolateral surface of the otoccipital.

The quadratojugal is well ossified; it articulates by its dorsoposterior face with the ventral ramus of the T-shaped squamosal. The squamosal has three rami; the posteroventral ramus widens towards its free (posterior) end as it moves away from its base; this ramus is flattened anterodorsally, it is slightly shorter than the posterodorsal ramus and longer than the zygomatic or anterior ramus. The posterodorsal ramus is flattened dorsoventrally, and its root is very close to the columella; the small zygomatic ramus is flattened laterally. Both branches (posterodorsal and anterior) become pointed towards their free ends and do not articulate with any bony structure.

The mandible is slim and completely edentate. The mentomeckelians are small, medially separated from each other, in the shape of a cylinder widened towards their ends; they are in contact posteriorly with the dentaries, which are short, acuminate towards the posterior end, and flattened anterodorsally. From the middle of its posterior border and with its posterior end, the dentary bones articulate with the anterior face of the angulosplenial. The angulosplenial is long, arcuate, and expanded at its posterior end; it articulates broadly by its anterolateral face with the posteromedial face of the slim and relatively small dentaries. The only ossified portions of the hyoid apparatus are the two posteromedial processes, which are moderately expanded anteriorly and posteriorly. Both posteromedial processes present a steep anteroventral inclination and are moderately separated from one another at the anterior ends; the separation between them increases posteriorly.

Postcranium (Fig. 32): There are eight non-imbricate presacral vertebrae. The first presacral vertebra (cervical vertebra) is wider than posterior vertebrae and has no diapophyses. The cervical vertebra has a type I cotylar arrangement. The cervical cotyles receive the occipital condyles of the cranium, which are widely separated from each other, leaving a foramen magnum of 21.69% of the maximum skull width.

Presacral vertebrae II–VIII bear well-developed diapophyses. The transverse processes of the presacrals increase in length as they move away from the skull, with the transverse processes of presacral II being the shortest. The transverse processes of presacral II are horizontal and have a dorsoventral flattening and slightly widened lateral free ends. The transverse processes of presacral III are slightly rotated forwards and present an anteroposterior flattening; in addition, their lateral free ends are evidently wider. From presacral IV to VII, the transverse processes are rotated 90° and are also flattened anteroposteriorly; these processes are not completely ossified toward their ends. In width, the processes of presacral III are followed by those of presacral II, the second widest slightly expanded distally, and those of presacral IV, the third widest, with their edges parallel along its entire length. Transverse processes of presacrals V–VIII are the smallest and similar in size (length and width) between them. This vertebrae of this species are characterized by having a holochordal centrum.

The sacrum bears moderately expanded diapophyses. Transverse processes are oriented laterally and slightly dorsally, with an angle of dorsal opening of ~140°, and articulate distally with the ilia, a few millimetres anterior to its front end. The sacrum is articulated caudally with the coccyx or urostyle by a bicondylar articulation. The long and thin urostyle is slightly longer than the presacral portion of the vertebral column (the presacral portion of the vertebral column is 91.85% of the urostyle) and bears a well-developed longitudinal ridge, which is largest anteriorly (at the point of its articulation with the sacrum) and gradually decreases in height posteriorly. The urostyle does not have complete transverse processes nor remnants and is not fully ossified at its posterior end. The sacrum–ilia articulation is not visible in the micro-CT scan. The ilia articulate posteromedially with each other and posteriorly with the ischia and present a long shaft.

In the pectoral girdle, the clavicles are long and slim, oriented anteromedially, curved with an anterior opening concavity, with the medial tips articulated between them. The coracoids are stout, with the anterior edge curved, with a pronounced anterior opening concavity, and with a straight posterior edge; their medial tips are separate from each other, and their sternal and glenoidal ends are widened, the sternal ones more than the glenoidal ones. The scapula is long, with the anterior edge slightly oriented anteromedially. Epicoracoids are visible. The sternum has no well-ossified elements. The omosternum is absent.

Manus and pes (Fig. 33): All phalanges are well ossified, with a phalangeal formula for the fingers and toes of 2-2-3-3 and 2-2-3-4-3, respectively. The increasing order of finger length is I < II < IV < III, and that of toes is I < II < III < V < IV. Distal phalanges of all toes and fingers are narrower distally, with the tip pointed. Bones of the carpus and metacarpus are completely ossified.

Distribution, natural history, and conservation status (Fig. 3): *Urkuphryne merinoi* is known from the surroundings of Protective Forest Cerro Golondrinas from 2500 to 2800 m a.s.l. in Western Montane Forest. Surrounding the protective forest, in both highlands and lowlands, there are deforested areas, some in regeneration, near human settlements and artificial open areas for agriculture and cattle raising. Individuals were collected in secondary forest, in the afternoon (between 12:30 and 13:30 h) on mossy rock walls with high humidity or buried in leaf litter, the adult male QCAZ 66091 was found vocalizing at 12:30 h buried in soil; and at night (19:00–22:30 h) on very damp rock walls ~150 cm from the ground, on leaf litter and mossy soils near creeks, or buried ~3 cm deep in soil. All females found were next to clutches with 8–12 eggs. One female (QCAZ 41813) was collected between 9:00 and 10:30 h on the roadside in a mossy habitat with herbaceous plants, buried under moss next to a clutch of white eggs.

Because of the lack of information on population size and geographical range, we assign *U. merinoi* to the Data Deficient IUCN Red List Category (based on [IUCN Standards and Petitions Committee 2023](#)).

Etymology: The specific name *merinoi* is a noun in the genitive case and is a patronym for Andrés Merino-Viteri, an Ecuadorian herpetologist, professor at Pontificia Universidad Católica del Ecuador (PUCE). During his career, Andrés Merino has contributed significantly to the study of chytridiomycosis and possible consequences of climate change in anurans. At PUCE, he is director of The Threatened Amphibian Conservation Initiative of Ecuador ‘Balsa de los Sapos’, one of Ecuador’s largest and long-lasting *ex situ* amphibian conservation projects in the world.

Embryonic development in *U. merinoi* and *P. personinus*

The *U. merinoi* clutch (Fig. 34A) was collected in the daytime, among moss with a lot of humidity on a rock wall. It was next to an adult female, presumably its mother. We were unable to observe behaviours related to mating or fertilization. It had 12 eggs, with relatively transparent jelly coats. Out of 12 eggs, 9 had developing embryos and 3 were unfertilized. Unfertilized eggs

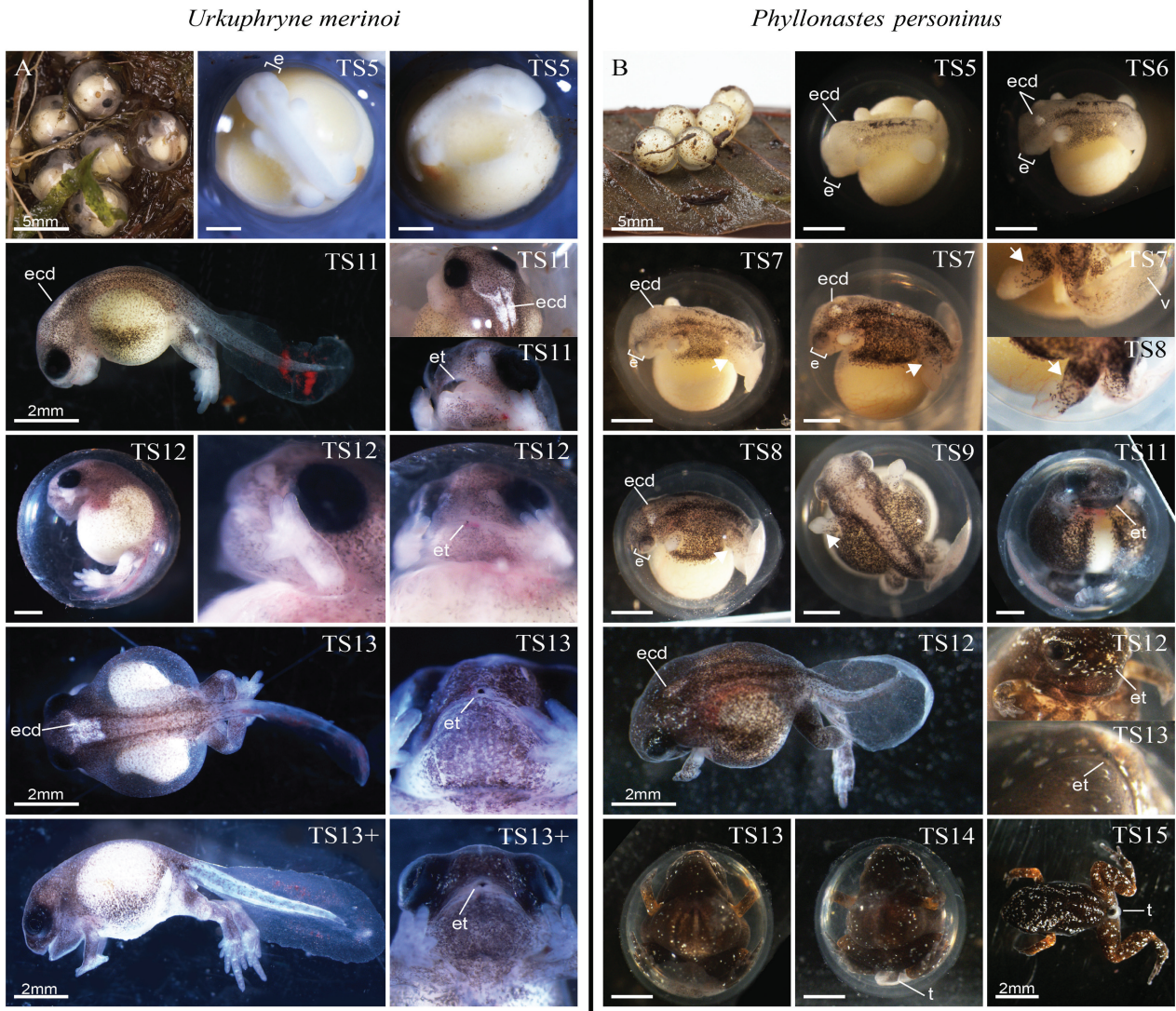


Figure 34. Early development of *Urkophryne merinoi* and *Phyllonastes personinus*. A, *U. merinoi*, clutch of female QCAZ 66078. B, *P. personinus*, clutch of couple QCAZ 71452–71453. Abbreviations: e, eye; ecd, endolymphatic calcium deposits; et, egg tooth; t, tail; v, fin vasculature. All scales are 1 mm unless otherwise specified.

had a diameter of 4.03 ± 0.02 mm (SD). The embryos were at two stages: TS5 and TS11. Five embryos were at stage TS5 and had a length (from snout to tail tip) of 4.63 ± 0.01 mm. All these embryos failed to develop. The remaining four embryos were at stage TS11 and had a total length of 10.40 ± 0.33 mm. Development of these four embryos was followed until TS13+, when the last embryo died.

The *P. personinus* couple was found and collected in amplexus and transported to the laboratory. The clutch was laid during transport; thus, we were not able to observe mating or fertilization behaviours. The nest was deposited in a terrarium in the laboratory with leaf litter (Fig. 34B). It had two embryos and three unfertilized eggs. Unfertilized eggs had a diameter of 2.15 ± 0.01 mm. The remaining two embryos were at TS5 and had a total length of 2.97 ± 0.05 mm. Only one of these embryos hatched as a froglet.

For both species, embryos at TS5 have the shape and structures of most direct-developing embryos, with distinctive limb and tail buds and with a head with visible eyes. In both species,

branchial arches and external gills were not apparent, and posterior limb buds were larger than the anterior ones. TS5 embryos in both species apparently lack oocyte-derived pigment, because both have clear unpigmented yolk and white embryonic integument. In *P. personinus*, melanocytes (neural crest-derived melanophores) are spread on the integument from the most dorsal part of the body but have not yet covered the yolk or the limb buds. Also, no retinal pigmentation was observed at this stage. Stages TS6–TS9 were recorded only in *P. personinus*. In TS6, pigmentation has advanced to the head and limb buds. At this stage, endolymphatic calcium deposits are rounded structures that protrude prominently from the posterior dorsal region of the head. During TS7 the eye develops retinal pigmentation distinct from the unpigmented lens vesicle (pupil), and melanocytes cover the whole dorsal body. By TS9, melanocytes and the body wall have covered one-third of the yolk surface and the endolymphatic calcium deposits, which now have a triangular shape. Compared with anterior limbs, at TS7, posterior limbs show more growth and differentiation, with distinctive paddles

and knee joint constrictions. Forelimbs seem to develop joint constrictions later (TS9). At TS10, we detected hindlimb movement, and autopod paddles showed finger differentiation (not shown). Between TS6 and TS7, translucent membranous fins with vascularization were first apparent in the tail.

Urkuphryne merinoi TS11 embryos are paler and seem to have less melanocytes that are spread across the whole body except for the ventral midline. In this species, endolymphatic calcium deposits were still visible and covered the dorsal surface of the hindbrain bilaterally, with projections towards the eyes.

In both species, the egg tooth is visible as an unpigmented monocuspid structure. Between TS12 and TS13, the egg tooth becomes keratinized and darkly pigmented. This was more evident in *U. merinoi*.

The tail develops to its maximum length by TS11 in *P. personinus* and by TS13 in *U. merinoi*. The tail of *U. merinoi* seems to be thinner and larger than that of *P. personinus*; however, both have symmetrical fins over the dorsoventral axis. The progress between TS13 and TS14 implies the reduction of yolk mass and the reabsorption of the tail, which remained as a translucent vestige in the *P. personinus* froglet. The progress from TS11 to TS13 in *U. merinoi* lasted 10 days. The progress from TSS to hatching in *P. personinus* lasted 32 days.

DISCUSSION

A first step to solve the polyphyly of *Noblella*

Our phylogeny (Supporting Information, Fig. S1), the most comprehensive to date for the Holoadeninae subfamily, confirms the polyphyly of *Noblella*, a result reported in previous studies (e.g. Catenazzi and Tito 2019, Reyes-Puig et al. 2019, 2021, Catenazzi et al. 2020, Reyes-Puig et al. 2020, Motta et al. 2021). The revalidation of the genus *Phyllonastes* partly solves this problem. Our proposal requires that the holotype of *N. peruviana*, the type specimen of *Noblella*, belongs to the southern clade. *Noblella peruviana* lacks genetic data, which could cast doubt on our clade assignment. However, there is convincing geographical, morphological, and environmental evidence indicating that *N. peruviana* belongs to the southern clade. First, there is a large geographical gap between the northern clade and the range of *N. peruviana* (>1200 km; Fig. 3). Given that closely related species usually (but not always) have geographically closer ranges, it is much more likely that *N. peruviana* belongs to the southern clade (e.g. Catenazzi and Tito 2019, Reyes-Puig et al. 2019, 2020, 2021, Catenazzi et al. 2020, Motta et al. 2021). Second, the species most similar to *N. peruviana* is *N. thiuni* (Catenazzi & Tito, 2019), a species from the southern clade (Fig. 2). Third, *N. peruviana* has morphological characteristics absent in *Phyllonastes* (for details, see 'Systematic accounts'). Finally, the *N. peruviana* type locality is cold and dry, outside the environmental envelope of the northern clade (Fig. 9). Its mean annual temperature is 7.8°C. In contrast, localities of species of the northern clade are warmer, with mean annual temperatures ranging from 9.8°C to 25.3°C. Habitat type is also markedly different, with *N. peruviana* occurring in Puna vegetation, a grassy and dry open habitat in the highlands of Perú; most *Phyllonastes*, in contrast, occur in evergreen montane forests. These marked ecological differences are additional evidence that *N. peruviana* belongs to the southern clade.

Our results confirm the paraphyly of *Noblella* and *Psychrophrynella* within the southern clade (Fig. 2), a finding made by prior studies (e.g. Catenazzi and Tito 2019, Motta et al. 2021, Reyes-Puig et al. 2021). One way to address this paraphyly would be to assign all species from the southern clade to the genus *Noblella* and treat *Psychrophrynella* as a synonym of *Noblella*, especially given that our ancestral character reconstruction does not suggest any notable morphological differences between them. However, we refrain from making the taxonomic change owing to incomplete information on the morphological variation between the clades, which could justify recognizing them as separate genera in the future. We prefer to avoid creating taxonomic instability.

The discovery and description of the six new species of *Phyllonastes* represents a 75% increase in the species content of this clade, a result similar to that of other groups of Brachycephaloidea, where the combination of genetic and morphological data has revealed a large proportion of undescribed species (e.g. Elmer and Cannatella 2008, Páez and Ron 2019, Ortega et al. 2022). Moreover, the richness of *Phyllonastes* is probably still underestimated. Our study alone revealed a total of 17 confirmed candidate species within the northern clade (Fig. 4). Other unconfirmed candidate species remain undescribed owing to insufficient morphological data required to confirm their taxonomic status. Furthermore, *P. myrmecoides* is shown to be paraphyletic (Fig. 4), suggesting the existence of cryptic diversity within its large distribution range (tropical Amazonian forest from eastern Ecuador to northwestern Brazil).

Urkuphryne, a new monotypic genus

A remarkable result from our study was the discovery of *Urkuphryne*, a new genus of Holoadeninae frogs. Based on recently collected material from northern Ecuador, this discovery highlights that highly divergent amphibian lineages still await discovery [see also Fouquet et al. (2024) and Arroyo et al. (2022) for a recent description of new genera and families of Brachycephaloidea]. The combination of molecular and morphological data (Figs 2, 4, 5; Supporting Information, Table S1) revealed an old phylogenetic divergence (23 Mya) and distinctive morphological traits (Figs 5, 28–33), clearly distinguishing it from its sister clade, *Phyllonastes*. These unique characteristics, in comparison to *Phyllonastes* and other Brachycephaloidea (= Terrarana) genera, justify its classification as a new, monotypic genus.

The autapomorphies of the genus are the arrangement of the vomerine teeth and the absence of distal expansion of toes. Our results show that, like other Terrarana, *Urkuphryne* exhibits reproductive mode 23 of Haddad and Prado (2005) (or its equivalent: mode 17 of Duellman and Trueb 1986), characterized by directly developing terrestrial eggs (Fig. 34). Females lay large eggs in small numbers in nests buried under leaf litter. The presence of an adult female next to the eggs suggests parental care. Moreover, the description of the embryonic development and reproductive mode in *Urkuphryne* advances our understanding of the natural history of Brachycephaloidea, a group for which reproductive information is scarce.

Urkuphryne belongs to the subfamily Holoadeninae, a clade of frogs remarkable for having many genera, but, paradoxically, low species richness relative to clades of a comparable

age within Brachycephaloidea. According to a recent estimate (Portik *et al.* 2023), Holoadeninae originated ~40 Mya (similar to our estimate of ~44 Mya). They are sister to Pristimantinae, a clade consisting of seven genera: *Lynchius* Hedges *et al.*, 2008, *Oreobates* Jiménez de la Espada, 1872, *Phrynopus*, *Pristimantis*, *Serranobatrachus* Arroyo *et al.* 2022, *Tachiramantis* Heinicke *et al.* 2015, and *Yunganastes* Padial *et al.* 2007 (Portik *et al.* 2023, Frost, 2023) and 697 species (Frost 2023). Despite having the same age, Holoadeninae have 73 species, only ~1/10 of Pristimantinae. The reasons for the striking difference in diversification rates are unclear.

Convergent evolution in Terrarana

Morphological resemblance in phylogenetically distant clades in Terrarana inhabiting similar ecosystems suggest convergent evolution (Hedges *et al.* 2008, Duellman and Lehr 2009, Catenazzi *et al.* 2020). *Phyllonastes* and *Noblella* provide an example of morphological similarity (Hedges *et al.* 2008, Heinicke *et al.* 2009, 2017, De la Riva *et al.* 2018, von May *et al.* 2018, Catenazzi *et al.* 2020) despite a long divergence time (~38 Mya). Both clades evolved convergently acuminate toe tips and lack of vomerine teeth, which explains their assignment to a single genus by De la Riva *et al.* (2008b).

Molecular systematics have revealed that clades of Terrarana that were considered phylogenetically close as result of morphological convergence, were evolutionarily distant (e.g. *Eleutherodactylus* and *Bahiuss*) (Motta *et al.* 2021). Therefore, reorganization into separate genera was necessary to solve widespread paraphyly and polyphyly problems (Hedges *et al.* 2008, Motta *et al.* 2021). Solving of those problems was started by Hedges *et al.* (2008) and several subsequent studies (e.g. Heinicke *et al.* 2009, 2015, De la Riva *et al.* 2018, Catenazzi *et al.* 2020). Our study provides an additional example of morphological convergence between Holoadeninae clades with *Phyllonastes* and *Noblella*.

Biogeography and diversification

Our biogeographical reconstruction shows an unexpected asymmetry in the direction of colonization events across the Andes in the *Phyllonastes*–*Urkuphryne* clade. The group originated >25 Mya in the Pacific slopes of the Andes. Since then, colonization across the Andes has been sporadic, with only five events. All those events took place from the Pacific slopes (*trans*-Andean distribution) to the Amazonian slopes (*cis*-Andean; Fig. 6) of the Andes. Therefore, our results indicate that the Pacific slopes have acted as a biogeographical museum, a region where old lineages have persisted (*sensu* Rangel *et al.* 2018). Although the group originated on the Pacific slopes, species richness on the Amazonian slopes is higher (11 species vs. 8 on the Pacific slopes) indicating that diversification rates have also been higher. This suggests that the Amazonian slopes have acted as a biogeographical cradle, a region where speciation predominates. This could exemplify how the Andes can be both a biogeographical museum (i.e. Chocó region and Pacific slopes) and a cradle of diversity (i.e. Amazonian slopes) for forest species separated by non-forested mountain tops and high valleys.

A similar biogeographical pattern was reported in the *P. lacrimosus* species group, which, despite an origin on the Pacific

slopes, has much higher species richness on the Amazonian slopes (Ron *et al.* 2020). The generality of this pattern has yet to be tested, but possible causes could be the species–area effect (i.e. forested areas are more extensive on the Amazonian slopes) and the drier conditions that predominate on the Pacific slopes south from 3°S of latitude.

Embryonic development in *Urkuphryne* and *Phyllonastes* (Fig. 34)

Amphibians with direct development do not have tadpoles, and most adult features appear during embryogenesis (Hanken 1999, McDiarmid and Altig 1999). In Terrarana (Brachycephaloidea), direct development seems to be a synapomorphy (Heinicke *et al.* 2009, Padial *et al.* 2014), according to the multiple descriptions of embryonic development in species of the genera *Eleutherodactylus*, *Adelophryne* Hoogmoed and Lescure, 1984, *Brachycephalus* Fitzinger, 1826, *Ischnocnema* Reinhardt and Lütken, 1862, *Pristimantis*, *Oreobates*, and *Haddadus* Hedges *et al.* 2008 (Noble 1925, Gitlin 1944, Jameson 1961, Townsend and Stewart 1985, Pombal 1999, Nokhbatolfighahai *et al.* 2010, Goldberg *et al.* 2012, 2020, Goldberg and Candioti 2015, de Lima *et al.* 2016). From these descriptions, it seems that terraranan species produce large unpigmented eggs, and embryos develop an expanding epidermal fold (body wall), an egg tooth, and a tail with large and highly vascularized fins. According to our observations, *U. merinoi* and *P. personinus* clearly follow the general developmental pattern of Terrarana. From ours and previous descriptions, it is also clear that there can be developmental differences among Terrarana groups, particularly regarding body pigmentation, formation of external gills, limb differentiation, and tail structure (Goldberg and Candioti 2015, Vera Candioti *et al.* 2020).

Body pigmentation and epidermal folds

Phyllonastes personinus shows early melanocyte differentiation and migration, like *Adelophryne maranguapensis* Hoogmoed *et al.*, 1994 embryos (de Lima *et al.* 2016). *Urkuphryne merinoi* embryos apparently have delayed melanocyte differentiation, like *Eleutherodactylus coqui*, *Ischnocnema henselii* (Peters, 1870), and the afrobatrachian *Arthroleptis xenodactyloides* Hewitt, 1933 (Townsend and Stewart 1985, Schweiger *et al.* 2017, Goldberg *et al.* 2020). In *E. coqui*, it has been shown that the definitive epidermis expands from the dorsal embryonic region, together with melanocytes, and progressively covers the yolk mass, in a phenomenon equivalent to the formation of the opercular folds in tadpoles (Elinson and Fang 1998). In some non-Terrarana direct developers, such as *A. xenodactyloides*, the myobatrachid *Metacrinia nichollsi* (Harrison, 1927), and rhacophorids of the genus *Pseudophilautus* Laurent, 1943, the epidermal folds cover the anterior limb buds, which develop inside and then break out after finger differentiation (Anstis 2008, Anstis *et al.* 2011, Schweiger *et al.* 2017). In Terrarana, including *U. merinoi* and *P. personinus*, these epidermal folds do not cover the limbs.

Limb development

Direct-developing embryos simultaneously form fore- and hind-limb buds immediately after the end of neurulation, during TS4 (Hanken *et al.* 2001). Similar to most direct developers

in Terrarana, *U. merinoi* and *P. personinus* embryos develop autopods and articulations earlier in the hindlimb buds than in the forelimb buds.

Formation of gills

Most terraranans lack external embryonic gills, except for some species within Eleutherodactylidae, such as *E. coqui* (Townsend & Stewart, 1985). Still, external gills are apparently absent in embryos of *Eleutherodactylus nubicola* Dunn, 1926, *Eleutherodactylus abbotti* Cochran, 1923, and *Eleutherodactylus flavescens* Noble, 1923 (Noble 1925).

Tail and caudal fin development

Reduction or absence of external gills in Terrarana might be related with the presence of a large tail with highly vascularized fins, which might have a respiratory function (Townsend and Stewart 1985). In every Terrarana embryo so far described, including *U. merinoi* and *P. personinus*, the tail is twisted, with the dorsal and ventral tail fins growing laterally, often covering the ventral surface of the embryo (Townsend and Stewart 1985, Nokhbatolfighahai et al. 2010, de Lima et al. 2016). In *Haddadus binotatus* Spix, 1824, *Oreobates barituensis* Vaira and Ferrari, 2008, and *Pristimantis urichi* Boettger, 1894, these fins appear to be lateral projections, rather than dorsoventral projections (Nokhbatolfighahai et al. 2010, Goldberg et al. 2012, Goldberg and Candiotti 2015). In these species, the tail fins are asymmetric and cover most of the embryo.

Egg tooth

A unique feature present in Terrarana is the formation of an egg tooth. This structure has not been observed in embryos of non-terraranans (Townsend and Stewart 1985, Bahir et al. 2005, Anstis 2008, Schweiger et al. 2017). Similar to other Terrarana species, in *U. merinoi* and *P. personinus*, the egg tooth developed first as an unpigmented unicuspid structure by TS11, which then keratinized by later stages. To compare, *Brachycephalus ephippium* Spix, 1824 and *Haddadus binotatus* have single bicupid egg teeth (Pombal 1999, Goldberg and Candiotti 2015).

CONCLUSIONS

We confirm the polyphyly of the genus *Noblella* by presenting a highly supported phylogeny. Based on molecular, morphological, and environmental evidence, we recommend its separation into two genera: *Noblella* and *Phyllonastes*. *Noblella* contains eight recognized species distributed in southern Peru and Bolivia, and *Phyllonastes* contains 15 recognized species, six newly described in this contribution, distributed in Ecuador, the Amazonian Tropical Rainforest from southeastern Colombia to northern and central Peru, and northwestern Brazil. In addition, we include genetic, morphological, and osteological evidence that allows us to propose the description of a new genus of strabomantid distributed in northern Ecuador: *Urkuphryne*.

Note added during the review process

While our article was under review, a publication by von May et al. (2024) (hereafter, von May et al.) appeared in the journal *Diversity* (published by MDPI) reporting the phylogenetic position of *Noblella peruviana* and *Psychrophrynella bagrecito*,

the type species for *Noblella* and *Psychrophrynella*, respectively. Although with fewer sampled species for the northern clade (19 species here vs. 10 in von May et al.), the phylogeny of von May et al. is consistent with ours. Incongruences involve weakly supported nodes, at least in one of the phylogenies. For example, in the paper by von May et al., the northern clade (= *Phyllonastes*) is sister to *Bahius*, whereas in our phylogeny *Phyllonastes* is sister to *Urkuphryne* (not sampled by Von May et al.), and both are sister to *Barycholos*.

von May et al. confirmed our assignment of *N. peruviana* to the southern clade. Based on the phylogenetic position of *N. peruviana* and *P. bagrecito*, von May et al. synonymized *Psychrophrynella* under *Noblella* and, in a similar manner to our publication, resurrected *Phyllonastes* for the northern clade of *Noblella* s.l. The inclusion of both type species in a phylogeny is a welcome step forward for advancing the systematics of the group.

Also, von May et al. included *N. lynchi* in a phylogeny for the first time, and their results are consistent with our assignment of this species to the northern clade and, therefore, to *Phyllonastes*, based on morphological evidence. However, we disagree with the reclassification of *Noblella duellmani* into *Phyllonastes*, because both its morphological traits and its geographical distribution align it more closely with the southern clade, contrary to the assertion by von May et al. Geographically, *N. duellmani* is situated closer to confirmed records of the southern clade (see Fig. 3); the nearest record of this clade (*Psychrophrynella vilcabambensis* = *Noblella vilcabambensis*) lies ~390 km away from *N. duellmani*, and the closest record of the northern clade (*Phyllonastes lynchi*) is ~490 km away. Additionally, according to our analyses of environmental envelopes, *N. duellmani* lies within climate conditions typical for the southern clade (Fig. 9). Morphologically, *N. duellmani* exhibits several characteristics more frequently found in species of the southern clade: (1) absence of a tympanic membrane and tympanic annulus; (2) presence of a supratympanic fold; (3) absence of supernumerary palmar tubercles; (4) absence of an inner tarsal tubercle; (5) absence of papillae on fingers and toes; and (6) absence of circumferential grooves on the toes (Lehr et al. 2004) (the presence of circumferential grooves is a synapomorphy of *Phyllonastes*). We thus recommend reinstating *N. duellmani* under *Noblella* as the available evidence suggests closer affiliation with the southern clade.

We also note that in the new combination proposed by von May et al., '*Phyllonastes personina*', the genus *Phyllonastes* (masculine in gender) does not agree with the gender of the species '*personina*' (feminine). Therefore, the correct binomen is *Phyllonastes personinus* comb. nov.

The combined evidence presented here and by Von May et al. supports the resurrection of the genus *Phyllonastes*. It should be noted that the priority principle applies only to nomenclatural acts, not to taxonomic decisions such as the resurrection of a genus. Therefore, one study does not invalidate the other, and both studies present complementary data to support the same taxonomic proposal.

SUPPLEMENTARY DATA

Supplementary data is available at *Zoological Journal of the Linnean Society* online.

ACKNOWLEDGEMENTS

For specimen collections, we thank Aída Ortiz, Alberto Sánchez, Alex Achig, Ana Almendáriz, Ana Mashendo, Andrea Calispa, Andrea Correa, Andrea Narváez, Andrés Merino, Carla Garzón, Carlos Castro, Carlos Ruiz, Carmen Córdoba, Cristian Melo, Cristina Toapanta, Dan Cogalniceanu, Daniel Rivadeneira, Darwin Nuñez, David Cannatella, David Gower, David Mantilla, David Velalcázar, Diana Pazmiño, Diana Székely, Diego Almeida, Diego Paucar, Eduardo Toral, Edwin Carrillo, Elicio Tapia, Eloy Nusirquia, Fernanda Gordon, Fernando Ayala, Fernando Nogales, Francisco Timias, Francy Mora, Gabriel Clavijo, Gabriela Olmedo, George Fletcher, Giovanni Onore, Ignacio De la Riva, Ignacio Segovia, Ítalo Tapia, Javier Aznar, Javier Pinto, Jean Marc Touzet, Jefferson Mora, Jenny Morocho, Jorge Brito M., Joselyn Durán, Josué Quintanchala, Juan Carlos Santos, Juan Fernando Dueñas, Juan Guayasamín, Juan Pablo Reyes-Puig, Julio Molineros, Leonardo Cedeño, Leónora Orejuela, Ligia Pandiguana, Lindali Tapia, Luis Coloma, Ma. Mercedes Gavilanes, Malki Bustos, Manuel Cajamarca, Marcel Caminer, María del Mar Moretta, Mariana Piruch, Mark Wilkinson, Martin Cohen, Mauricio Ortega, Miguel Urgiles, Monica Paez, Nadia Páez, Néstor Acosta, Octavio Jiménez Robles, Pablo Venegas, Paloma Lima, Pamela Baldeón, Paul Székely, Polibio Malte, Raffaele Gattelli, Raquel Betancourt, Raúl Sandoya, Ricardo Gavilanes, Rubén Jarrín, Salomón Ramírez, Samael Padilla, Santiago Arroyo, Santiago Burneo, Santiago Recalde, Sebastián Valverde, Silvia Aldás, Teresa Camacho, Valeria Ayo, Victor Utreras, Xavier Cisneros, and Yerka Sagredo. We also thank Luke Mahler Ph.D., Ken Toyama, and Christopher Boccia from the Department of Ecology & Evolutionary Biology of Toronto University for assisting access to CT-Scan facilities and helping us with the landmark's analyses. We are grateful to Fernando Ayala, Santiago Guamán and Diego Paucar for their help for accessing QCAZ specimens; to Mario Yáñez-Muñoz for his support and encouragement, allowing access to DHMECN specimens deposited at the National Institute of Biodiversity INABIO, and providing detailed information for specimens under his care; to Carolina Reyes-Puig, David Brito and Emilia Peñaherrera for their help accessing ZSFQ specimens; to Ana Belén Carrillo, Sebastián Espinoza-Ulloa, Liliana Jaramillo, and Claudia Terán for their help with DNA extraction and laboratory work; to Julio Carrión, Gustavo Pazmiño, Diego Quirola and Jose Vieira who offered photo assistance; to Emilia Peñaherrera for helping with ecological niche models and maps; to David Brito and Emilia Peñaherrera for supporting lab work at ZSFQ.

FUNDING

Field and laboratory work in Ecuador were funded by Secretaría Nacional de Educación Superior, Ciencia, Tecnología e Innovación del Ecuador SENESCYT (Arca de Noé initiative; SRR and Omar Torres principal investigators) and grants from Pontificia Universidad Católica del Ecuador, Dirección General Académica. Field and lab work by DFCH was supported by the Smithsonian Women's Committee, Smithsonian Institution (2002 Research Training Program, National Museum of Natural History), Secretaría de Educación Superior, Ciencia, Tecnología e Innovación (SENESCYT, Programa "Becas de Excelencia"), Universidad San Francisco de Quito, and "Proyecto Descubre Napo", an initiative of Universidad San Francisco de Quito in association with Wildlife Conservation Society and funded by the Gordon and Betty Moore Foundation as part of the project: WCS Consolidating Conservation of Critical Landscapes (mosaics) in the Andes.

CONFLICT OF INTEREST

All the authors declare that there are not conflicts of interest.

DATA AVAILABILITY STATEMENT

The data underlying this article are available in the manuscript, its supplementary material, and in Zenodo, at <https://doi.org/10.5281/zenodo.14498155>

REFERENCES

- Acevedo A, Lampo M, Cipriani R. The cane or marine toad, *Rhinella marina* (Anura, Bufonidae): two genetically and morphologically distinct species. *Zootaxa* 2016;**4103**:574–86. <https://doi.org/10.11646/zootaxa.4103.6.7>
- Adams DC, Collyer M, Kaliontzopoulou A. Geometric morphometric analyses of 2D/3D landmark data. *CRAN* 2020. <https://github.com/geomorphR/geomorph>.
- Adams DC, Otarola-Castillo E. Geomorph: an R package for the collection and analysis of geometric morphometric shape data. *Methods in Ecology and Evolution* 2013;**4**:393–9. <https://doi.org/10.1111/2041-210X.12035>
- Aguiayo-Vedia CR, Harvey MB. Dos nuevas especies de *Phrynopis* (Anura: Leptodactylidae) de los bosques nublados de Bolivia. *Revista de Biología Tropical* 2001;**49**:333–45.
- AmphibiaWeb. *AmphibiaWeb: Information on Amphibian Biology and Conservation*. 2021. <http://amphibiaweb.org/> (11 November 2024, date last accessed).
- Anstis M. Direct development in the Australian myobatrachid frog *Metacrinia nicholli* from Western Australia. *Records of the Western Australian Museum* 2008;**24**:133–50. [https://doi.org/10.18195/issn.0312-3162.24\(2\).2008.133-150](https://doi.org/10.18195/issn.0312-3162.24(2).2008.133-150)
- Anstis M, Parker F, Hawkes TIM *et al.* Direct development in some Australopapuan microhylid frogs of the genera *Austrochaperina*, Australia and Papua New Guinea. *Zootaxa* 2011;**3052**:1–50.
- Arroyo S, Targino M, Rueda-Solano LA *et al.* A new genus of terraranas (Anura: Brachycephaloidea) from northern South America, with a systematic review of *Tachiramantis*. *Systematics and Biodiversity* 2022;**20**:1–25. <https://doi.org/10.1080/14772000.2022.2123865>
- Bahir MM, Meegaskumbura M, Manamendra-Arachchi K *et al.* Reproduction and terrestrial direct development in Sri Lankan shrub frogs (Ranidae: Rhacophorinae: *Philautus*). *Raffles Bulletin of Zoology* 2005;**12**:339–50.
- Barbour T. A list of Antillean reptiles and amphibians. *Zoologica: scientific contributions of the New York Zoological Society* 1930;**11**:61–116. <https://doi.org/10.5962/p.203735>
- Bokermann WCA. *Lista Anotada das Localidades Tipo de Anfíbios Brasileiros*. São Paulo: Serviço de Documentação, Universidade Rural São Paulo, 1966.
- Bokermann WCA. Três espécies novas de *Eleutherodactylus* do sudeste da Bahia, Brasil (Anura, Leptodactylidae). *Revista Brasileira de Biologia* 1975;**34**:11–8.
- Bossuyt F, Milinkovitch MC. Convergent adaptive radiations in Madagascan and Asian ranid frogs reveal covariation between larval and adult traits. *Proceedings of the National Academy of Sciences of the United States of America* 2000;**97**:6585–90. <https://doi.org/10.1073/pnas.97.12.6585>
- Boulenger GA. An account of the reptiles and batrachians collected by Mr. W. F. H. Rosenberg in western Ecuador. *Proceedings of the Zoological Society of London* 1898;**66**:107–28. <https://doi.org/10.1111/j.1096-3642.1898.tb03134.x>
- Canedo C, Haddad CF. Phylogenetic relationships within anuran clade Terrarana, with emphasis on the placement of Brazilian Atlantic rainforest frogs genus *Ischnocnema* (Anura: Brachycephalidae). *Molecular Phylogenetics and Evolution* 2012;**65**:610–20. <https://doi.org/10.1016/j.ympev.2012.07.016>
- Caramaschi U, Pombal JP. Notes on the type-series of *Holoaden bradei* B. Lutz and *Holoaden luederwaldti* Miranda-Ribeiro (Anura, Brachycephalidae). *Revista Brasileira de Zoologia* 2006;**23**:1261–3.
- Carrión-Olmedo JC, Ron SR. A new cryptic species of the *Pristimantis lacrimosus* group (Anura, Strabomantidae) from the eastern slopes

- of the Ecuadorian Andes. *Evolutionary Systematics* 2021;**5**:151–75. <https://doi.org/10.3897/evolsyst.5.62661>
- Catenazzi A, Mamani L, Lehr E *et al.* New genus of terrestrial-breeding frogs (Holoadeninae, Strabomantidae, Terrarana) from Southern Peru. *Diversity* 2020;**12**:184. <https://doi.org/10.3390/d12050184>
- Catenazzi A, Ttito A. A new species of *Psychrophrynella* (Amphibia, Anura, Craugastoridae) from the humid montane forests of Cusco, eastern slopes of the Peruvian Andes. *PeerJ* 2016;**4**:e1807.
- Catenazzi A, Ttito A. *Psychrophrynella glauca* sp. n., a new species of terrestrial-breeding frogs (Amphibia, Anura, Strabomantidae) from the montane forests of the Amazonian Andes of Puno, Peru. *PeerJ* 2018;**6**:e4444. <https://doi.org/10.7717/peerj.4444>
- Catenazzi A, Ttito A. *Noblella thiuni* sp. n., a new (singleton) species of minute terrestrial-breeding frog (Amphibia, Anura, Strabomantidae) from the montane forest of the Amazonian Andes of Puno, Peru. *PeerJ* 2019;**7**:e6780. <https://doi.org/10.7717/peerj.6780>
- Catenazzi A, Ttito A, Diaz MI *et al.* *Bryophryne phuyuhampatu* sp. n., a new species of Cusco Andes frog from the cloud forest of the eastern slopes of the Peruvian Andes (Amphibia, Anura, Craugastoridae). *ZooKeys* 2017;**685**:65–81. <https://doi.org/10.3897/zookeys.685.12152>
- Catenazzi A, Uscapi V, von May R. A new species of *Noblella* (Amphibia, Anura, Craugastoridae) from the humid montane forests of Cusco, Peru. *ZooKeys* 2015;**516**:71–84. <https://doi.org/10.3897/zookeys.516.9776>
- Chaparro JC, Padijal JM, Gutiérrez RC *et al.* A new species of Andean frog of the genus *Bryophryne* from southern Peru (Anura: Craugastoridae) and its phylogenetic position, with notes on the diversity of the genus. *Zootaxa* 2015;**3994**:94–108. <https://doi.org/10.11646/zootaxa.3994.1.4>
- Chernomor O, von Haeseler A, Minh BQ. Terrace aware data structure for phylogenomic inference from supermatrices. *Systematic Biology* 2016;**65**:997–1008. <https://doi.org/10.1093/sysbio/syw037>
- Cochran DM. Frogs of southeastern Brazil. *Bulletin of the United States National Museum* 1955;**206**:1–423. <https://doi.org/10.5479/si.03629236.206.1>
- Condori FP, Acevedo-Rincón L, Mamani AJ *et al.* A new species of terrestrial-breeding frog of the genus *Psychrophrynella* (Anura: Strabomantidae) from the Cordillera de Vilcabamba, southeastern Peru. *Amphibian & Reptile Conservation* 2020;**14**:127–37.
- Dayrat B. Towards integrative taxonomy. *Biological Journal of the Linnean Society* 2005;**85**:407–15. <https://doi.org/10.1111/j.1095-8312.2005.00503.x>
- De la Riva I. A new species of *Phrynopus* from Bolivia (Anura: Leptodactylidae). *Herpetologica* 1992;**48**:111–4.
- De la Riva I. Bolivian frogs of the genus *Phrynopus*, with the description of twelve new species (Anura: Brachycephalidae). *Herpetological Monographs* 2007;**21**:241–77. <https://doi.org/10.1655/07-011.1>
- De la Riva I, Burrowes PA. A new species of *Psychrophrynella* (Anura: Craugastoridae) from the Cordillera Real, Department La Paz, Bolivia. *Zootaxa* 2014;**3887**:459–70. <https://doi.org/10.11646/zootaxa.3887.4.4>
- De la Riva I, Chaparro JC, Castroviejo-Fisher S *et al.* Underestimated anuran radiations in the high Andes: five new species and a new genus of Holoadeninae, and their phylogenetic relationships (Anura: Craugastoridae). *Zoological Journal of the Linnean Society* 2018;**182**:129–72. <https://doi.org/10.1093/zoolinnean/zlx020>
- De la Riva I, Chaparro JC, Padijal JM. A new, long-standing misidentified species of *Psychrophrynella* Hedges, Duellman & Heinicke from Departamento Cusco, Peru (Anura: Strabomantidae). *Zootaxa* 2008a;**1823**:42–50.
- De la Riva I, Chaparro JC, Padijal JM. The taxonomic status of *Phyllonastes* Heyer and *Phrynopus peruvianus* (Noble) (Lissamphibia, Anura): resurrection of *Noblella* Barbour. *Zootaxa* 2008b;**1685**:67–8.
- De la Riva I, Köhler J. A new minute leptodactylid frog, genus *Phyllonastes*, from humid montane forests of Bolivia. *Journal of Herpetology* 1998;**32**:325–9.
- de Lima AVP, Reis AH, Amado NG *et al.* Developmental aspects of the direct-developing frog *Adelophryne maranguapensis*. *Genesis* 2016;**54**:257–71. <https://doi.org/10.1002/dvg.22935>
- del Pino EM, Ávila ME, Pérez OD *et al.* Development of the dendrobatid frog *Colostethus machalilla*. *The International Journal of Developmental Biology* 2004;**48**:663–70. <https://doi.org/10.1387/ijdb.041861ed>
- Dubois A, Ohler A, Pyron RA. New concepts and methods for phylogenetic taxonomy and nomenclature in zoology, exemplified by a new ranked cladonomy of recent amphibians (Lissamphibia). *Megataxa* 2021;**5**:1–738. <https://doi.org/10.11646/megataxa.5.1.1>
- Duellman WE. A new species of leptodactylid frog, genus *Phyllonastes*, from Peru. *Herpetologica* 1991;**47**:9–13.
- Duellman WE, Lehr E. *Terrestrial-breeding frogs (Strabomantidae) in Peru*. Munster, Germany: Nature und Tier, 2009.
- Duellman WE, Trueb L. *Biology of Amphibians*. Baltimore, MD, USA: The Johns Hopkins University Press Baltimore, 1986.
- Edgar RC. MUSCLE: multiple sequence alignment with high accuracy and high throughput. *Nucleic Acids Research* 2004;**32**:1792–7. <https://doi.org/10.1093/nar/gkh340>
- Elinson RP, Fang H. Secondary coverage of the yolk by the body wall in the direct developing frog, *Eleutherodactylus coqui*: an unusual process for amphibian embryos. *Development Genes and Evolution* 1998;**208**:457–66.
- Elmer KR, Cannatella DC. Three new species of leaf litter frogs from the upper Amazon forests: cryptic diversity within *Pristimantis* “ockendeni” (Anura: Strabomantidae) in Ecuador. *Zootaxa* 2008;**1784**:11–38. <https://doi.org/10.11646/ZOOTAXA.1784.1.2>
- Esselstyn JA, Garcia HJD, Saulog MG *et al.* A new species of *Desmalopex* (Pteropodidae) from the Philippines, with a phylogenetic analysis of the Pteropodini. *Journal of Mammalogy* 2008;**89**:815–25. <https://doi.org/10.1644/07-MAMM-A-285.1>
- Faivovich J, Haddad CFB, Garcia PCA *et al.* Systematic review of the frog family Hylidae, with special reference to the Hylinae: phylogenetic analysis and taxonomic revision. *Bulletin of the American Museum of Natural History* 2005;**294**:1–240.
- Fouquet A, Kok PJR, Recoder RS *et al.* Relicts in the mist: two new frog families, genera and species highlight the role of Pantepui as a biodiversity museum throughout the Cenozoic. *Molecular Phylogenetics and Evolution* 2024;**191**:107971. <https://doi.org/10.1016/j.ympev.2023.107971>
- Frost DR. *Amphibian Species of the World: an Online Reference, version 6.2*. American Museum of Natural History, 2023. <https://amphibiansoftheworld.amnh.org> (11 November 2024, date last accessed).
- GBIF.org. GBIF Occurrence, 2023. <https://doi.org/10.15468/dl.gpgmw> (25 January 2024, date last accessed?).
- Garzón-Santomar C, Sánchez-Nivicela JC, Mena Valenzuela PR *et al.* *Reptiles y Aves de la provincia de El Oro: Una guía de identificación de especies del páramo al manglar*. Quito, Ecuador: Serie de Publicaciones GADPEO – INABIO, 2019.
- Gitlin D. The development of *Eleutherodactylus portoricensis*. *Copeia* 1944;**1944**:91–8. <https://doi.org/10.2307/1438760>
- Goebel AM, Donnelly JM, Atz ME. PCR primers and amplification methods for 12S ribosomal DNA, the control region, cytochrome oxidase I, and cytochrome b in bufonids and other frogs, and an overview of PCR primers which have amplified DNA in amphibians successfully. *Molecular Phylogenetics and Evolution* 1999;**11**:163–99. <https://doi.org/10.1006/mpev.1998.0538>
- Goldberg J, Candiotti FV. A tale of a tail: variation during the early ontogeny of *Haddadus binotatus* (Brachycephaloidea: Craugastoridae) as compared with other direct developers. *Journal of Herpetology* 2015;**49**:479–84. <https://doi.org/10.1670/14-072>
- Goldberg J, Candiotti FV, Akmentins MS. Direct-developing frogs: ontogeny of *Oreobates barituensis* (Anura: Terrarana) and the development of a novel trait. *Amphibia-Reptilia* 2012;**33**:239–50. <https://doi.org/10.1163/156853812x638527>
- Goldberg J, Taucce PPG, Quinzio SI *et al.* Increasing our knowledge on direct-developing frogs: the ontogeny of *Ischnocnema henselii* (Anura: Brachycephalidae). *Zoologischer Anzeiger* 2020;**284**:78–87.
- Griffiths I. The phylogeny of *Smithillius limbatus* and that status of the Brachycephalidae (Amphibia, Salientia). *Proceedings of the Zoological Society of London* 1959;**132**:457–87. <https://doi.org/10.1111/j.1469-7998.1959.tb05531.x>

- Guayasamin JM, Terán-Valdez A. A new species of *Noblella* (Amphibia: Strabomantidae) from the western slopes of the Andes of Ecuador. *Zootaxa* 2009;**2161**:47–59.
- Günther ACLG. Neue Batrachier in der Sammlung des britischen Museums. *Archiv für Naturgeschichte* 1858;**24**:319–28. <https://doi.org/10.5962/bhl.part.5288>
- Haddad C, Prado CP. Reproductive modes in frogs and their unexpected diversity in the Atlantic Forest of Brazil. *BioScience* 2005;**55**:207–17. [https://doi.org/10.1641/0006-3568\(2005\)055\[0207:RMIFAT\]2.0.CO;2](https://doi.org/10.1641/0006-3568(2005)055[0207:RMIFAT]2.0.CO;2)
- Hanken J. Larvae in Amphibian development and evolution. In: *The Origin and Evolution of Larval Forms*. San Diego: Academic Press, 1999, 61–108.
- Hanken J, Carl TF, Richardson MK et al. Limb development in a ‘nonmodel’ vertebrate, the direct-developing frog *Eleutherodactylus coqui*. *Journal of Experimental Zoology* 2001;**291**:375–88. <https://doi.org/10.1002/jez.1136>
- Harvey MB, Almendáriz A, Brito-M J et al. A new species of *Noblella* (Anura: Craugastoridae) from the Amazonian Slopes of the Ecuadorian Andes with Comments on *Noblella lochites* (Lynch). *Zootaxa* 2013;**3635**:001–14.
- Hedges SB, Duellman WE, Heinicke MP. New World direct-developing frogs (Anura: Terrarana): molecular phylogeny, classification, biogeography, and conservation. *Zootaxa* 2008;**1737**:1–182.
- Heinicke MP, Barrio-Amorós CL, Hedges SB. Molecular and morphological data support recognition of a new genus of New World direct-developing frog (Anura: Terrarana) from an under-sampled region of South America. *Zootaxa* 2015;**3986**:151–72. <https://doi.org/10.11646/zootaxa.3986.2.1>
- Heinicke MP, Diaz LM, Hedges SB. Origin of invasive Florida frogs traced to Cuba. *Biology Letters* 2011;**7**:407–10. <https://doi.org/10.1098/rsbl.2010.1131>
- Heinicke MP, Duellman WE, Hedges SB. Major Caribbean and Central American frog faunas originated by ancient oceanic dispersal. *Proceedings of the National Academy of Sciences of the United States of America* 2007;**104**:10092–7. <https://doi.org/10.1073/pnas.0611051104>
- Heinicke MP, Duellman WE, Trueb LA et al. A new frog family (Anura: Terrarana) from South America and an expanded direct-developing clade revealed by molecular phylogeny. *Zootaxa* 2009;**2211**:1–35.
- Heinicke MP, Lemmon AR, Lemmon EM et al. Phylogenomic support for evolutionary relationships of New World direct-developing frogs (Anura: Terrarana). *Molecular Phylogenetics and Evolution* 2017;**118**:145–55. <https://doi.org/10.1016/j.ympev.2017.09.021>
- Heyer WR. Studies on the genus *Leptodactylus* (Amphibia, Leptodactylidae) III. A redefinition of the genus *Leptodactylus* and a description of a new genus of leptodactylid frogs. *Contributions in Science* 1969;**155**:1–14. <https://doi.org/10.5962/p.241143>
- Heyer WR. Taxonomic notes on frogs from the Madeira and Purus rivers, Brazil. *Papéis Avulsos de Zoologia* 1977;**31**:141–62. <https://doi.org/10.11606/0031-1049.1977.31.p141-162>
- Hime PM, Lemmon AR, Moriarty Lemmon EC et al. Phylogenomics reveals ancient gene tree discordance in the amphibian tree of life. *Systematic Biology* 2021;**70**:49–66. <https://doi.org/10.1093/sysbio/2Fsyaa034>
- Hoogmoed MS, Lescure J. A new genus and two new species of minute leptodactylid frogs from northern South America, with comments upon *Phyzelaphryne* (Amphibia: Anura: Leptodactylidae). *Zoologische Meddelingen* 1984;**58**:85–115.
- Huson DH, Bryant D. Application of phylogenetic networks in evolutionary studies. *Molecular Biology and Evolution* 2006;**23**:254–67. <https://doi.org/10.1093/molbev/msj030>
- Instituto Nacional de Biodiversidad, Fundación Ecominga, Sumak Kawsay; et al. Anfibios y Reptiles del Corredor Ecológico Llanganates-Sangay. *Serie de Publicaciones Instituto Nacional de Biodiversidad Publicación Miscelánea* 2023;**17**:1–70.
- IUCN Standards and Petitions Committee. *Guidelines for Using the IUCN Red List Categories and Criteria. Version 15.1. Prepared by the Standards and Petitions Committee*, 2023. <https://www.iucnredlist.org/documents/RedListGuidelines.pdf> (25 January 2024, date last accessed).
- Jameson DL. The development of *Eleutherodactylus latrans*. *Copeia* 1961;**1950**:44–109. <https://doi.org/10.2307/1437581>
- Jiménez de la Espada M. Nuevos batracios americanos. *Anales de la Sociedad Española de Historia Natural* 1872;**1**:84–8.
- Kalyaanamoorthy S, Minh BQ, Wong TKF et al. ModelFinder: fast model selection for accurate phylogenetic estimates. *Nature Methods* 2017;**14**:587–9. <https://doi.org/10.1038/nmeth.4285>
- Karger DN, Wilson AM, Mahony C et al. Global daily 1 km land surface precipitation based on cloud cover-informed downscaling. *Scientific Data* 2021;**8**:307.
- Köhler JA. New species of *Phyllonastes* Heyer from the Chapare region of Bolivia, with notes on *Phyllonastes carrascoicola*. *Spixiana* 2000;**23**:47–53.
- Lehr E. Taxonomic status of some species of Peruvian *Phrynopis* (Anura: Leptodactylidae), with the description of a new species from the Andes of southern Peru. *Herpetologica* 2006;**62**:331–47. [https://doi.org/10.1655/0018-0831\(2006\)62\[331:tsoaso\]2.0.co;2](https://doi.org/10.1655/0018-0831(2006)62[331:tsoaso]2.0.co;2)
- Lehr E, Aguilar C, Lundberg M. A new species of *Phyllonastes* from Peru (Amphibia, Anura, Leptodactylidae). *Journal of Herpetology* 2004;**38**:214–8. <https://doi.org/10.1670/135-03a>
- Lehr E, Catenazzi A. A new species of minute *Noblella* (Anura: Strabomantidae) from southern Peru: the smallest frog of the Andes. *Copeia* 2009a;**2009**:148–56. <https://doi.org/10.1643/ch-07-270>
- Lehr E, Catenazzi A. Three new species of *Bryophryne* (Anura: Strabomantidae) from the region of Cusco, Peru. *South American Journal of Herpetology* 2009b;**4**:125–38. <https://doi.org/10.2994/057.004.0204>
- Lehr E, Catenazzi A. Two new species of *Bryophryne* (Anura: Strabomantidae) from high elevations in southern Peru (region of Cusco). *Herpetologica* 2010;**66**:308–19. <https://doi.org/10.1655/09-038.1>
- Lehr E, Fritzsich G, Mueller A. Analysis of Andes frogs (*Phrynopis*, Leptodactylidae, Anura) phylogeny based on 12S and 16S mitochondrial rDNA sequences. *Zoologica Scripta* 2005;**34**:593–603.
- Lutz B. Anfibios novos e raros das Serras Costeiras do Brasil (New or rare frogs from the Coastal Ranges of Brazil). *Memórias do Instituto Oswaldo Cruz* 1958;**56**:373–99. <https://doi.org/10.1590/s0074-02761958000200002>
- Lynch JD. Evolutionary relationships, osteology, and zoogeography of leptodactylid frogs. *Museum of Natural History Miscellaneous Publications* 1971;**53**:1–238.
- Lynch JD. A review of the Andean leptodactylid frog genus *Phrynopis*. *Occasional Papers of the Museum of Natural History* 1975;**35**:1–51.
- Lynch JD. Two new species of frogs of the genus *Euparkerella* (Amphibia: Leptodactylidae) from Ecuador and Perú. *Herpetologica* 1976;**32**:48–53.
- Lynch JD. New species of minute leptodactylid frogs from the Andes of Ecuador and Peru. *Journal of Herpetology* 1986;**20**:423–31. <https://doi.org/10.2307/1564505>
- Lynch JD, Duellman WE. *Frogs of the Genus Eleutherodactylus in Western Ecuador: Systematics, Ecology, and Biogeography*. Kansas: Natural History Museum, University of Kansas, 1997.
- Maddison WP, Maddison DR. *Mesquite: a Modular System for Evolutionary Analysis. Version 3.70*, 2019. <http://mesquiteproject.org> (25 January 2024, date last accessed).
- Mamani L, Catenazzi A, Ttito A et al. A new species of *Bryophryne* (Anura: Strabomantidae) from the Cordillera de Vilcabamba, southeastern Peruvian Andes. *Phyllomedusa* 2017;**16**:129–41. <https://doi.org/10.11606/issn.2316-9079.v16i2p129-141>
- McDiarmid RW, Altig R. *Tadpoles: the Biology of Anuran Larvae*. Chigago, IL, USA: University of Chicago Press, 1999.
- Miranda-Ribeiro A. Algumas considerações sobre *Holoaden lüderwaldti* e generos correlatos. *Revista do Museu Paulista* 1920;**12**:319–20.
- Miranda-Ribeiro A. Alguns batrachios novos das colleções do Museo Nacional. *O campo* 1937;**8**:66–9.
- Moen DS, Wiens JJ. Phylogenetic evidence for competitively driven divergence: body-size evolution in Caribbean treefrogs

- (Hylidae: *Osteopilus*). *Evolution* 2009;**63**:195–214. <https://doi.org/10.1111/j.1558-5646.2008.00538.x>
- Motta AP, Chaparro JC, Pombal JP. Molecular phylogenetics and taxonomy of the Andean genus *Lynchius* Hedges, Duellman, and Heinicke 2008 (Anura: Craugastoridae). *Herpetological Monographs* 2016;**30**:119–42.
- Motta AP, Taucce GPP, Haddad BCF *et al.* A new terraranan genus from the Brazilian Atlantic Forest with comments on the systematics of Brachycephaloidea (Amphibia: Anura). *Journal of Zoological Systematics and Evolutionary Research* 2021;**59**:663–79. <https://doi.org/10.1111/jzs.12452>
- Nguyen LT, Schmidt HA, von Haeseler A *et al.* IQ-TREE: a fast and effective stochastic algorithm for estimating maximum-likelihood phylogenies. *Molecular Biology and Evolution* 2015;**32**:268–74. <https://doi.org/10.1093/molbev/msu300>
- Noble GK. Five new species of Salientia from South America. *American Museum Novitates* 1921;**29**:1–7.
- Noble GK. An outline of the relation of ontogeny to phylogeny within the Amphibia. I. *American Museum Novitates* 1925;**165**:1–2.
- Nokhbatolfighahai M, Mitchel NJ, Downie JR. Surface ciliation and tail structure in direct-developing frog embryos: a comparison between *Myobatrachus gouldii* and *Pristimantis* (= *Eleutherodactylus*) *urichi*. *Herpetological Journal* 2010;**20**:59–68.
- Oppel M. *Die Ordnung, Familien und Gattungen der Reptilien als Prodrum einer Naturgeschichte derselben*. München: Joseph Lindauer, 1811.
- Ortega JA, Brito J, Ron SR. Six new species of *Pristimantis* (Anura: Strabomantidae) from Llanganates National Park and Sangay National Park in Amazonian cloud forests of Ecuador. *PeerJ* 2022;**10**:e13761. <https://doi.org/10.7717/peerj.13761>
- Padial JM, Castroviejo-Fisher S, De la Riva I. The phylogenetic relationships of *Yunganastes* revisited (Anura: Terrarana). *Molecular Phylogenetics and Evolution* 2009;**52**:911–5. <https://doi.org/10.1016/j.ympev.2009.05.006>
- Padial JM, Chaparro JC, Castroviejo-Fisher S *et al.* A revision of species diversity in the Neotropical genus *Oreobates* (Anura: Strabomantidae), with the description of three new species from the Amazonian slopes of the Andes. *American Museum Novitates* 2012;**3752**:1–55. <https://doi.org/10.1206/3752.2>
- Padial JM, Chaparro JC, De la Riva I. Systematics of *Oreobates* and the *Eleutherodactylus discoidalis* species group (Amphibia, Anura), based on two mitochondrial DNA genes and external morphology. *Zoological Journal of the Linnean Society* 2008;**152**:737–73. <https://doi.org/10.1111/j.1096-3642.2007.00372.x>
- Padial JM, De La Riva I. A response to recent proposals for integrative taxonomy. *Biological Journal of the Linnean Society* 2010;**101**:747–56. <https://doi.org/10.1111/j.1095-8312.2010.01528.x>
- Padial JM, Miralles A, De la Riva I *et al.* The integrative future of taxonomy. *Frontiers in Zoology* 2010;**7**:16. <https://doi.org/10.1186/1742-9994-7-16>
- Padial JM, Grant T, Frost DR. Molecular systematics of terraranas (Anura: Brachycephaloidea) with an assessment of the effects of alignment and optimality criteria. *Zootaxa* 2014;**3825**:1–132. <https://doi.org/10.11646/zootaxa.3825.1.1>
- Páez NB, Ron SR. Systematics of *Huicundomantis*, a new subgenus of *Pristimantis* (Anura, Strabomantidae) with extraordinary cryptic diversity and eleven new species. *ZooKeys* 2019;**868**:1–112. <https://doi.org/10.3897/zookeys.868.26766>
- Parker HW. A new brachycephalid frog from Brazil. *Annals and Magazine of Natural History* 1926;**18**:201–3.
- Parker HW. The systematic status of some frogs in the Vienna Museum. *Annals and Magazine of Natural History* 1932;**10**:341–4. <https://doi.org/10.1080/00222933208673582>
- Peters WCH. Über zwei Giftschlangen aus Afrika und über neue oder weniger bekannte Gattungen und Arten von Batrachiern. *Monatsberichte der Königlich Preussische Akademie des Wissenschaften zu Berlin*, 1873:411–8.
- Pombal JP. Oviposição e desenvolvimento de *Brachycephalus ephippium* (Spix) (Anura, Brachycephalidae). *Revista Brasileira de Zoologia* 1999;**16**:967–76.
- Ponssa ML, Candiotti MFV. Patterns of skull development in anurans: size and shape relationship during postmetamorphic cranial ontogeny in five species of the *Leptodactylus fuscus* group (Anura: Leptodactylidae). *Zoomorphology* 2012;**131**:349–62. <https://doi.org/10.1007/s00435-012-0164-1>
- Portik DM, Streicher JW, Wiens JJ. Frog phylogeny: a time-calibrated, species-level tree based on hundreds of loci and 5242 species. *Molecular Phylogenetics and Evolution* 2023;**188**:107907–72. <https://doi.org/10.1016/j.ympev.2023.107907>
- Pyron RA, Wiens JJ. A large-scale phylogeny of Amphibia including over 2800 species, and a revised classification of extant frogs, salamanders, and caecilians. *Molecular Phylogenetics and Evolution* 2011;**61**:543–83. <https://doi.org/10.1016/j.ympev.2011.06.012>
- QGIS.org. *QGIS Geographic Information System*. 2023.
- R Core Team. *R: a Language and Environment for Statistical Computing*. Vienna, Austria: R Foundation for Statistical Computing, 2021.
- Rangel T, Edwards N, Holden P *et al.* Modeling the ecology and evolution of biodiversity: biogeographical cradles, museums, and graves. *Science* 2018;**361**:eaar5453.
- Raxworthy CJ, Ingram CM, Rabibisoa N *et al.* Applications of ecological niche modeling for species delimitation: a review and empirical evaluation using day geckos (*Phelsuma*) from Madagascar. *Systematic Biology* 2007;**56**:907–23. <https://doi.org/10.1080/10635150701775111>
- Reichle S, Aguayo-Vedia CR, Cortez C. Geographic distribution: *Phyllonastes myrmecoides*. *Herpetological Review* 2004;**35**:283.
- Reyes-Puig C, Guayasamin JM, Koch C *et al.* A new species of the genus *Noblella* (Amphibia: Strabomantidae) from Ecuador, with new information for *Noblella worleyae*. *Acta Herpetologica* 2021;**16**:63–87. https://doi.org/10.36253/a_h-10742
- Reyes-Puig C, Maynard RJ, Trageser SJ *et al.* A new species of *Noblella* (Amphibia: Strabomantidae) from the Rio Manduriacu Reserve on the Pacific slopes from Ecuadorian Andes. *Neotropical Biodiversity* 2020;**6**:162–71. <https://doi.org/10.1080/23766808.2020.1809287>
- Reyes-Puig JP, Reyes-Puig C, Ron SR *et al.* A new species of terrestrial frog of the genus *Noblella* Barbour, 1930 (Amphibia: Craugastoridae) from the Llanganates-Sangay Ecological Corridor, Tungurahua, Ecuador. *PeerJ* 2019;**7**:e7405. <https://doi.org/10.7717/peerj.7405>
- Ron SR, Carrión J, Caminer M *et al.* Three new species of frogs of the genus *Pristimantis* (Anura, Strabomantidae) with a redefinition of the *P. lacrimosus* species group. *ZooKeys* 2020;**993**:121–55.
- Ron SR, Merino-Viteri A, Ortiz DA. *Anfibios del Ecuador. Version 2024.0. Museo de Zoología, Pontificia Universidad Católica del Ecuador*, 2024. <https://bioweb.bio/faunaweb/amphibiaweb> (11 November 2024, date last accessed).
- Rueden CT, Schindelin J, Hiner MC *et al.* ImageJ2: ImageJ for the next generation of scientific image data. *BMC Bioinformatics* 2017;**18**:529. <https://doi.org/10.1186/s12859-017-1934-z>
- Santa-Cruz R, von May R, Catenazzi A *et al.* A new species of terrestrial-breeding frog (Amphibia, Strabomantidae, *Noblella*) from the Upper Madre De Dios Watershed, Amazonian Andes and Lowlands of Southern Peru. *Diversity* 2019;**11**:145–20. <https://doi.org/10.3390/d11090145>
- Schweiger S, Naumann B, Larson JG *et al.* Direct development in African squeaker frogs (Anura: Arthroleptidae: Arthroleptis) reveals a mosaic of derived and plesiomorphic characters. *Organisms Diversity & Evolution* 2017;**17**:693–707. <https://doi.org/10.1007/s13127-017-0335-5>
- Smith SA, Stephens PR, Wiens JJ. Replicate patterns of species richness, historical biogeography, and phylogeny in Holarctic treefrogs. *Evolution* 2005;**59**:2433–50.
- Townsend DS, Stewart MM. Direct development in *Eleutherodactylus coqui* (Anura: Leptodactylidae): a staging table. *Copeia* 1985;**1985**:423–36. <https://doi.org/10.2307/1444854>
- Trifinopoulos J, Nguyen LT, von Haeseler A *et al.* W-IQ-TREE: a fast online phylogenetic tool for maximum likelihood analysis. *Nucleic Acids Research* 2016;**44**:W232–5. <https://doi.org/10.1093/nar/gkw256>
- Trueb L. Patterns of cranial diversity among the Lissamphibia. In: Hanken J, Hall BK (eds), *The Skull: Patterns of Structural and Systematic*

- Diversity*, Vol. 2. Chicago, IL, USA: Chicago University Press, 1993, 255–343.
- Valencia JH, Ortega-Andrade HM, Laborde J *et al.* Species richness, composition, distribution and conservation status of the amphibians and reptiles of the Cordillera del Cóndor, a region between Ecuador and Peru. *Community Ecology* 2023;**24**:61–72. <https://doi.org/10.1007/s42974-023-00132-y>
- Vences M, Guayasamin JM, Miralles A *et al.* To name or not to name: criteria to promote economy of change in Linnaean classification schemes. *Zootaxa* 2013;**3636**:201–44. <https://doi.org/10.11646/ZOOTAXA.3636.2.1>
- Vera Candiotti F, Goldberg J, Akmentins MS *et al.* Skeleton in the closet: hidden diversity in patterns of cranial and postcranial ontogeny in Neotropical direct-developing frogs (Anura: Brachycephaloidea). *Organisms Diversity & Evolution* 2020;**20**:763–83. <https://doi.org/10.1007/s13127-020-00467-8>
- Vieites DR, Wollenberg KC, Andreone F *et al.* Vast underestimation of Madagascar's biodiversity evidenced by an integrative amphibian inventory. *Proceedings of the National Academy of Sciences of the United States of America* 2009;**106**:8267–72. <https://doi.org/10.1073/pnas.0810821106>
- von May R, Catenazzi A, Corl A *et al.* Divergence of thermal physiological traits in terrestrial breeding frogs along a tropical elevational gradient. *Ecology and Evolution* 2017;**7**:3257–67. <https://doi.org/10.1002/ece3.2929>
- von May R, Diaz MI, Ttito A *et al.* The rediscovery of *Noblella peruviana* after more than 115 years helps resolve the molecular phylogeny and taxonomy of *Noblella* (Amphibia, Anura, Strabomantidae). *Diversity* 2024;**16**:613. <https://doi.org/10.3390/d16100613>
- von May R, Lehr E, Rabosky DL. Evolutionary radiation of earless frogs in the Andes: molecular phylogenetics and habitat shifts in high-elevation terrestrial breeding frogs. *PeerJ* 2018;**6**:e4313. <https://doi.org/10.7717/peerj.4313>
- Wiley EO. The evolutionary species concept reconsidered. *Systematic Zoology* 1978;**27**:17–26. <https://doi.org/10.2307/2412809>
- Zhang J, Kapli P, Pavlidis P *et al.* A general species delimitation method with applications to phylogenetic placements. *Bioinformatics* 2013;**29**:2869–76. <https://doi.org/10.1093/bioinformatics/btt499>